

POLYMER CAPSULES  
BY  
LIVING RADICAL POLYMERIZATION

By  
MIR MUKKARAM ALI, M.Sc.

A thesis  
Submitted to the School of Graduate Studies  
in Partial Fulfillment of the Requirements  
For the Degree  
Doctor of Philosophy

McMaster University

© By Mir Mukkaram Ali, September 2004

# POLYMER CAPSULES BY LIVING RADICAL POLYMERIZATION

DOCTOR OF PHILOSOPHY  
(Chemistry)

McMaster University  
Hamilton, Ontario

TITLE: Polymer Capsules by Living Radical Polymerization

AUTHOR: Mir Mukkaram Ali (McMaster University)

SUPERVISOR: Professor Harald D. H. Stöver

NUMBER OF PAGES: xxvii, 192

## ABSTRACT

A novel technique for encapsulation by *in situ* suspension Atom Transfer Radical Polymerization (ATRP) was developed. The capsule wall-forming material was a crosslinked terpolymer based on diethylene glycol dimethacrylate (DEGDMA) crosslinker; a hydrophobic oil-soluble monomer, methyl methacrylate (MMA), and either polar oil soluble poly(ethylene glycol) monomethyl ether methacrylate (MPEGMA) or water soluble poly(ethylene glycol) methacrylate (PEGMA).

Narrow disperse ( $M_w/M_n < 1.2$ ) and linear MMA/MPEGMA (9 – 30 mol% MPEGMA) and MMA/PEGMA (10 – 40 mol% PEGMA) copolymers of controlled molecular weight (MW) were prepared in high yields (>90 and >80 wt.%, respectively) using tosyl chloride initiator and Cu(I)Cl – dinonyl dipyriddy catalyst in diphenyl ether (DPE) solution at 70 °C. Copolymer analysis by  $^1\text{H}$  and  $^{13}\text{C}$  NMR showed quantitative incorporation of both MPEGMA and PEGMA into the copolymers.

Suspension copolymerization of MMA with either MPEGMA or PEGMA in a DPE oil phase also yielded narrow disperse ( $M_w/M_n < 1.3$ ) copolymers of controlled MW in high yields (>80 wt.%), indicating that the ATRP catalyst was confined to the oil droplets.  $^1\text{H}$  NMR confirmed the incorporation of both MPEGMA and PEGMA into the copolymers forming in the oil phase, despite significant partitioning of MPEGMA and especially PEGMA into the water phase.

In crosslinking suspension ATR terpolymerizations of MMA, MPEGMA and DEGDMA crosslinker, a transition in particle morphology from solid to hollow and multi-hollow capsular particles was observed upon increasing the MPEGMA content (0 –

31 mol%) in the feed. Analogous conventional free radical polymerizations (CFRP) gave only solid polymer particles. Similarly, ATR terpolymerization of MMA, PEGMA and DEGDMA gave capsules at 17 mol% PEGMA, while CFRP only gave capsules at higher amounts PEGMA (24 mol%) in the feed. Both systems illustrated that the slow rate of ATRP favors the thermodynamically favored capsular morphology when compared to analogous CFRP experiments, and hence should permit capsule formation for more polar fills compared to CFRP.

## ACKNOWLEDGEMENTS

I am grateful to Professor Harald D. H. Stöver for the opportunity to conduct my Doctoral Research in his Laboratory. Dr. Stöver is a dependable friend and a good leader in addition to being an excellent scientific advisor. His ability to identify and positively respond to several of my academic as well as social needs is deeply appreciated. As well, his willingness to venture into new areas of research and to continually support my endeavors was instrumental to the success of my doctoral research. The critical comments and constructive suggestions made by Dr. John F. Valliant and Dr. Brian E. McCarry who served as members of my Ph.D. Supervisory Committee helped mould this work in terms of content and direction. Their participation is gratefully acknowledged.

I also thank a number of past and present members of the Stöver Polymer Group whose contributions are too many and varied to be listed here. Special thanks are due to Dr. Nicholas Burke; a number of his scientific suggestions were incorporated into my work. Nick has a unique personality and his ability and willingness to help out is gratefully acknowledged. I also wish to thank Wen Hui Li for sharing her expertise in the area of suspension polymerization. Dr. Anna Shulkin, Dr. Lisa M. Croll, Dr. Xiangchung Yin, Erica Robinson, Xia Yan, and Mohammad Jafar Mazumdar, thank you all very much for being such great friends and colleagues.

I am immensely grateful to my parents, Dr. Mir Moazzam Ali and Nuzhath Jehan Siddiqui, to whom I owe the ability to meet challenges, make the best use of opportunities, and be persistent with whatever task I undertake in life. Their continued love, care and concern, despite my lengthy and attention demanding academic and other

pursuits over the years, leaves me with a deep sense of being truly fortunate. I acknowledge and remain deeply appreciative of the support I have received from my wife Rubina B. Siddiqi, who has cheerfully put up with my busy schedule during the final year of my doctoral program which comprised of a rush of experiments followed by long and arduous quiet writing. I thank my sister Kulsoom Fatima and my brother Mir Mohammad Ali for support and encouragement they have offered throughout my educational and other endeavors.

In closing, I am most grateful to God Almighty who has opened new doors of wonderful opportunities before me over the years and who has guided me with principles and values that have molded my character and performance for the better.

## TABLE OF CONTENTS

ABSTRACT.....	iv
ACKNOWLEDGEMENTS.....	vi
TABLE OF CONTENTS.....	vii
LIST OF SCHEMES, TABLES, FIGURES AND ABBREVIATIONS.....	xi
<b>1.0 INTRODUCTION.....</b>	<b>1</b>
<b>1.1 Polymer capsules.....</b>	<b>4</b>
1.1.1 Methods of polymer capsule preparation.....	4
1.1.2 Controlling factors in encapsulation by in situ radical polymerization.....	8
1.1.3 Morphology of polymer particles prepared by in situ radical polymerization.....	12
<b>1.2 Atom Transfer Radical Polymerization (ATRP).....</b>	<b>19</b>
1.2.1 ATRP Mechanism.....	21
1.2.2 Kinetics of Atom Transfer Radical Polymerization.....	23
1.2.3 Parameters affecting the activation and deactivation rate constants ( $k_a$ and $k_d$ ).....	24
1.2.4 Measurement of the activation and deactivation rate constants ( $k_a$ and $k_d$ ) in ATRP.....	30
1.2.5 Dependence of the activation and deactivation rate constants ( $k_a$ and $k_d$ ) in ATRP on initiator, copper halides, ligands, and polymerization solvent.....	35
1.2.6 ATRP in aqueous suspension/emulsion conditions.....	41
<b>1.3 Statement of Problem and Research Proposal.....</b>	<b>47</b>

<b>2.0 POLYMERIC CAPSULES PREPARED BY <i>IN SITU</i> SYNTHESIS AND CROSS-LINKING OF AMPHIPHILIC COPOLYMERS BY ATOM TRANSFER RADICAL POLYMERIZATION.....</b>	<b>56</b>
<b>2.1 Introduction.....</b>	<b>57</b>
<b>2.2 Results and Discussion.....</b>	<b>61</b>
2.2.1 Copolymer synthesis in diphenyl ether.....	61
2.2.2 Partitioning of PegMA into the water phase.....	73
2.2.3 Copolymer synthesis in suspension conditions.....	75
2.2.4 Encapsulation of diphenyl ether.....	82
<b>2.3 Conclusions.....</b>	<b>87</b>
<b>2.4 Experimental section.....</b>	<b>89</b>
<b>3.0 WELL DEFINED AMPHIPHILIC THERMOSENSITIVE COPOLYMERS BASED ON POLY(ETHYLENE GLYCOL) MONOMETHACRYLATE AND METHYL METHACRYLATE PREPARED BY ATOM TRANSFER RADICAL POLYMERIZATION.....</b>	<b>97</b>
<b>3.1 Introduction.....</b>	<b>98</b>
<b>3.2 Results and Discussion.....</b>	<b>100</b>
3.2.1 HPLC analysis of PEGMA macromonomer.....	100
3.2.2 Isolation and analysis of mono-functional PEGMA.....	104
3.2.3 ATRP synthesis of poly(ethylene glycol) monomethacrylate.....	104
3.2.4 ATRP copolymerization of PEGMA and MMA.....	112

3.2.5	Copolymer composition and microstructure.....	121
3.2.6	Temperature induced phase transitions of aqueous homopolymer and copolymer solutions.....	126
3.3	<b>Conclusions.....</b>	126
3.4	<b>Experimental section.....</b>	128
4.0	<b>INTERFACIAL LIVING RADICAL COPOLYMERIZATION OF OIL AND WATER SOLUBLE COMONOMERS YIELDS COMPOSITE-WALLED POLYMER CAPSULES.....</b>	138
4.1	<b>Introduction.....</b>	139
4.2	<b>Results and Discussion.....</b>	142
4.2.1	Choice of monomers, solvents and ATRP initiator-catalyst system for suspension polymerization.....	142
4.2.2	PEGMA partitioning between water and oil phases.....	143
4.2.3	ATRP synthesis of poly(MMA- <i>co</i> -PEGMA) in solution and suspension conditions.....	147
4.3	<b>Polymer capsules by crosslinking suspension ATRP.....</b>	162
4.4	<b>Conclusions and future perspectives.....</b>	171
4.5	<b>Experimental section.....</b>	173
5.0	<b>CONCLUSIONS.....</b>	185
5.1	<b>Summary.....</b>	185

<b>5.2 The Poly(MMA-<i>co</i>-MPEGMA) system.....</b>	<b>185</b>
<b>5.3 The Poly(MMA-<i>co</i>-PEGMA) solution polymerization system.....</b>	<b>186</b>
<b>5.4 The Poly(MMA-<i>co</i>-PEGMA) suspension polymerization system.....</b>	<b>187</b>
<b>5.5 Future work.....</b>	<b>188</b>
<b>APPENDIX I.....</b>	<b>191</b>
<b>APPENDIX II.....</b>	<b>192</b>

## LIST OF SCHEMES, TABLES, FIGURES AND ABBREVIATIONS

### List 1. List of Schemes in Chapter 1.

<u>Scheme No.</u>	<u>Scheme Caption</u>	<u>Page No.</u>
1	Possible equilibrium configurations corresponding to the three sets of relations for $S_i$ . The medium is phase 2.	10
2	Structures of AIBN, ABCVA and KPS.	13
3	Structures of some chain transfer agents.	17
4	Mechanism of Atom Transfer Radical Polymerization.	20
5	Elementary reactions in the ATRP equilibrium.	25
6	Some R-X compounds used as ATRP initiators or representative of polymeric end groups in ATRP (except <i>ET</i> and <i>AN</i> ).	26
7	Kinetic isolation of the activation process.	31
8	Model reaction for measurement of deactivation rate constant of phenyl ethyl bromide.	33
9	Pathway for deactivation rate constant measurement.	34
10	Complex formation equilibrium in polar and non-polar solvents.	40
11	Mechanism of “reverse” ATRP.	43

**List 2. List of Tables in Chapter 1.**

<u>Table No.</u>	<u>Table Caption</u>	<u>Page No.</u>
1	Calculated (DFT) and Experimental (from Ref. 5) BDE's of some R-X systems.	25

**List 3. List of Tables in Chapter 2.**

<u>Table No.</u>	<u>Table Caption</u>	<u>Page No.</u>
1	Solubility characteristics of some organic solvents.	62
2	Reaction conditions for encapsulation of diphenyl ether using 20 mol% crosslinking monomer and an increasing MPEGMA:MMA ratio.	83

**List 4. List of Figures in Chapter 1.**

<u>Figure No.</u>	<u>Figure Caption</u>	<u>Page No.</u>
1	Structures of ligands and copper (I) halides.	28
2	Correlation of $E_{1/2}$ with $K_{eq}^{app}$ for ATRP of methyl acrylate using several N-based ligands.	29
3	Structures of ATRP initiators used as models for polymer chain end groups.	36
4	Structures of some nitrogen based ligands used for ATRP	37

catalysts.

5	Structures of commonly used surfactants and stabilizers for suspension and emulsion ATRP.	42
6	Water soluble azo-based initiators used in “reverse” ATRP. Half lives at 90 °C in water are about 7 -10 minutes.	44

**List 5. List of Figures in Chapter 2.**

<u>Figure No.</u>	<u>Figure Caption</u>	<u>Page No.</u>
1	Plots of experimental molecular weight ( $M_n(\text{SEC})$ ) vs conversion for copolymerization of MMA and MPEGMA in DPE at 10, 25 and 40 wt % total monomer loading. $[\text{MMA}]_0:[\text{MPEGMA}]_0:[\text{TSC}]_0: [\text{Cu}(\text{dNBpy})_2\text{Br}]_0 = 60:14:1:1$ at 70 °C.	63
2	Size exclusion chromatographs showing the molecular weight profile of P(MMA-co-MPEGMA) containing 18 mol% MPEGMA at 10 wt% (90% conversion), 25 wt% (96% conversion), and 40 wt% (99% conversion) total monomer loading, respectively (top to bottom of stack) in diphenyl ether at 70°C. The reaction conditions are those presented in Figure 1.	64
3	Plots of Polydispersity Index ( $M_w/M_n$ ) vs conversion for	66

copolymerization of MMA and MPEGMA in DPE at 10 25 and 40 wt % total monomer loading.  $[MMA]_0:[MPEGMA]_0:[TSC]_0:[Cu(dNBpy)_2Br]_0 = 60:14:1:1$  at 70 °C. Error expected in Mw/Mn measurements is  $\pm 0.02$ .

- |   |  |    |
|---|--|----|
| 4 | Kinetic profiles for copolymerization of MMA and MPEGMA in DPE at 10, 25 and 40 wt % total monomer loading. $[MMA]_0:[MPEGMA]_0:[TSC]_0:[Cu(dNBpy)_2Br]_0 = 60:14:1:1$ at 70 °C. The dotted lines are only meant to guide the eye.       | 67 |
| 5 | Plots of experimental ( $M_n(SEC)$ ) and theoretical ( $M_n(Theo)$ ) molecular weight vs conversion for copolymerization of MMA and MPEGMA (%MPEGMA = 0.0, 9.5, 18 and 39) in DPE at 25 wt%. $[TSC]_0:[Cu(dNBpy)_2Br]_0 = 1:1$ at 70 °C. | 68 |
| 6 | Polydispersity vs conversion for copolymerization of MMA and MPEGMA (mol% MPEGMA = 0. 9.5, 18 and 39) in DPE at 25 wt%. $[TSC]_0:[Cu(dNBpy)_2Br]_0 = 1:1$ at 70 °C.  | 69 |
| 7 | Kinetics of copolymerization of MMA and MPEGMA (mol% MPEGMA = 0, 9.5, 18 and 39) in DPE at 25 wt%. $[TSC]_0:[Cu(dNBpy)_2Br]_0 = 1:1$ at 70 °C.   | 71 |

8	Size exclusion chromatographs of, A. PMMA at 98% conversion; P(MMA- <i>co</i> -MPEGMA) containing, B. 9.5% MPEGMA at 97% conversion, high molecular weight peak (HMWP) is 12 % of total peak area; C. 18 mol% MPEGMA at 96% conversion, HMWP is 17 % of total peak area; D. 39 mol% MPEGMA at 94% conversion, HMWP is 20 % of total peak area. The reaction conditions are those presented in Figures 5.	72
9	Aqueous Size Exclusion Chromatographs of (a) 2% (w/w) aqueous MPEGMA in 0.1M NaNO <sub>3</sub> and 100 ppm NaN <sub>3</sub> (solid line) (b) Aqueous phase of MPEGMA partitioning experiment done at 70 °C between 80 mL distilled water and 20 mL 10% (w/w) MPEGMA solution in diphenyl ether (dotted line). Injection volume: 30 μL. Elution solvent: Aqueous 0.1M NaNO <sub>3</sub> and 100 ppm NaN <sub>2</sub> ; Flow rate: 0.8 mL/min; Column Temperature: 35 °C; Refractive Index detector temperature: 30 °C.	74
10	Aqueous Size Exclusion Chromatography calibration curve for MPEGMA based on total area under the five component peaks. Chromatographic conditions as in Figure 9.	75
11	Kinetics of solution and suspension copolymerization of	77

MMA and MPEGMA (18 mol% MPEGMA).  
 $[MMA]_0:[MPEGMA]_0:[TSC]_0:[Cu(dNBpy)_2Br]_0 =$   
 60:14:1:1; 25% total monomer in DPE; oil (monomers +  
 DPE) /water ratio in suspension = 1:4; both polymerizations  
 at 70 °C. The dashed lines are meant only to guide the eye.

- |    |   |    |
|----|---|----|
| 12 | <p>Plots of molecular weight and polydispersity versus conversion for solution and suspension copolymerization of MMA and MPEGMA (18 mol% MPEGMA).<br/> <math>[MMA]_0:[MPEGMA]_0:[TSC]_0:[Cu(dNBpy)_2Br]_0 =</math><br/>         60:14:1:1; 25% total monomer in DPE; oil (monomers + DPE) /water ratio in suspension = 1:4; both polymerizations at 70 °C.</p> | 78 |
| 13 | <p>Molecular weight distributions of P(MMA-<i>co</i>-MPEGMA) (18 mol% MPEGMA) prepared by solution polymerization (dashed line) and solution-suspension polymerization (solid line) both at 96% conversion. Reaction conditions as in Figure 11.</p>  | 79 |
| 14 | <p>(a) Carbon-13 NMR of final P(MMA-<i>co</i>-MPEGMA) (18 mol% MPEGMA) in CDCl<sub>3</sub>; (b) J-modulated spin sort spectrum of P(MMA-<i>co</i>-MPEGMA); (c) Expansion (<math>\delta_C = 50</math></p>  | 80 |

- 60 ppm) of spectra (a) and (b).
- 15 Carbon-13 spectra ( $\delta_C = 50 - 60$  ppm) of P(MMA-*co*-MPEGMA) in CDCl<sub>3</sub> with Cr(acac)<sub>3</sub> in a gated decoupling experiment; (a) prepared by solution polymerization at quantitative conversion; (b) 2 hour in suspension polymerization at 82 % conversion. 81
- 16 ESEM micrograph showing suspension polymer particles of P(MMA-*co*-MPEGMA) crosslinked with DEGDMA. [MMA]<sub>0</sub>: [MPEGMA]<sub>0</sub>: [DEGDMA]<sub>0</sub>: [TSC]<sub>0</sub>: [Cu(dNBpy)<sub>2</sub>Br]<sub>0</sub> = 30 : 7 : 9 : 1 : 1; 32% total monomer in DPE; suspension = 11% monomers + DPE and 1% PVA (rel. to water) at 70 °C. 84
- 17 TEM micrographs showing internal morphology of suspension particles using DPE as oil phase: A. MPEGMA-0 particles (conv.= 90%) prepared by CFRP. B. MPEGMA-0 particles (conv.= 99%) prepared by ATRP. C. MPEGMA-8 particles (conv.= 98%) prepared by ATRP. D. MPEGMA-15 particles (conv.= 98%) prepared by ATRP. E. MPEGMA-31 particles (conv.= 92%) prepared by ATRP. F. MPEGMA-31 particles (conv.= 100%) prepared by CFRP. 86

**List 6. List of Tables in Chapter 3.**

<u>Table No.</u>	<u>Table Caption</u>	<u>Page No.</u>
1	LC-MS data for crude PEGMA.	101-102
2	Refractive indices of some oligo ethylene glycols and dimethacrylate derivatives	103
3	Dielectric constants and solubility parameters of some ATRP solvents	106
4	Hydrophilic lypophilic balance of P(PEGMA) and P(PEGMA-co-MMA)	115

**List 7. List of Figures in Chapter 3.**

<u>Figure No.</u>	<u>Figure Caption</u>	<u>Page No.</u>
1	Overlaid HPLC chromatograms of crude (solid line) and purified (dotted line) PEGMA (Aldrich). Chromatographic conditions as follows: reverse phase C-18 column; mobile phase: methanol/water = 1:1; flow rate = 0.5 mL/minute; column temp.= 35 °C; refractive index detector temp.= 30 °C; sample conc. = 3 wt.%; injection vol. = 20 µL; run time = 150 minutes. Non-functional PEG components (Z2–Z21), mono-functional PEG-MA components (M1–M27) and di-	105

	functional PEG-DMA (D2-D30) elute in the 5-8, 8 – 30 and 30 – 150 minute ranges, respectively.	
2	Molecular weight and polydispersity profiles for polymerization of PEGMA in DPE and XYL at 25 wt% monomer loading. [TSC] <sub>o</sub> : [Cu(dNBpy) <sub>2</sub> Br] <sub>o</sub> : [PEGMA] = 1:1:30 at 70 °C.	109
3	Conversion and kinetic profiles for polymerization of PEGMA in DPE and XYL. Conditions as in Figure 2.	110
4	Molecular weight and polydispersity profiles for polymerization of PEGMA in CXL and ETH at 25 wt% monomer loading. [TSC] <sub>o</sub> : [Cu(dNBpy) <sub>2</sub> Br] <sub>o</sub> : [PEGMA] = 1:1:30 at 70 °C.	112
5	Conversion and kinetic profiles for polymerization of PegMA in CXL and ETH at 25 wt% monomer loading. [TSC] <sub>o</sub> : [Cu(dNBpy) <sub>2</sub> Br] <sub>o</sub> : [PEGMA] = 1:1:30 at 70 °C.	114
6	Molecular weight and polydispersity profiles for copolymerization of MMA with PEGMA (mol% PEGMA = 18) in CXL at 25 wt%. [TSC] <sub>o</sub> : [Cu(dNBpy) <sub>2</sub> Br] <sub>o</sub> : [MMA] : [PEGMA] = 1:1:60:14 at 70 °C.	116
7	Conversion and kinetic profiles for copolymerization of MMA with PEGMA (mol% PEGMA = 18) in CXL.	118

Conditions as in Figure 6.

- 8 Plots of experimental ( $M_n(\text{SEC})$ ) and theoretical ( $M_n(\text{Theo})$ ) molecular weight vs conversion for copolymerization of MMA with PEGMA (%PEGMA = 10, 18, 24, 30 and 40 mol % PEGMA) in DPE at 25 wt%. [TSC]<sub>0</sub>: [Cu(dNBpy)<sub>2</sub>Br]<sub>0</sub> = 1:1 at 70 °C. 119
- 9 Conversion profiles for polymerization of P(MMA-*co*-PEGMA) (%PEGMA = 10, 18, 24, 30 and 40 mol % PEGMA) in DPE using conditions of Figure 8. Errors in conversion measurements at 10, 18, 24, and 30 mol% PEGMA are similar to those shown for the 40 mol% PEGMA copolymerization, but are omitted for clarity. 120
- 10 Polydispersity profiles for polymerization of P(MMA-*co*-PEGMA) (%PEGMA = 10, 18, 24, 30 and 40 mol % PEGMA) in DPE using conditions of Figure 8. 121
- 11 Kinetic profiles for polymerization of P(MMA-*co*-PEGMA) (%PEGMA = 10, 18, 24, 30 and 40 mol % PEGMA) in DPE using conditions of Figure 8. 122
- 12 <sup>1</sup>H NMR spectrum of P(MMA-*co*-PEGMA) copolymer (in CDCl<sub>3</sub>) containing 18 mol% PEGMA. 123

13	Evolution of PEGMA content in P(MMA- <i>co</i> -PEGMA) copolymer with conversion as determined by <sup>1</sup> H NMR spectroscopy.	124
14	Turbidity versus temperature curves of 1 wt.% aqueous solutions of water soluble P(MMA- <i>co</i> -PEGMA) containing 24, 30, and 40 mol% PEGMA showing the phase transition temperatures (42.7, 49.8 and 55.8 °C, respectively) of the copolymers (as determined by location of the point of inflection).	125

**List 8. List of Tables in Chapter 4.**

<u>Table No.</u>	<u>Table Caption</u>	<u>Page No.</u>
1	Partition coefficients of PEGMA in selected organic solvents.	146
2	Summary of suspension copolymerizations of MMA and PEGMA.	153
3	Morphology of suspension polymer particles	165
4	Suspension polymer particle size and size distribution data	166

List 9. List of Figures in Chapter 4.

<u>Figure No.</u>	<u>Figure Caption</u>	<u>Page No.</u>
1	Size exclusion chromatogram of a 5% (w/w) solution of PEGMA in 100ppm NaN <sub>3</sub> .	144
2	PEGMA calibration curve using SEC chromatograms of 1 to 8 % (w/w) standard aqueous PEGMA solutions. The total area under the SEC peaks representing PEGMA components bearing 1 to 27 ethylene oxide units in the pendant PEG chain was used as a measure of PEGMA concentration.	145
3	Molecular weight versus conversion plots for solution copolymerization of MMA with PEGMA (mol% PEGMA = 19) at 25 wt% monomer loading in the solvents shown. [TSC] <sub>0</sub> : [Cu(dNBpy) <sub>2</sub> Br] <sub>0</sub> : [MMA] : [PEGMA] = 1:1:60:14 at 70 °C. DPE results are reproduced from Ref. 28.	148
4	Polydispersity versus conversion for solution copolymerization of MMA with PEGMA (mol% PEGMA = 19) at 25 wt% monomer loading in the solvents shown. [TSC] <sub>0</sub> : [Cu(dNBpy) <sub>2</sub> Br] <sub>0</sub> : [MMA] : [PEGMA] = 1:1:60:14 at 70 °C. DPE results are reproduced from Ref. 28.	149
5	SEC chromatograms of P(MMA-co-PEGMA) (mol%	150

PEGMA = 19) prepared in CXN at 25 wt% monomer loading at 28, 40, 49, 58, 64 and 80% conversion (top to bottom of stack). [TSC]<sub>o</sub>: [Cu(dNBpy)<sub>2</sub>Br]<sub>o</sub>: [MMA] : [PEGMA] = 1:1:60:14 at 70 °C.

- 6 Conversion profiles for solution copolymerization of MMA with PEGMA (mol% PEGMA = 19) at 25 wt% monomer loading in the solvents shown. [TSC]<sub>o</sub>: [Cu(dNBpy)<sub>2</sub>Br]<sub>o</sub>: [MMA] : [PEGMA] = 1:1:60:14 at 70 °C. DPE results are reproduced from Ref. 28. 151
- 7 Kinetic plots for solution copolymerization of MMA with PEGMA (mol% PEGMA = 19) at 25 wt% monomer loading in the solvents shown. [TSC]<sub>o</sub>: [Cu(dNBpy)<sub>2</sub>Br]<sub>o</sub>: [MMA] : [PEGMA] = 1:1:60:14 at 70 °C. DPE results are reproduced from Ref. 28. 152
- 8 SEC chromatograms of P(MMA-co-PEGMA) prepared by suspension polymerization at 70 °C; Samples taken at 1hr into suspension polymerization (top) and at reaction end (bottom); Oil:Water = 1:2; 25 wt% monomer loading in oil phase; [TSC]<sub>o</sub>: [Cu(dNBpy)<sub>2</sub>Br]<sub>o</sub>: [MMA] : [PEGMA] = 1:1:38:16 (30 mol% PEGMA). 154

9	SEC chromatograms of P(MMA-co-PEGMA) prepared by suspension polymerization using 1% (w/w) PVP (top) and no suspension stabilizer (bottom); Samples taken at 1hr into suspension polymerization; Oil:Water = 1:2; 25 wt% monomer loading in oil phase; [TSC] <sub>o</sub> : [Cu(dNBpy) <sub>2</sub> Br] <sub>o</sub> : [MMA] : [PEGMA] = 1:1:38:16 (30 mol% PEGMA) at 70 °C.	158
10	Molecular weight profiles of suspension polymerization of P(MMA-co-PEGMA) at 70 °C; Oil:Water = 1:2; 25 wt% monomer in oil phase; [TSC] <sub>o</sub> : [Cu(dNBpy) <sub>2</sub> Br] <sub>o</sub> : [MMA] : [PEGMA] = 1:1:90:10.4; 1:1:60:14; 1:1:38:16 (10, 19, and 30mol% PEGMA); PEGMA-30-PVP done with 1% (w/w) PVP in water phase of suspension.	159
11	Polydispersity profiles of suspension polymerization of P(MMA-co-PEGMA); conditions as in Figure 10.	160
12	Kinetics of suspension polymerization of P(MMA-co-PEGMA); conditions as in Figure 10.	161
13	Conversion profiles of suspension polymerization of P(MMA-co-PEGMA); conditions as in Figure 10. Errors in conversion measurements in the 10, 19 and 30 mol%	162

PEGMA copolymerization are similar to those shown for the PEGMA-30-PVP experiment but have been omitted for clarity.

- 14                      Optical micrographs (500 ×) of suspension polymer particles                      166  
prepared by ATRP at 70 °C using an oil:water ratio of 1:2  
with 1% (w/w) PVA in the water phase, 17 mol% cross-  
linker (DEGDMA) and A. 13 mol% PEGMA, B. 17 mol%  
PEGMA and C. 24 mol% PEGMA; Image A was acquired  
using reflected light only, while B and C were acquired using  
both reflected and transmitted light.
- 15                      Transmission electron micrographs of suspension polymer                      167  
particles prepared by convention radical polymerization (A,  
B, C and D) and ATRP (E, F, G and H) at 70 °C using DPE  
oil phase, oil:water = 1:2, and 17 mol% cross-linker  
(DEGDMA). In both series (A to D and E to H) the PEGMA  
concentration was increased incrementally (A,E = 8 mol%;  
B,F = 13 mol%; C,G = 17 mol%; D, H = 24 mol%).
- 16                      Transmission electron micrographs of suspension polymer                      168  
particles prepared by convention radical polymerization at 24  
mol% PEGMA (A) and ATRP at 17 (B) and 24 mol%  
PEGMA (C and D) at 70 °C using DPE oil phase, oil:water =

1:2, and 17 mol% cross-linker (DEGDMA).

17                      Environmental scanning electron micrographs of suspension                      170  
polymer particles prepared by conventional free radical  
polymerization at 24 mol% PEGMA (A and D) and ATRP at  
17 (B and E) and 24 mol% PEGMA (C and F) at 70 °C using  
DPE oil phase, oil:water = 1:2, and 17 mol% cross-linker  
(DEGDMA). The scale bar is 50 microns in micrographs A,  
B, C and F, and 35 and 15 microns in D and E, respectively.

**List of Abbreviations used in Thesis.**

<u>Term</u>	<u>Abbreviation used in Thesis</u>
Atom Transfer Radical Polymerization	ATRP
Bipyridine	Bpy
Butyl Acrylate	BA
Conventional Free Radical Polymerization	CFRP
Copper (I) Bromide	Cu(I)Br
Diethylene glycol dimetharylate	DEGDMA
Dimethyl Acrylamide	DMAM
Dinonyl Bipyridine	dNBpy
Ethyl bromo <i>iso</i> -butyrate	EBiB
Methyl Acrylate	MA
Methyl Methacrylate	MMA
Pentamethyl diethylene triamine	PMDETA
Poly(ethylene glycol) methacrylate	PEGMA
Poly(ethylene glycol) monomethyl ether methacrylate	MPEGMA
Styrene	STY
Tosyl Chloride	TSC

## 1.0 Introduction

Microcapsules are defined as spherical particles in the 50 nanometer to 2 millimeter size range composed of a polymer matrix or wall that encapsulates an active component.<sup>1</sup> Reasons for microencapsulation include sustained or delayed release of the active component,<sup>2,3</sup> targeting of an active drug to specific locations within the body,<sup>4,5</sup> protection of the active components from the environment to impart prolonged stability,<sup>6,7</sup> separation of incompatible components,<sup>8</sup> masking taste,<sup>9</sup> or converting liquids and tacky solids into free-flowing powders.<sup>10</sup> As such, microencapsulation is employed in a diverse range of industries dealing with medicine, agriculture, electronics, adhesives, detergents, perfumes and fragrances, as well as the printing and toner industries. Choice of the size of the microcapsules employed depends on the requirements of the application. For instance, high resolution electronic inks and drug delivery applications require nanometer size capsules, while micron sized capsules are suitable for most other applications.

Polymer microcapsules are often prepared by dispersing the active ingredient along with polymer or polymer precursors in the form of micron sized droplets in a second immiscible phase. This is followed by chemically or physically induced polymer precipitation at the interface causing the active ingredient/component to become engulfed within a polymer wall. The chemical and physical properties of the wall forming polymer are controlled through the choice of monomers and this in turn determines the encapsulation technique employed. If polymers based on vinyl monomers are desired, *in situ* suspension or emulsion polymerization is used for encapsulation. Alternatively,

preformed natural or synthetic polymers can be employed using the suspension cross-linking, coacervation, or solvent extraction/evaporation techniques. On the other hand, interfacial polycondensation is used if condensation polymers are the preferred wall forming material. A brief introduction to these methods is presented in Section 1.1.1 below.

*In situ* suspension polymerization of vinyl monomers is an attractive encapsulation method as capsules form from monomeric starting materials in one step and because a wide range of wall properties are accessible through the diverse chemistries of vinyl monomers.<sup>11</sup> This technique typically involves droplets of an oil phase containing both the active ingredient and monomer(s) dispersed in an aqueous continuous phase. As polymerization proceeds, the growing polymer phase separates within the oil droplets giving an oil-polymer-water three phase system. Reservoir type core-shell capsules where a polymer shell completely engulfs the oily core form only if the lowest energy conformation of this three phase system is one where the polymer occupies the oil-water interface. In this system comprised of three immiscible phases the most stable configuration is one that minimizes the interfacial surface energy. As such, the polymer occupies the oil-water interface only if the oil-water interfacial tension is greater than the sum of the oil-polymer and polymer-water interfacial tensions.<sup>12</sup> That is, a capsular morphology forms provided that the polymer is more polar than the oil phase but less polar than the aqueous phase. Furthermore, experimental conditions must permit polymer forming in the oil droplets to diffuse to the oil-water interface. This kinetic requirement is met when the viscosity of the oil phase and molecular weight of the

polymer are low, enabling free and efficient diffusion of the polymer within the oil droplets.

Atom Transfer Radical Polymerization (ATRP) is a living/controlled radical polymerization technique<sup>13</sup> that has recently been applied to a wide range of vinyl monomers including (meth)acrylates, styrenic monomers, as well as acrylamides.<sup>14</sup> Like other living polymerization techniques, ATRP is characterized by fast initiation early in the polymerization and growth of all polymer chains at an equal rate until most of the monomer in the system is consumed. That is, polymer molecular weight increases linearly with conversion to form narrow disperse polymers whose final molecular weight is determined by the initial monomer to initiator ratio. In addition, as a radical polymerization ATRP is tolerant to water and other protic solvents and proceeds with desirably high rates at relatively low temperatures. As such, ATRP has been successfully extended to emulsion and suspension polymerization conditions.<sup>15</sup>

This research describes the preparation of crosslinked polymer capsules by *in situ* suspension Atom Transfer Radical Polymerization. The choice of a living polymerization is based on the following hypotheses. First, the slow linear increase of molecular weight with conversion in ATRP will help maintain low viscosity conditions in the oil droplets, minimizing diffusion limitations and yielding the thermodynamic morphology under a given set of encapsulation conditions. Secondly, the living nature of ATRP will allow synthesis of highly amphiphilic copolymers based on oil and water soluble comonomers in suspension conditions despite partitioning of the water soluble monomer into the water phase. As well, composite walled polymer capsules exhibiting a hydrophilic comonomer

rich outer surface may be accessible owing to the living nature of the initially formed inner capsule wall.

## 1.1 Polymer Capsules

### *1.1.1 Methods of polymer capsule preparation*

#### *a) Interfacial polycondensation*

Interfacial polycondensation involves the condensation polymerization of two complementary monomers each soluble in one phase of a two phase system usually comprised of an oil phase dispersed in an aqueous continuous phase.<sup>16</sup> The dispersed oil droplets serve as templates for the formation of polymer particles. Each monomer may partition to some extent in the phase where it is less soluble and consequently polycondensation begins where the product of the concentrations of the two monomers is highest. If the polymer formed at the interface is soluble in the oil droplets, it continues to grow within the droplets and solvent swollen microspheres or monolithic capsules are formed. An example is the formation of monolithic polycarbonate resin by interfacial reaction of bisphenol A [2,2'-bis-(4-hydroxylphenyl)-propane] dissolved in an alkaline aqueous phase with phosgene dissolved in dispersed chloroform droplets.<sup>16</sup> On the other hand, if the polymer formed at the interface is insoluble in the dispersed oil droplets, the initially formed oligomers grow until they become insoluble and precipitate at the interface giving a primary membrane around the droplets. This capsule wall usually thickens by diffusion of one or both monomers across the primary membrane. An example is the formation of polyamide capsules by interfacial reaction of hexamethylene diamine (HDA) dissolved in a dispersed alkaline water phase and sebacyl chloride

(SBC) dissolved in a continuous oil phase usually comprised of a 4:1 mixture of cyclohexane and chloroform. Initial reaction and membrane growth occurs predominantly on the oil side of the interface because HDA partitions into the oil phase but the solubility of SBC in water is negligible.<sup>16</sup>

*b) Coacervation*

Coacervation is the partial desolvation of dissolved polymer and results in the formation of a polymer-rich coacervate phase and a polymer-lean coacervation medium.<sup>17</sup> The coacervate phase is characterized by diminished polymer-solvent interactions and enhanced polymer-polymer interaction relative to a polymer solution, however unlike a polymer precipitate, the coacervate phase is highly solvated, typically containing > 80% solvent by weight. In aqueous medium, the process is referred to as simple coacervation if a solution of a single polymer desolvates triggered by changes in the properties of the solvent. For example, addition of ethanol to an aqueous gelatin solution induces coacervation as water molecules leave the hydration sphere of gelatin molecules to partake in the more favorable interaction with ethanol molecules.<sup>18</sup> Desolvation may also be triggered by enhanced polymer-polymer interactions upon mixing aqueous solutions of oppositely charged polyelectrolytes in a process known as complex coacervation. An example is the coacervation of positively charged acid-processed gelatin with a negatively charged carboxyl bearing polymer such as gum arabic.<sup>17</sup> Polymer coacervates appear initially as microscopic droplets (or coacervate nuclei), which in the absence of stabilizer and stirring, coalesce to larger droplets and eventually form a macroscopic coacervate phase. In encapsulation, the core

droplets/particles are dispersed (by stirring) in the coacervation medium and are gradually coated by newly formed coacervate nuclei. Subsequent hardening of the coacervate “wall” by either cross-linking (e.g., using glutaraldehyde in the gelatin-gum arabic system)<sup>19</sup> or solvent removal, gives stable capsules.

*c) Suspension Cross-linking*

In this technique, droplets of a solution of natural or preformed synthetic polymer containing the material to be encapsulated (active component) are dispersed in a continuous phase and gradual crosslinking induced precipitation of the polymer gives the desired polymer capsules.<sup>20</sup> For efficient encapsulation, it is critical that the active component has substantially greater affinity for the dispersed phase than the continuous phase. Upon cross-linking the viscosity of the dispersed phase droplets increases and breaking up of coalesced droplets becomes increasingly difficult by shearing. In the absence of a suspension stabilizer this leads to increase of droplet size and finally coagulation. Thus, to avoid coagulation a suspension stabilizer is added which forms a thin film around the dispersed droplets and prevents their coalescence. An ideal stabilizer is usually a polymeric or oligomeric substance that is insoluble in the droplet phase and has a low solubility in the suspension medium. Examples are poly(*N*-vinyl pyrrolidone) for oil in water suspensions and cellulose acetate for water in oil suspensions. As well, formation of a stable suspension prior to crosslinking is important to form discrete polymer particles (rather than aggregates of primary particles). This is accomplished by either making the suspension at low temperature to lower the rate of crosslinking or by addition of the crosslinking agent after a stable suspension has formed.

Protein microcapsules containing encapsulated drugs are prepared by both thermal and chemical cross-linking. Stirring an aqueous albumin solution (containing various drugs) in isooctane in the presence of a sorbitan trioleate stabilizer gives a stable water in oil suspension and subsequently raising the temperature to 50 - 85 °C effects thermal cross-linking to yield albumin microcapsules.<sup>21</sup> As well, hemoglobin microcapsules are prepared by stirring an aqueous gelatin solution in a chloroform/hexane (1:4) mixture and subsequent addition of terephthaloyl chloride cross-linker to the suspension. The hydrophobic nature of the cross-linker limits its reaction to the oil-water interface and core-shell (reservoir type) capsules are obtained.<sup>22</sup>

*d) Solvent extraction/evaporation*

In this approach, a solution of the wall forming polymer and material to be encapsulated is dispersed in a continuous phase and the solvent within the dispersed droplets is removed by either extraction or evaporation leading to polymer precipitation and yielding the desired microcapsules.<sup>23</sup> The removal of solvent from the polymer droplets is accompanied by a decrease in droplet volume (increase in interfacial surface area) and increase in the viscosity of the individual droplets. Both these changes tend to destabilize the suspension system. In particular, the highly viscous droplets coalesce much faster than they can redivide, driving the system towards coagulation which is prevented by the addition of suspension stabilizer that forms a thin film around the droplets and prevents their coalescence.

Cellulose microcapsules containing enzymes or whole cells are prepared by dissolving cellulose in a dimethylformamide (DMF) or dimethylsulfoxide (DMSO)

solution of *N*-ethylpyridinium chloride at 90 – 120 °C, mixing the cells or enzymes with the cooled cellulose solution and extrusion of the suspension in the form of droplets into a large volume of water.<sup>24</sup> Cellulose precipitation caused by extraction of the salt and organic solvent (DMF or DMSO) into the aqueous phase leads to entrapment of the cells/enzymes within cellulose particles. Like routine polymer precipitation by addition of a large volume of precipitant, the outward diffusion of solvent from the polymer droplets continues until all or most of it is removed during a relatively short period ( less than 10 -15 minutes). On the other hand, in solvent evaporation, the solvent is immiscible with the suspension medium, thus the medium is quickly saturated with the solvent. Consequently, solvent diffusion is driven by its gradual removal from the continuous phase by evaporation. Norethisterone, a synthetic hormone, was encapsulated in poly(lactide-*co*-glycolide) by suspending a dichloromethane solution of hormone and copolymer in water and applying reduced pressure to accelerate dichloromethane evaporation.<sup>25</sup>

#### *e) In situ polymerization*

Preparation of polymer capsules by *in situ* radical polymerization of vinyl monomers using a living polymerization technique is the subject of this research. As such, a detailed account of the *in situ* polymerization technique is presented in Sections 1.1.2 and 1.1.3 below.

##### *1.1.2 Controlling factors in encapsulation by in situ radical polymerization*

In the *in situ* radical polymerization method, the system initially consists of two immiscible phases, i.e., the dispersed monomer and solvent “combined” oil phase and the

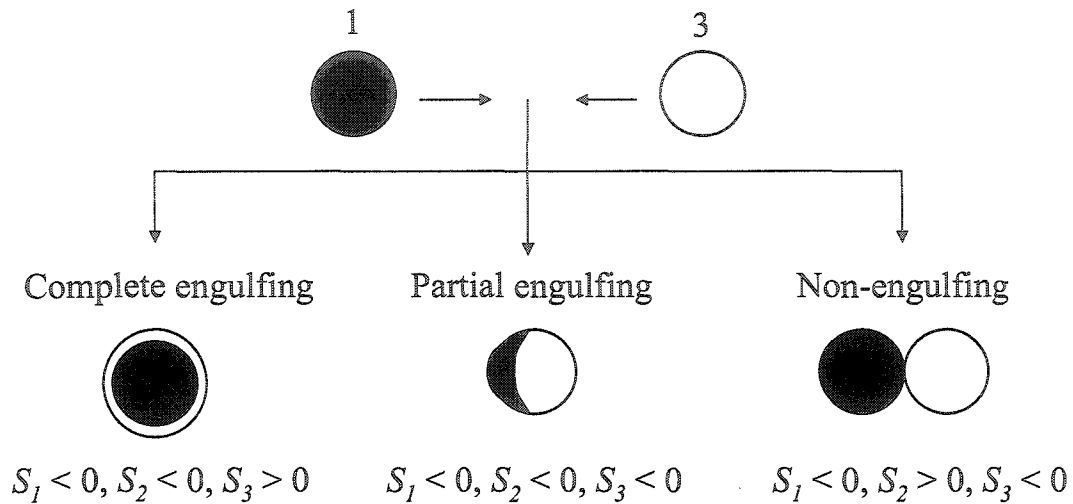
aqueous continuous phase. The solvent is chosen to be miscible with the monomer but to be a non-solvent for the polymer. Thus, upon initiation of polymerization, polymer forms in a mixture of non-solvent (usually a hydrocarbon such as hexadecane) and good solvent (usually the monomer serves as the good solvent in the binary mixture). Above a critical molecular weight and conversion, the polymer becomes immiscible in the oil droplets and begins to phase separate. At this point, the system consists of three mutually immiscible phases and the morphology of the resulting polymer particles is dictated by thermodynamic and kinetic considerations as described below.

*a) Thermodynamic considerations.*

Torza and Mason<sup>12</sup> pioneered a theory for predicting the equilibrium configuration of two immiscible liquid droplets, designated as phase 1 and phase 3, suspended in a third immiscible liquid, designated as phase 2. For simplicity it was assumed that the final equilibrium state is defined solely by the three interfacial tensions,  $\gamma_{12}$ ,  $\gamma_{13}$ , and  $\gamma_{23}$ .

$$S_i = \gamma_{jk} - (\gamma_{ij} + \gamma_{ik}) \dots \dots \dots (1)$$

Defining spreading coefficients,  $S_i$ , by equation (1), where the suffixes  $i$ ,  $j$ , and  $k$  represent the three immiscible phases, for the premise that  $\gamma_{12} > \gamma_{23}$ , it follows that  $S_1 < 0$ . Inspection of equation (1) shows that there are only three possible sets of values of  $S_i$ , corresponding to the three different equilibrium configurations illustrated in Scheme (1). These are, (a) complete engulfing, (b) partial engulfing and (c) non-engulfing.



Scheme 1. Possible equilibrium configurations corresponding to the three sets of relations for  $S_j$ . The medium is phase 2.

Thus, if  $\gamma_{12} > \gamma_{23}$  ( $S_1 < 0$ ), then phase 1 is completely engulfed by phase 3 when  $S_2 < 0$  and  $S_3 > 0$ , no engulfing occurs when  $S_2 > 0$  and  $S_3 < 0$ , and  $S_1, S_2, S_3 < 0$ , leads to partial engulfing and formation of two phase droplets with three interfaces.

Along these lines, Sundberg et al.<sup>26</sup> developed a model based on the Gibbs free energy change of the process of morphology development when mutually immiscible oil, polymer and water phases are brought together. They showed that the Gibbs free energy change per unit area for the process leading to core-shell morphology (with polymer phase completely engulfing the oil phase) is given by equation 2:

$$\Delta G = \gamma_{op} + \gamma_{pw}(1 - \phi_p)^{-2/3} - \gamma_{ow} \dots (2)$$

$$\text{Limit } \phi_p \rightarrow 0,$$

$$\Delta G = (\gamma_{op} + \gamma_{pw}) - \gamma_{ow} \dots (3)$$

where  $\gamma_{op}$ ,  $\gamma_{pw}$ , and  $\gamma_{ow}$ , are the oil-polymer, polymer-water, and oil-water interfacial tensions and  $\phi_p$  is the volume fraction of the polymer (in the polymer plus oil “combined” phase). In the limit as  $\phi_p$  tends to zero, equation (2) reduces to equation (3). Thus, when  $\gamma_{ow} > (\gamma_{op} + \gamma_{pw})$ , the core-shell morphology with the core oil being engulfed by the polymer is the thermodynamically favorable morphology.

*b) Kinetic considerations.*

Morphology predictions based on thermodynamics assume that the system in question is capable of attaining the thermodynamically stable equilibrium configuration within the time frame of the experiment. Consequently, such predictions are valid when viscosities of the three phases are low, allowing efficient diffusional transport and yielding the most stable morphology. In encapsulation by *in situ* polymerization, the viscosity of the oil phase is proportional to the concentration and molecular weight of the forming polymer. That is, the relative rates of initiation/propagation and diffusion become critical to the development of the equilibrium morphology. The essential question is whether or not a primary radical or short chain oligomer is able to diffuse throughout the oil droplet before it has grown to a chain length that virtually immobilizes it. An accurate description of diffusivity versus polymerization kinetics is quite complicated. However, Klumperman *et al.*<sup>27</sup> proposed using the Damköhler number ( $D_a$ ) to assess whether a given system is diffusion controlled.  $D_a$  is defined as follows:

$$D_a = \frac{k_p[M]d^2}{D} \dots(4)$$

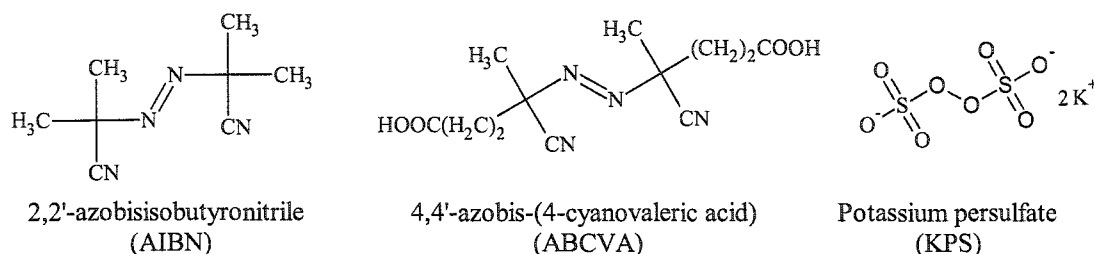
where  $D$  is the diffusion coefficient of a low molar mass species in a semi-dilute polymer solution,  $k_p$  is the propagation rate constant of a growing radical (or initiation rate constant of a primary radical),  $[M]$  is the monomer concentration at the locus of polymerization, and  $d$  is the relevant diffusion distance.  $D_a$  values below 1 are indicative of a system without transport limitations. Equation (4) shows that high rates of polymerization ( $k_p[M]$ ) and large diffusional distances ( $d$ ) drive the system towards diffusion control while low viscosity (high  $D$ ) of the medium removes transport limitations.

### ***1.1.3 Morphology of polymer particles prepared by in situ radical polymerization***

Polymer particles are prepared by the *in situ* radical polymerization technique using both “seeded” and “non-seeded” suspension/emulsion polymerization. In the seeded process, preformed mono-disperse latex seed particles prepared by conventional emulsion polymerization are suspended in an aqueous continuous phase and swollen by a second (different) monomer. Upon polymerization of the second monomer within the seed particles, the forming polymer phase separates from the seed polymer giving composite polymer particles. In the non-seeded process, polymerization occurs within oil droplets (of an aqueous emulsion/suspension) that are initially comprised of monomer and a solvent (usually a hydrocarbon) that is miscible with monomer but immiscible with the polymer. Upon polymerization, forming polymer phase separates within the oil droplets. In both seeded and non-seeded conditions, the final morphology of the polymer particles is governed by both kinetic and thermodynamic factors as discussed below.

a) *Seeded emulsion systems.*

In the polymerization of styrene in poly(methyl methacrylate) (PMMA) seeds, the formed poly(styrene) (PS) was completely engulfed by the PMMA seed polymer yielding the thermodynamically favored “inverted core-shell” morphology only when oil soluble initiator 2,2'-azobisisobutyronitrile (AIBN) or hydrophobic water soluble initiator 4,4'-azobis-(4-cyanovaleric acid) (ABCVA) (scheme 2 for structures) were used.<sup>28</sup>



Scheme 2. Structures of AIBN, ABCVA and KPS.

The experiments were conducted by a batch process using high swelling ratios (styrene: PMMA = 3:1) to ensure low viscosity at the locus of polymerization. Using AIBN, PS nucleation occurs within the swollen seed particles and the PS and PMMA domains are able to diffuse freely and attain the thermodynamically stable morphology wherein the more polar PMMA completely engulfs less polar PS. With ABCVA initiation, water phase initiation is followed by diffusion of the PS oligomers into the PMMA seeds and subsequent polymerization induced phase separation in low viscosity conditions yields the thermodynamic morphology. In contrast, when the water soluble potassium persulfate (KPS) initiator is used, morphology depends on the initiator

concentration. At low [KPS], PMMA completely engulfs PS, while upon increasing [KPS], the PMMA is sandwiched between two PS lobes. At even higher [KPS], PS engulfs the PMMA (core-shell) although phase separation between the PMMA and PS domains is incomplete with some PMMA remaining un-engulfed by PS and consequently, a rough “raspberry like” particle surface was observed. This core-shell morphology (PMMA core - PS shell) may be the combined result of lowered mobility of the PS chains due to anchoring at the interface (i.e. kinetic control) and the diminished difference between interfacial tensions between emulsion polymerized PS-styrene and water and that between emulsion polymerized PMMA-styrene and water (the latter is only slightly lower). Increasing chain mobility by addition of toluene or chain transfer agent (to lower polymer molecular weight), led to core-shell (PS shell - PMMA core) particles characterized by more complete phase separation between PS and PMMA domains and smooth particle surfaces.

In the polymerization of MMA in PS seeds at 70 °C using AIBN initiator in a batch process and low swelling ratios (MMA: PS = 1:1 and 1:2), the product consisted of a mixture of the thermodynamically favored half moon particles as well as the higher interfacial energy sandwich particles (PS sandwiched between PMMA domains).<sup>29</sup> Upon swelling the particles with toluene in a post polymerization step, all particles exhibited the thermodynamic morphology. This indicates that swelling with toluene decreases the diffusional resistance, enhancing polymer chain mobility so that the thermodynamically more favorable morphology can be achieved.

The dependence of morphology on the mobility of polymer chains at the locus of polymerization was further illustrated in the polymerization of styrene in PMMA seeds at 60 °C with *t*-butyl hydroperoxide or KPS initiation by batch and slow addition methods using a low swelling ratio of styrene: PMMA = 1:1.<sup>30</sup> In the slow addition experiments, viscosity was high due to the low monomer concentration in the seed particles. Consequently, the non-equilibrium core-shell morphology with PS engulfing the PMMA core resulted with either initiator. Addition of chain transfer agent led to penetration of the PS domains into the PMMA core reflecting the higher mobility of the lower molar mass polymers. Similarly interpenetration of PS and PMMA domains was observed in the batch experiments due to the relatively lower viscosity and the resulting higher mobility of the polymers. This illustrates that enhanced mobility drives the system towards the thermodynamically favored inverted core-shell (PS core - PMMA shell) morphology.

*b) Non-seeded emulsion/suspension systems.*

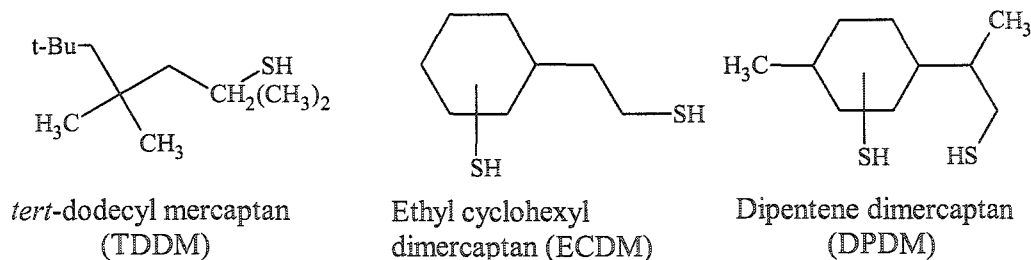
Sundberg *et al.* tested their model for morphology prediction, based on minimization of Gibb's free energy for the process of morphology development, using the *in situ* suspension polymerization of MMA.<sup>11</sup> Suspension polymerizations were conducted at 60 – 80 °C using decane or hexadecane and MMA as oil phase (MMA : hydrocarbon = 50:50 to 90:10 by wt.) and a series of emulsifiers (polymeric stabilizers e.g., pectin (PCT), poly(acrylic acid) (PAA) and carboxymethyl cellulose (CMC), and surfactants e.g., phosphatidyl choline (PC) and sodium dioctylsulfosuccinate (SDOS)) to modify the oil-water ( $\gamma_{ow}$ ) and polymer-water ( $\gamma_{pw}$ ) interfacial tensions at a constant oil-

polymer interfacial tension ( $\gamma_{op}$ ). Under optimized conditions using oil soluble initiators, capsular particles with PMMA completely engulfing hydrocarbon droplets were obtained provided that  $\gamma_{ow} > \gamma_{op} + \gamma_{pw}$  (observed with PCT, PAA and CMC). Moreover, when the inequality was reversed ( $\gamma_{ow} < \gamma_{op} + \gamma_{pw}$ ) (using PC and SDOS), half moon particles formed as predicted, indicating that the system is under thermodynamic control. In contrast, using water soluble initiators solid polymer particles with no encapsulated oil formed, indicating that the oligomers formed in the water phase are not trapped by the suspended oil droplets which merely serve as MMA reservoirs.

Morphology development of polymer particles prepared by *in situ* polymerization can be mimicked by dissolving preformed polymer in a binary mixture of a volatile solvent and a high boiling non-solvent for polymer followed by precipitation of the polymer in the oil phase upon removal of the solvent by evaporation. Sundberg *et al.* used an aqueous suspension of PMMA dissolved in a mixture of methylene chloride (volatile solvent) and decane (high boiling non-solvent), stabilized by sodium lauryl sulfate as emulsifier, to monitor the morphology of the oil droplets by optical microscopy.<sup>31</sup> PMMA precipitates in the oil droplets as methylene chloride diffuses out of the droplets into the aqueous phase and evaporates at the edge of the microscope slide. Thus, from the edge to the center of the slide, particles in different stages of morphology development were photographed simultaneously illustrating that “acorns” (one polymer zone on the periphery of a droplet) and “sandwiches” (two polymer zones somewhat surrounding a central oil zone) are precursors to capsular particles. Furthermore, a large number of the non-equilibrium “acorns” and “sandwiches” persisted after all methylene

chloride had evaporated indicating that very rapid removal of methylene chloride results in kinetic control.

In a significant contribution, McDonald *et al.*<sup>32</sup> reported that the encapsulation of *iso*-octane by emulsion polymerization of styrene using water soluble ammonium or sodium persulfate initiator was observed provided low molecular weight polymer is formed in the early stages of the process. Both seeded (using a high seed (styrene + *iso*-octane) : PS = 2000:1 ratio) and non-seeded conditions in a semi-batch process were employed with addition of a water miscible alcohol (methanol) to the aqueous phase. The process consisted of emulsion copolymerization of styrene with a small amount of methacrylic acid (MA) (styrene: MA = 28:1 by wt.) by slow addition of a stream of aqueous initiator solution in the presence of a chain transfer agent (shown in scheme 3).



Scheme 3. Structures of some chain transfer agents.

At low instantaneous conversion (20 – 40 %), a second stream containing a mixture of styrene, divinylbenzene-80, and MA (60:10:0.5 by wt.) was introduced. The initially formed low molecular weight polymer forms an interfacial polymer rich phase around the hydrocarbon/monomer droplets which then serves as the locus of further

polymerization and crosslinking yielding stable polymer shells. If instantaneous conversion is high (> 40%) when the crosslinker stream is added, microdomain capsules with polymer filling the entire particle are formed possibly due to the high viscosity of the oil phase that hinders diffusion of the polymer to the interface.

The molecular weight of the initial stage polymer decreased with increasing amounts of chain transfer agent, initiator, and alcohol present in the aqueous phase. Formation of capsular particles with complete encapsulation is maximized when the molecular weight of the initially formed polymer is low (typically 8000 Da) and increases over the course of polymerization, as is the case with dimercaptans. Formation of high molar mass polymer (> 100,000 Da) in the initial stage led to solid polymer particles with no hydrocarbon encapsulation. This suggests that the high mobility and better solubility in hydrocarbon of low molecular weight polymer favors its retention within the hydrocarbon droplets as well as the formation of a polymer rich phase at the oil-water interface.

In the absence of water miscible alcohol in the aqueous phase, encapsulation is limited, and the polymerization is similar to a traditional emulsion polymerization with the hydrocarbon layered on the surface of the particle. The alcohol played a crucial role by increasing the solubility of the hydrocarbon and monomer in the aqueous phase, lowering polymer molecular weight, oil-water and polymer-water interfacial tensions, and slowing down the polymerization kinetics.

Recently, the miniemulsion technique was used to prepare capsular polymer particles in the nanometer size range.<sup>12,33,34</sup> Miniemulsions are aqueous dispersions of

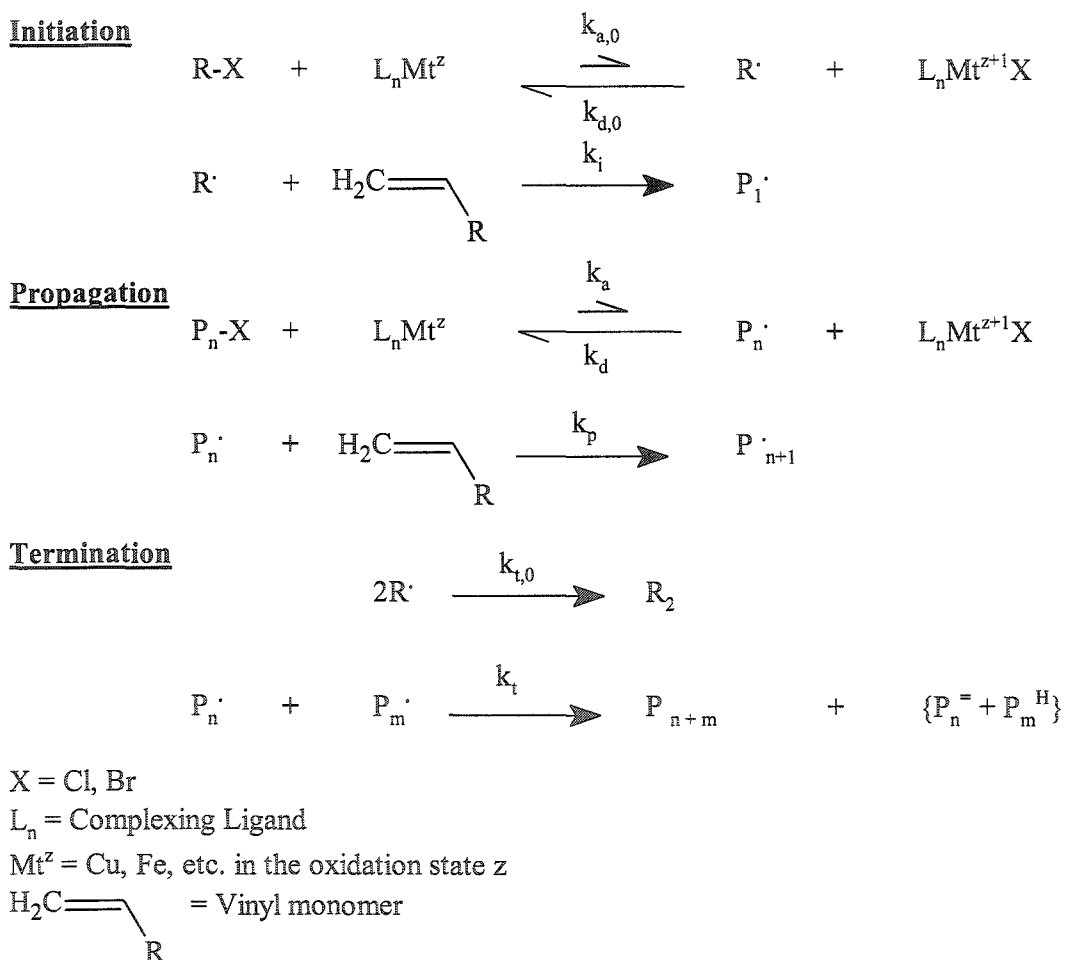
relatively stable 50-500 nm sized oil droplets prepared by shearing (usually by ultrasonication) a system containing oil (e.g., a water-insoluble monomer), water, a surfactant, and a highly water-insoluble compound (hydrophobe) to suppress Ostward ripening of the droplets. In miniemulsions, the final particle morphology is governed by the same thermodynamic and kinetic factors described above for emulsion and suspension polymerizations. The miniemulsion polymerization of butyl acrylate (BA) in hexadecane (HD) (BA:HD = 1:1) stabilized by sodium dodecylsulfate and initiated by oil soluble AIBN yielded the thermodynamically favored microdomain morphology with polymer filling the entire oil droplet.<sup>12</sup> In contrast, KPS initiation yielded core-shell particles with poly(BA) engulfing the HD core. This indicates that the charged sulfate end groups anchor the poly(BA) oligomers entering the oil droplets from the water phase onto the interface. Reduced polymer mobility hinders diffusion giving a kinetic core-shell morphology.

Analysis of the results reported above indicates that hollow capsular particles may be prepared by the *in situ* polymerization technique using experimental conditions that favor the capsular morphology by simultaneously effecting the kinetics and thermodynamics of the process of encapsulation. Appendix 1 provides a summary of the various techniques that the most prominent researchers working in this area have used.

## 1.2 Atom Transfer Radical Polymerization (ATRP)

The mechanistic aspects of ATRP in solution conditions are described in sections 1.2.1 to 1.2.5 below. While a basic understanding of the mechanism of ATRP presented

in sections 1.2.1 and 1.2.2 is necessary for an appreciation of the results of this work, detailed mechanistic discussion presented in sections 1.2.3 to 1.2.5 is meant to provide a basis for future work in the area of ATRP. An account of ATRP in heterogeneous suspension/emulsion polymerization conditions is presented in section 1.2.6.



Scheme 4. Mechanism of Atom Transfer Radical Polymerization.

### 1.2.1 ATRP Mechanism

Pioneered by Matyjaszewski *et al.*, ATRP is a recently developed living free radical polymerization technique.<sup>35</sup> The requirements for obtaining a living polymerization include fast initiation and polymer chain growth without irreversible chain transfer and chain termination.<sup>36</sup> In ATRP, initiator radicals are formed by a fast atom transfer redox reaction between an alkyl halide and a transition metal complex involving reduction of the alkyl halide to a free radical and one electron oxidation of the transition metal (represented by the rate constant of activation,  $k_{a,0}$ , Scheme 4).<sup>37</sup> The formed radicals undergo one of the following three reactions:

1. They can terminate ( $k_{t,0}$ ) by recombination or disproportionation. Recombination involves coupling of two radicals yielding a sigma bond between the two reacting radical centers. On the other hand, disproportionation involves abstraction (by one radical) of a hydrogen atom alpha to the second radical center, thereby generating a sigma and a pi-bond.
2. They can abstract a halogen atom from the oxidized form of the transition metal complex and convert to the dormant alkyl halide in a deactivation process ( $k_{d,0}$ ).
3. They can react with monomer, i.e. propagation ( $k_p$ ).

In addition to propagation, the polymeric radicals either terminate ( $k_t$ ) or deactivate by halogen abstraction from the oxidized form of the transition metal complex ( $k_d$ ) yielding a halogen capped dormant species. The dormant species is then reactivated by reaction with the reduced form of the transition metal complex ( $k_a$ ). Thus, polymerization

progresses by repeated activation, propagation and deactivation cycles. A living polymerization results if the following conditions are met:

1.  $k_{a,0} > k_p$ , i.e., initiation is fast relative to propagation. This ensures that all polymer chains are initiated early in the polymerization.
2. Both  $k_a$  and  $k_d$  are large, so activation/deactivation cycles are frequent and all polymer chains have the same chance of growth.
3.  $k_d \gg k_a$ , i.e., the equilibrium constant  $K_{eq} = k_a/k_d$  is small, so that the majority of polymer chains are dormant and termination reaction rates ( $k_{t,0}[R\cdot]^2$  and  $k_t [P_n\cdot] [P_m\cdot]$ ) are minimal.

Thus, for a well-controlled ATR polymerization of a given monomer, the alkyl halide, metal centre and ligands must be chosen such that  $K_{eq}$  is small to ensure low equilibrium radical concentrations. In addition, radical concentrations in ATRP are further lowered by the "Persistent Radical Effect". In the atom transfer reaction between the initiator (R-X) and Cu(I) species ( $L_nM^{z+}$ ), a reactive organic radical (R $\cdot$ ) and a stable Cu(II) species ( $L_nM^{z+1}X$ ) are formed. If no Cu(II) species is present in the system when the polymerization is initiated, then deactivation ( $k_{da}[XCu(II)]$ ) is slow, and radicals couple leading to an increase in Cu(II) concentration. With each radical termination event, 2 equivalents of Cu(II) will form irreversibly. For example, in the ATRP of styrene initiated by 1-phenyl ethyl bromide (0.1 M) using copper (I) bromide / 2 (bipyridine) catalyst (0.1 M) at 110 °C,  $K_{eq} \sim 10^{-8}$ , and  $[R\cdot]_0 = (K_{eq} [R-X] [Cu(Bpy)_2Br])^{0.5} \sim 10^{-5}$  mol/L.<sup>38</sup> At this very high concentration, the radicals undergo rapid bimolecular termination which reduces their concentration to  $10^{-7}$  mol/L. The Cu(II) species

concentration simultaneously increases to  $\sim 10^{-4}$  mol/L. Consequently, irreversible radical termination ( $k_t [P_n^\bullet] [P_m^\bullet]$ ) is negligible at these low equilibrium radical concentrations.

### 1.2.2 Kinetics of Atom Transfer Radical Polymerization

The rate of polymerization in ATRP is given by equation (5) below<sup>39</sup> (using symbols of Scheme 1):

$$\text{Rate} = \frac{-d[M]}{dt} = k_p [M] [P_n^\bullet] \dots (5)$$

Assuming that radical termination events are negligible due to the persistent radical effect, and application of the steady state approximation to radical concentration gives:

$$\frac{-d[M]}{dt} = k_p [M] [P_n^\bullet] = k_p [M] \frac{k_a [P_n - X] [Cu(I)]}{k_d [XCu(II)]} \dots (6)$$

Integration and rearrangement of equation (6) gives the following kinetic expression (equation (7)) for ATRP, where  $k_{app}$  is the apparent rate constant of polymerization:

$$\text{Ln} \left( \frac{[M]_0}{[M]_t} \right) = \frac{k_p k_a [P_n X] [Cu(I)]}{k_d [XCu(II)]} t = k_{app} t \dots (7)$$

Thus, linear dependence of  $\text{Ln}[M]_0/[M]_t$  on time is indicative of constant radical concentration in the ATR polymerization. Also, the evolution of polydispersity with conversion in ATRP is given by equation (8)<sup>39</sup> below, where “ $p$ ” is conversion:

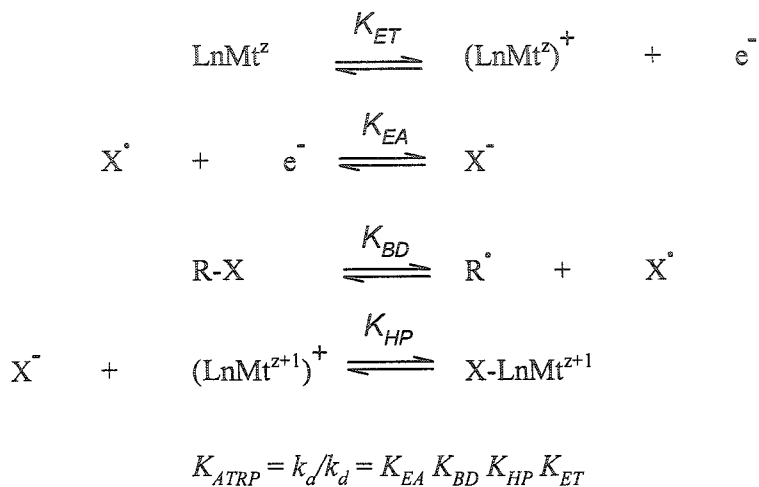
$$\frac{M_w}{M_n} = 1 + \left( \frac{k_p [P_n X]}{k_d [XCu(II)]} \right) \left( \frac{2}{p} - 1 \right) = 1 + \frac{2}{k_a [Cu(I)] t} \dots (8)$$

Equation (6) shows that the rate of polymerization is first order with respect to the monomer and the copper (I) concentrations ( $[M]$  and  $[Cu(I)]$ , respectively), and inverse first order with respect to copper (II) concentration ( $[XCu(II)]$ ). Not only does the rate of polymerization depend on the rate of propagation,  $k_p$ , which is specific for each monomer, but also on the rate constants of activation,  $k_a$ , and deactivation,  $k_d$ . A high value of  $k_a/k_d$  gives a high rate of polymerization.

Equation (8) shows that a narrow molecular weight distribution ( $M_w/M_n$ ) is obtained at higher conversion, higher  $k_d$  relative to  $k_p$ , higher concentration of deactivator ( $XCu(II)$ ), and higher molecular weights, i.e.,  $1/[P-X]$ . At the limit of a large  $k_a$  and small  $k_d$ , the desired high rate of polymerization is obtained, but ATRP simply becomes a conventional redox-initiated radical polymerization process resulting in a highly polydisperse polymer. Thus, the optimal ratio of  $k_a$  and  $k_d$  is critical to obtaining a well controlled ATR polymerization.

### *1.2.3 Parameters affecting the activation and deactivation rate constants ( $k_a$ and $k_d$ )*

The overall ATRP equilibrium may be expressed in terms of the four elementary reactions shown in Scheme 5. Thus, the ATRP equilibrium constant ( $K_{eq} = k_a/k_d$ ) can be expressed as the product of the equilibrium constants for electron transfer to the metal complex ( $K_{ET}$ ), electron affinity of the halogen ( $K_{EA}$ ), homolytic bond dissociation of the alkyl halide ( $K_{BD}$ ), and the heterolytic cleavage of the  $X-Mt^{n+1}$  bond or halogenophilicity ( $K_{HP}$ ).



Scheme 5. Elementary reactions in the ATRP equilibrium.

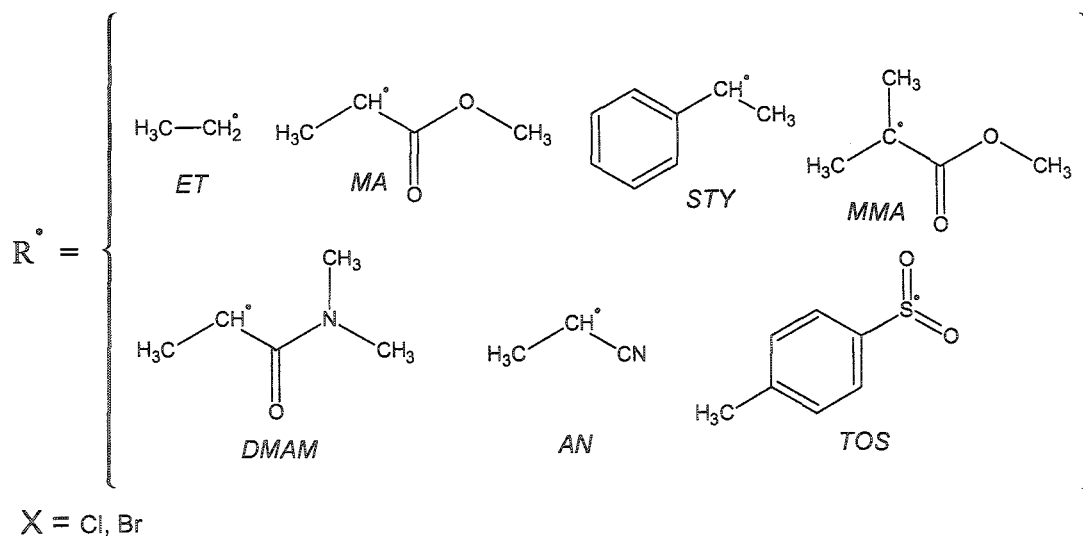
**Table 1. Calculated (DFT) and Experimental BDE's of some R-X systems (Ref. 5).**

R	$\Delta H_{298}^0$ / kcal mol <sup>-1</sup> for Cl (DFT)	BDE's / kcal mol <sup>-1</sup> for Cl (Exptl.)	$\Delta H_{298}^0$ / kcal mol <sup>-1</sup> for Br (DFT)	BDE's / kcal mol <sup>-1</sup> for Br (Exptl.)
<i>et</i>	83.1	84.2 ± 0.8	73.1	70.0 ± 1.0
<i>dmam</i>	72.5	-	64.8	-
<i>ma</i>	69.9	72.1 <sup>a</sup>	61.4	-
<i>sty</i>	68.5	-	59.9	-
<i>mma</i>	66.9	-	58.9	-
<i>an</i>	65.9	63.9 <sup>b</sup>	57.2	-
<i>tos</i>	55.2	-	53.1	55.3 ± 1

<sup>a</sup> For the related methyl-2-chloroacetate; <sup>b</sup> For the related 2-chloroethanenitrile.

$K_{BD}$  and  $K_{EA}$  are determined by the structure of the alkyl group and the identity of the halogen, and  $K_{ET}$  and  $K_{HP}$  are governed by the properties of the metal center and ligands that constitute the ATRP catalyst.

Currently, bond dissociation energy (BDE) data for the carbon-halogen bond of alkyl halides (R-X) that are structurally similar to dormant species derived from vinyl monomers commonly polymerized by ATRP are lacking in the literature.<sup>40</sup> Thus, Matyjaszewski *et al.* recently employed the density functional theory (DFT) approach to estimate BDE's for several R-X systems relevant to ATRP (Scheme 6).<sup>41</sup> Table 1 shows that the BDE values obtained by DFT calculations compare well with experimentally available data for related systems. For all R-groups, the BDE's of R-Cl are greater than those of R-Br systems and the BDE (R-Cl)/BDE (R-Br) ratio remains between 1.1 to 1.2. For both chloride and bromide series, variation of BDE's as a function of R-group follows the order ET > DMAM > MA > STY > MMA > AN > TOS (see scheme 6 for abbreviations used), as expected based on the stabilities of the formed radicals.



Scheme 6. Structures of alkyl radicals (R<sup>•</sup>) and halides (X) derived from ATRP initiators or representative of polymeric end groups in ATRP (except ET and AN).

According to scheme 5, for the same catalytic systems (metal center and ligand), bond dissociation energies of alkyl halides should correlate directly with atom transfer equilibrium constants. Thus, the relative values of  $K_{eq}$  obtained using DFT calculated BDE data<sup>a</sup> should correspond to experimental  $K_{eq}$  values of ATRP equilibria under the same conditions (solvent, temperature, ligands, etc.). Relative to *MA*, the experimentally obtained values of  $K_{eq}$  of ATRP systems at 363 K, followed the trend *MA*-Br (1) < *STY*-Br (20) < *MMA*-Br (300) < *AN*-Br (3000).

The corresponding relative values of  $K_{eq}$  calculated by DFT at 363 K are *MA*-Br (1) < *STY*-Br (6) < *MMA*-Br (30) < *AN*-Br (700), confirming the direct correlation between BDE's and ATRP equilibrium constants.

For a given alkyl halide (R-X), the ATRP equilibrium constant depends on the activity of the catalyst which in turn is determined by its redox potential ( $K_{ET}$ ) and its halogenophilicity ( $K_{HP}$ ) (Scheme 5). Thus, for transition metal complexes that have similar halogenophilicity (such as complexes of a given transition metal), the redox potential ( $E_{1/2}$ ) should correlate directly with  $K_{eq}$ . Use of  $E_{1/2}$  values as a measure of  $K_{ET}$  is strictly inappropriate because redox potentials usually provide information on outer sphere electron transfer between the metal complex and the selected electrode, while ATRP proceeds *via* an inner sphere electron transfer mechanism.<sup>42,43</sup> However, they provide a convenient means of studying the effect of ligand structure and halogen on the activity of ATRP catalysts.

---

<sup>a</sup>  $K_{eq}$  values were calculated from Gibbs free energy data obtained by combination of  $\Delta H$  (BDE) and  $T\Delta S$  values derived from DFT calculations at 363 K.

Matyjaszewski *et al.*<sup>44</sup> correlated the redox potentials of a number of Cu(I) complexes to the structure of several nitrogen based ligands and halides (Figure 1) and to the corresponding ATRP equilibrium constants. The  $E_{1/2}$  values of all copper (I) chloride complexes were lower (by  $\sim 100$  mV) than the corresponding copper (I) bromide complexes. That is, the chloride complexes are stronger reducing agents; thus consideration of  $K_{eq}$  values alone would lead to the conclusion that chloride complexes would give higher  $K_{eq}$  values and polymerization rates compared to the corresponding bromide complexes. However, due to the stronger C-Cl bonding compared to the C-Br bonding (which overcompensates Cu-Br versus Cu-Cl bonding), experimentally observed rates of ATRP using bromide complexes are higher than those using the corresponding chloride complexes.

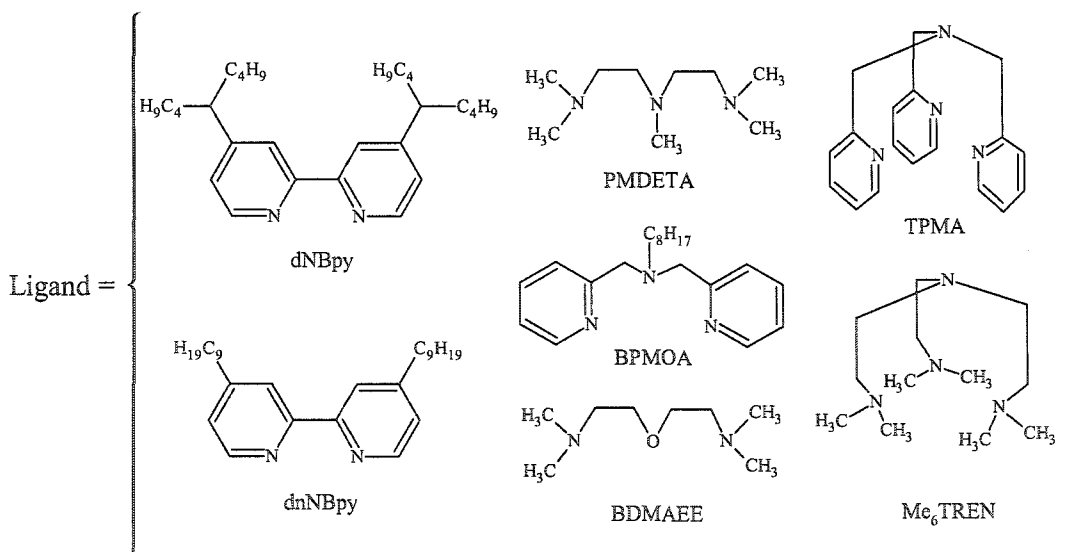


Figure 1. Structures of ligands and copper (I) halides.

The  $E_{1/2}$  values of both the Cu (I) chloride and bromide complexes followed the order Bpy > dNBpy or dnNBpy > BPMA > PMDETA > TPMA > Me<sub>6</sub>TREN, that is, Me<sub>6</sub>TREN and Bpy gave the strongest and weakest reducing catalysts, respectively. The  $E_{1/2}$  values may be correlated with the structure of the ligand in several ways. For example, reducing power increases with the number of N-atoms and binding efficiency (i.e. the Chelate effect): bidentate ligand < tridentate ligand < tripodal ligand. Also, the aliphatic amines which are more nucleophilic than aromatic amines better stabilize Cu(II) species: BPMA < PMDETA; TPMA < Me<sub>6</sub>TREN. As well, Cu(II) is a stronger Lewis acid than Cu(I) and will complex better with stronger nucleophiles (trialkyl amines vs. pyridines).

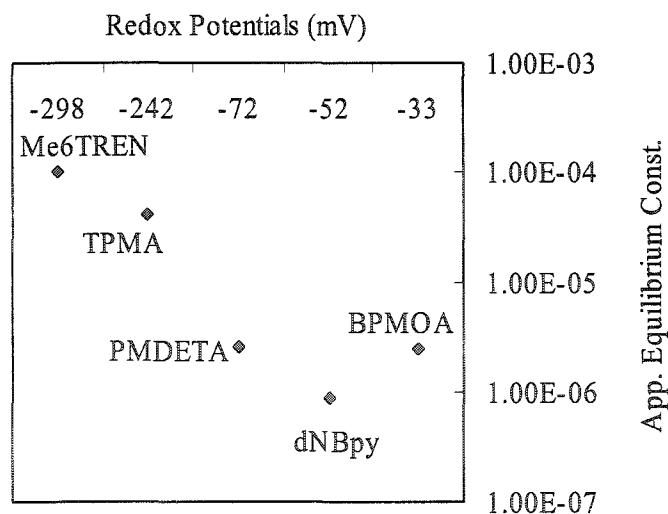


Figure 2. Correlation of  $E_{1/2}$  with  $K_{eq}^{app}$  for ATRP of methyl acrylate using several N-based ligands.

A linear correlation between the apparent ATRP equilibrium constant,  $K_{eq}^{app}$ , and the  $E_{1/2}$  values was found for a series of ligands in the bulk ATRP of methyl acrylate initiated by ethyl 2-bromopropionate at 50 °C (Figure 2). Thus, stronger reducing catalysts gave higher values of  $K_{eq}^{app}$ , and higher rates of ATR polymerization.  $K_{eq}^{app}$ , is defined in Equation 9.

$$K_{eq}^{app} = \frac{K_{eq}}{[Cu^{II}]} = \frac{d \ln([M]_0/[M]_t)}{dt \times k_p \times [Cu^I]_0 \times [I]_0} \dots (9)$$

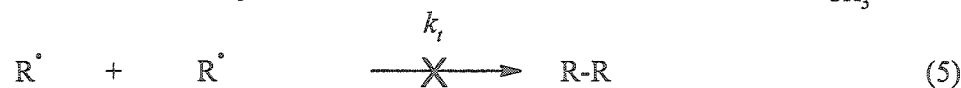
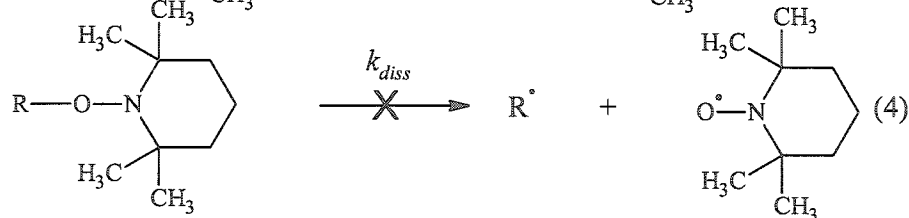
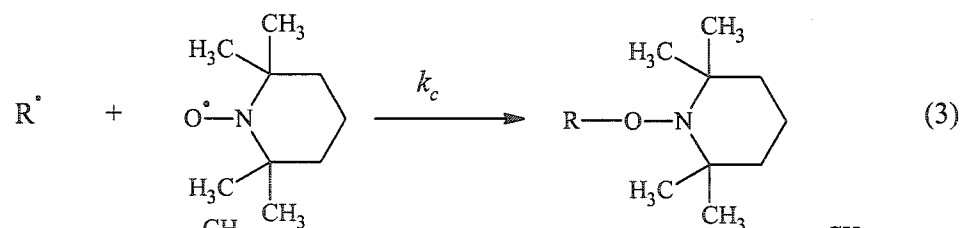
It is noteworthy that, in addition to  $K_{eq}$  and  $k_p$ , the rate of ATRP depends on the concentrations of the Cu(I) and Cu(II) species (Equation 6). Thus, a large value of  $K_{eq}$ , may generate a high concentration of radicals that rapidly terminate forming excess Cu(II), and the overall reaction is slower than that expected from the high  $K_{eq}$  value. For example, although the polymerization of methyl methacrylate (MMA) with dNBpy as ligand is much faster than that of styrene and methyl acrylate, the opposite was found with PMDETA as ligand, due to a much higher  $K_{eq}$  value, which leads to excessive termination resulting in low activator (Cu(I)) concentration as well as low solubility of the Cu(II)/PMDETA complex in the polymerization medium.<sup>45</sup>

#### *1.2.4 Measurement of the activation and deactivation rate constants ( $k_a$ and $k_d$ ) in ATRP.*

The successful ATRP of a particular monomer requires careful adjustment of the structures and concentrations of initiators, metals, ligands, halide atoms, solvents, as well reaction temperature. The overall rate of polymerization and the level of control during polymerization are governed by the choice of these variables through affecting  $k_a$  and  $k_d$ .

Thus, the measurement of the activation and deactivation rate constants for model systems as well as polymeric systems is necessary for better understanding of ATRP systems and further development.

The activation rate constants of alkyl halide initiators or oligomeric macroinitiators are typically measured by kinetic isolation of the activation process<sup>46</sup> (1) from the deactivation process (2) (Scheme 7) by (nearly quantitative) trapping (3) of the formed alkyl radicals using a large excess of a stable organic radical such as 2,2,6,6-tetramethylpiperidiny-1-oxy (TEMPO).



Scheme 7. Kinetic isolation of the activation process.

The deactivation process (2) is negligible under these conditions since  $k_d < k_c$  and  $[\text{Cu}^{\text{I}}\text{X}_2] < [\text{TEMPO}]$  and so is the thermal decomposition of the alkoxyamine<sup>47</sup> (4) at low reaction temperature (35 °C). Similarly, coupling of alkyl radicals (5) can be neglected due to the presence of a large excess of radical scavenger (TEMPO). Under these conditions, the rate of disappearance of the alkyl halide is given by equation (10):

$$-\frac{d[\text{R-X}]}{dt} = k_a[\text{R-X}][\text{Cu}^{\text{I}}\text{X}] \dots (10)$$

$$[\text{Cu}^{\text{I}}\text{X}]_t = [\text{Cu}^{\text{I}}\text{X}]_0 - ([\text{R-X}]_0 - [\text{R-X}]_t) \dots (11)$$

$$\ln\left(\frac{[\text{R-X}]_0}{[\text{R-X}]_t}\right) + \ln\left(\frac{[\text{Cu}^{\text{I}}\text{X}]_0 - [\text{R-X}]_0 - [\text{R-X}]_t}{[\text{Cu}^{\text{I}}\text{X}]_0}\right) = ([\text{Cu}^{\text{I}}\text{X}]_0 - [\text{R-X}]_0)k_a t \dots (12)$$

Since  $[\text{Cu}^{\text{I}}\text{X}]$  and  $[\text{R-X}]$  are related by equation (11), when  $[\text{R-X}]_0 \neq [\text{Cu}^{\text{I}}\text{X}]_0$ , solving equations (10) and (11) gives equation (12) where the subscripts 0 and  $t$  denote concentrations at times 0 and  $t$ , respectively.

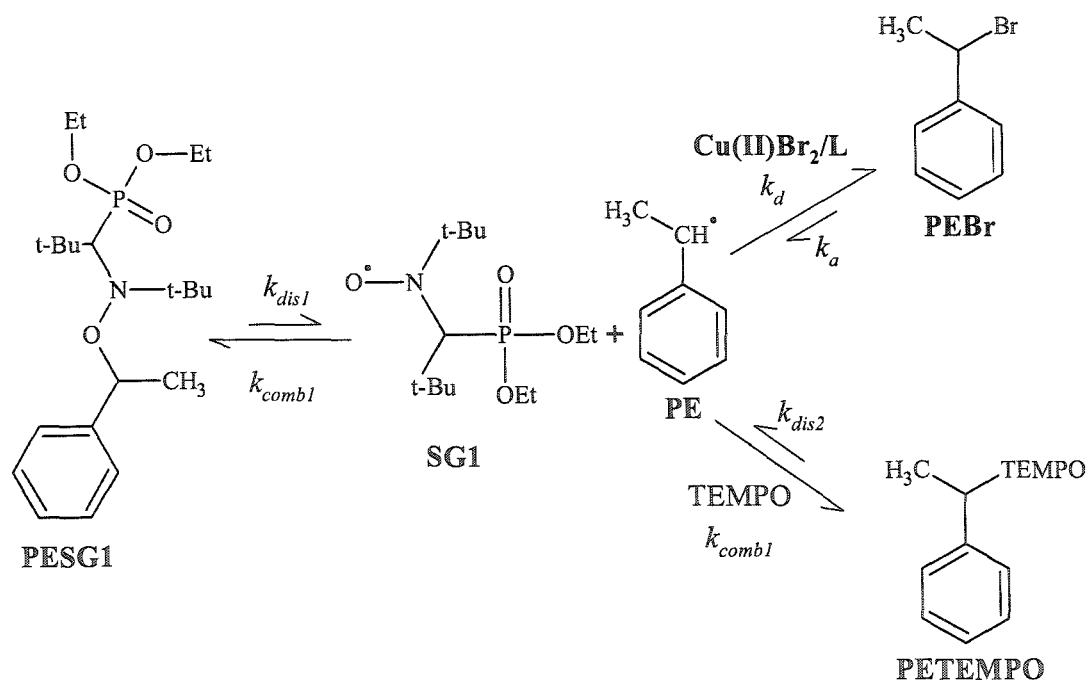
Monitoring  $[\text{R-X}]$  as a function of time (by HPLC, GPC, GC or NMR) and plotting the left hand side of equation (12) versus time gives a straight line whose slope corresponds to  $([\text{Cu}^{\text{I}}\text{X}]_0 - [\text{R-X}]_0)k_a$ . Alternatively, the kinetic analysis can be further simplified by using a large excess of  $[\text{Cu}^{\text{I}}\text{X}]$  (versus  $[\text{R-X}]$ ) so that equation (10) may be written as equation (13). In this case, an apparent rate constant of activation,  $k_{app}$ , is defined as the product of  $k_a$  and  $[\text{Cu}^{\text{I}}\text{X}]_0$  which solves to give equation (14):

$$-\frac{d[\text{R-X}]}{dt} = k_a[\text{R-X}][\text{Cu}^{\text{I}}\text{X}] \approx k_{app}[\text{R-X}] \dots (13)$$

$$\ln\left(\frac{[\text{R-X}]_0}{[\text{R-X}]_t}\right) = k_{app}t \dots (14)$$

Plotting equation (14) gives a straight line whose slope corresponds to the apparent rate constant of activation,  $k_{app}$ .

The deactivation rate constant of a common ATRP initiator (as well as model for poly(styrene) end group) may be determined by generating the phenyl ethyl (PE) radical *via* thermal dissociation of 1-(N,N-(2-methylpropyl-1)-(1-diethylphosphono-2,2-dimethylpropyl-1)-N-oxyl)-1-phenylethane (PESG1), and comparing its rate of deactivation by reaction with  $\text{Cu(II)Br}_2/\text{L}$ , with its rate of coupling with TEMPO



Scheme 8. Model reaction for measurement of deactivation rate constant of phenyl ethyl bromide.

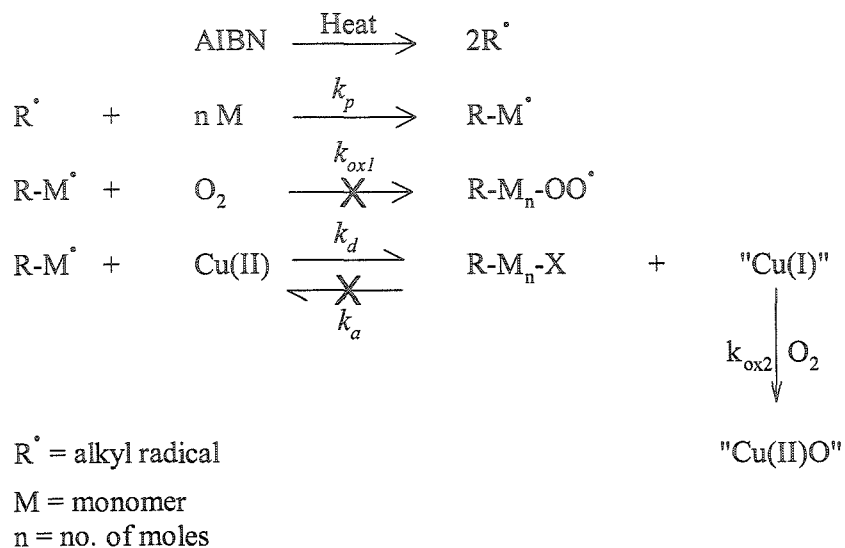
(Scheme 8).<sup>48</sup> Thus, by comparing the amounts of PEBr and PETEMPO formed, the deactivation rate constant ( $k_d$ ) is calculated relative to the combination rate constants ( $k_{comb2}$ ) (Equations 15, 16) available in the literature.<sup>49,50</sup>

$$\frac{d[PEBr]}{d[PETEMPO]} = \frac{k_d}{k_{comb2}} \frac{[Cu(II)Br_2/L][PE^*]}{[TEMPO][PE^*]} \dots (15)$$

$$k_d = k_{comb2} \frac{[TEMPO]}{[Cu(II)Br_2/L]} \frac{d[PEBr]}{d[PETEMPO]} \dots (16)$$

The nitroxide SG1 is chosen for this experiment because its large dissociation constant ( $k_{dis1} = 4.0 \times 10^{-5} \text{ M}^{-1}\text{s}^{-1}$ ) at a relatively low temperature (75°C) ensures sufficient generation of radicals without significant dissociation of PETEMPO ( $k_{dis2} = 2.8 \times 10^{-6} \text{ M}^{-1}\text{s}^{-1}$ ). As well, its smaller combination rate constant ( $k_{comb1} = 5.6 \times 10^6 \text{ M}^{-1}\text{s}^{-1}$ ) minimizes interference with the trapping reactions.<sup>51</sup>

A more general method for measurement of deactivation rate constants is based on the principle of reverse ATRP under homogeneous conditions (Scheme 9).<sup>52</sup> In this method, radicals formed by thermal decomposition of AIBN react with monomer (M) to yield polymeric radicals, until they are either deactivated by reaction with Cu(II) to give a dormant polymer chain and Cu(I) species, or are trapped by oxygen. Oxygen reacts preferentially with Cu(I) species, which are present in much higher concentrations than the active radicals, to form oxo, peroxy, or other stable Cu(II) complexes, which cannot reactivate the dormant polymer chains ( $k_{ox2}$ ).



Scheme 9. Pathway for deactivation rate constant measurement.

Under these conditions, at low conversion, the degree of polymerization ( $DP_n$ ) increases according to Equation (17):

$$\frac{1}{DP_n} = \frac{1}{DP_{n0}} + \frac{k_d[\text{Cu(II)}]_0}{k_p[\text{M}]_0} \dots (17)$$

Plotting  $1/DP_n$  versus  $[\text{Cu(II)}]_0$  gives a straight line whose slope corresponds to  $k_d/k_p [\text{M}]_0$ .

### ***1.2.5 Dependence of the activation and deactivation rate constants ( $k_a$ and $k_d$ ) in ATRP on initiator, copper halides, ligands, and polymerization solvent.***

In general, studies of ATRP systems using ATRP initiators as models for corresponding polymer chain end groups give  $k_a$  and  $k_d$  values that are in good agreement with those obtained using macroinitiators and from real ATR polymerizations.

a) Effect of alkyl halide on  $k_a$  and  $k_d$ .

The structure of the alkyl group as well as the identity of the halogen substituent govern the reactivity of the alkyl halide. The greater the stability of the alkyl radical that forms upon halogen transfer to the catalyst, the higher the  $k_a$  value and lower the  $k_d$  value. For example, in the Cu(I)Br/dNBpy system and acetonitrile solvent at 35 °C, the  $k_a$  value ( $M^{-1}s^{-1}$ ) of PEBr (0.085) > BzBr (0.043) and EBriB (0.60) > MBrP (0.052) (See Figure 3 for structures of alkyl halides).<sup>53</sup> Similarly, in the Cu(I)Br/PMDETA system and a number of solvent of differing polarity at 35 °C, the  $k_a$  values had relative magnitudes in the order EBriB (30) >> MBrP (3) > *t*-BBrP (1).<sup>43</sup> Since the rates of activation depend primarily on the stability of the formed radicals and steric effects, the 3-fold faster activation of MBrP relative to the bulkier *t*-BBrP (but having similar radical stability),

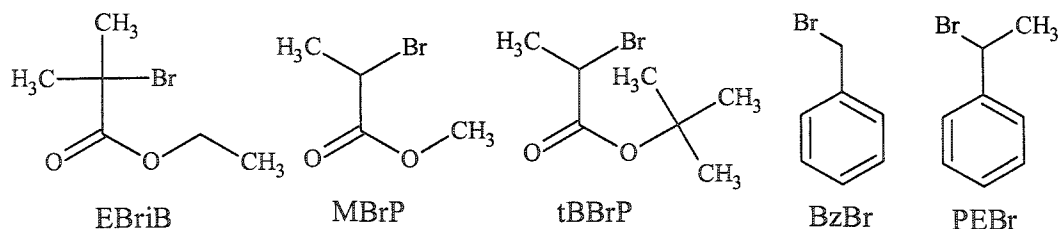


Figure 3. Structures of ATRP initiators used as models for polymer chain end groups.

indicates that the atom transfer process involves a bimolecular step of Br atom transfer from alkyl halide to copper through an inner sphere electron transfer (ISET).

The deactivation rate constants decrease with increasing stability of the alkyl radicals (or polymeric radical). The  $k_d$  values ( $M^{-1}s^{-1}$ ) in the ATRP of methyl methacrylate, styrene, and butyl acrylate using Cu(II)Br<sub>2</sub>/TPB systems (Figure 4) at 90

$^{\circ}\text{C}$ , measured using a method based on reverse ATRP (described earlier), were  $1.4 \times 10^4$ ,  $3.0 \times 10^4$ , and  $3.5 \times 10^5$ , respectively.<sup>52</sup> That is, the higher stability of the MMA and St end groups makes their  $k_d$  values an order of magnitude smaller than that of the less stable BA radical.

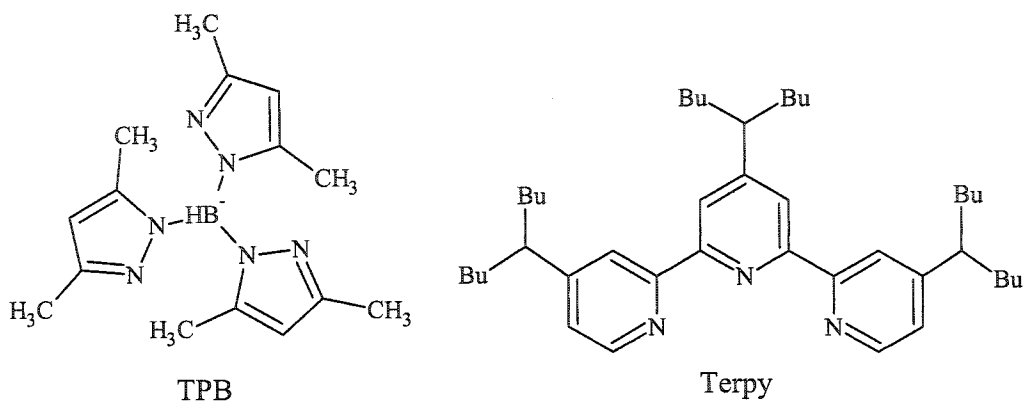


Figure 4. Structures of some nitrogen based ligands used for ATRP catalysts.

b) *Effect of the nature of the halide on  $k_a$  and  $k_d$ .*

The halide atom on the alkyl halide and the copper salt both strongly influence  $k_a$  and  $k_d$  values. In the Cu(I)Br/ diheptyl bipyridyl (dHBpy) system and toluene solvent at  $110\text{ }^{\circ}\text{C}$ , the  $k_a$  value ( $\text{M}^{-1}\text{s}^{-1}$ ) of PEBr (0.42) is larger than that of PECl (0.018) using the Cu(I)Cl/dHBpy system under otherwise identical conditions. This indicates the C-Cl bond is much stronger than the C-Br bond. Also, the  $k_a$  value ( $\text{M}^{-1}\text{s}^{-1}$ ) of the mixed PEBr- $\{\text{Cu(I)Cl/dHBpy}\}$  and PECl- $\{\text{Cu(I)Br/dHBpy}\}$  systems is 0.52 and 0.010, respectively. The lower  $k_a$  value of PECl- $\{\text{Cu(I)Br/dHBpy}\}$  system (0.010) than the PECl- $\{\text{Cu(I)Cl/dHBpy}\}$  system (0.018) and the higher  $k_a$  value of the PEBr- $\{\text{Cu(I)Cl/dHBpy}\}$  system (0.52) than the PEBr- $\{\text{Cu(I)Br/dHBpy}\}$  system infers that Cu(I)Cl is a stronger reducing agent than Cu(I)Br.<sup>54</sup> Matyjaszewski *et al.*<sup>55</sup> reported better control of

polymerization using the mixed halogen system with an alkyl bromide and Cu(I)Cl and explained it in terms of an increase in the relative rate of initiation to that of propagation.

The deactivation rate constant ( $k_d$ ), of the PE radical using Cu(II)Br<sub>2</sub>/2dNBpy system in acetonitrile at 35 °C is larger than that with the Cu(II)Cl<sub>2</sub>/2dNBpy system ( $2.5 \times 10^7$  versus  $4.3 \times 10^6$ ),<sup>53</sup> indicating that the Cu-Br bond is weaker than the Cu-Cl bond.

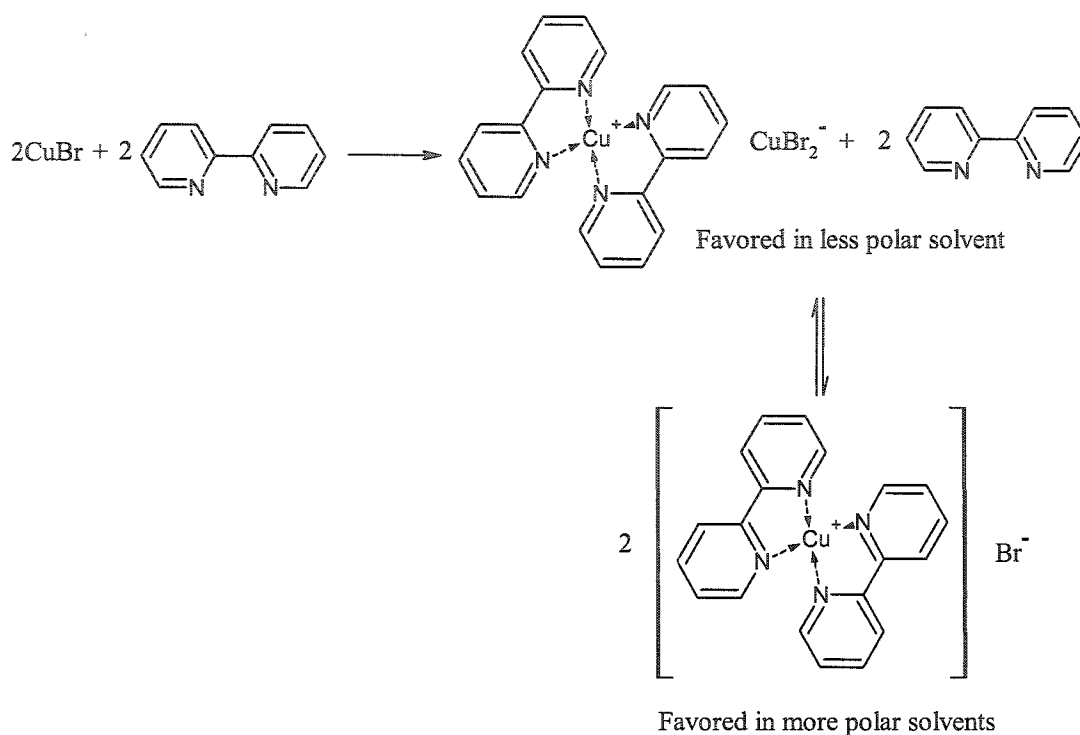
*c) Effect of ligand structure on  $k_a$  and  $k_d$ .*

Ligands effect  $k_a$  and  $k_d$  values ( $M^{-1}s^{-1}$ ) through the electronic and steric properties of the catalyst. The activation rate constants of the PEBr-Cu(I)Br/2dNBpy (0.085), PEBr-Cu(I)Br/PMDETA (0.12) and PECl-Cu(I)Cl/Me<sub>6</sub>TREN(1.5) systems in acetonitrile at 35 °C followed the order dNBpy < PMDETA < Me<sub>6</sub>TREN ( $k_a$  of PEBr-Cu(I)Br/Me<sub>6</sub>TREN is too large to be measured using HPLC for monitoring changes in alkyl halide concentration). The corresponding  $k_d$  values ( $M^{-1}s^{-1}$ ) at 75 °C were  $2.5 \times 10^7$ ,  $6.1 \times 10^6$  and  $1.4 \times 10^7$  (for PEBr-Cu(I)Br/Me<sub>6</sub>TREN), indicating that more nucleophilic aliphatic ligands stabilized the Cu(II) species better than less nucleophilic aromatic ligands.<sup>53</sup> The  $k_a$  value ( $M^{-1}s^{-1}$ ) of the PEBr-Cu(I)Br/Me<sub>6</sub>TREN system at 35 °C, measured using the stopped flow technique,<sup>56</sup> is  $(1.2 \pm 0.3) \times 10^3$ , confirming the above trend. However, a subtle change in the catalyst geometry and/or electronic properties reverses this trend. For example,  $k_a$  values ( $M^{-1}s^{-1}$ ) of PEBr in acetonitrile at 35 °C, using homoleptic PMDETA (0.1) and TERPY (0.42) (see Scheme 13 for structure of TERPY) follow the order aromatic TERPY > aliphatic PMDETA.<sup>48</sup>

*d) Effect of solvent on  $k_a$  and  $k_d$ .*

Solvent affects  $k_a$  by changing the structure of the catalyst and the free ion/ion pair ratio of the copper species.<sup>42,43</sup> Measurements of  $k_a$  of EBriB at 35 °C using Bpy/Cu(I)Br ratios of 0.5 to 4, showed that in polar acetonitrile (dielectric constant,  $\epsilon = 35.94$ ), the maximum value of  $k_a$  ( $= 0.243 \text{ M}^{-1}\text{s}^{-1}$ ) resulted at Bpy/Cu(I)Br = 2:1, while in a binary mixture containing 58.5 wt.% non-polar chlorobenzene ( $\epsilon = 5.62$ ) its maximum value ( $= 0.098 \text{ M}^{-1}\text{s}^{-1}$ ) resulted at Bpy/Cu(I)Br = 1:1. This implies that catalyst structure depends on the polarity of the medium (Scheme 10).

The apparent rate constant based on added Cu(I) species therefore doubles in polar solvents because only half the Cu(I)Br is in the active  $\text{Cu}(\text{Bpy})_2^+$  form in the less polar medium. With the non-coordinating  $\text{PF}_6^-$  copper salt ( $\text{Cu}(\text{I})\text{PF}_6$ ), maximum  $k_a$  values were obtained at Bpy/Cu(I)Br = 2:1 in both polar and non-polar media, indicating that here only the active  $\text{Cu}(\text{Bpy})_2^+$  species results irrespective of solvent polarity.



Scheme 10. Complex formation equilibrium in polar and non-polar solvents.

The activation rate constant,  $k_a$  for EBriB with  $\text{Cu(Bpy)}_2^+ \text{PF}_6^-$  in acetonitrile was 1.5 times larger than that in the non-polar binary solvent mixture, possibly due to a greater proportion of more active free ions in the polar medium. For the same reason, addition of 56 wt. % water to acetonitrile led to a four fold increase in  $k_a$  (of EBriB using  $\text{Cu(Bpy)}_2^+ \text{Br}^-$ ).

In a binary solvent mixture of acetonitrile and 13.7 wt. % tetra(ethylene glycol dimethyl ether) (TEGDME),  $k_a$  (of EBriB using  $\text{Cu(Bpy)}_2^+ \text{Br}^-$ ) fell to half its value

relative to acetonitrile. Oxyethylene solvents, however, are known to accelerate ATRP.<sup>57</sup> Thus, this unexpected lowering of the  $k_a$  implies that the higher rate of ATRP in such solvents is the result of a lower  $k_d$  value rather than a higher  $k_a$  value. In this binary solvent composition, the maximum  $k_a$  value resulted at Bpy/Cu(I)Br = 2:1, indicating that  $\text{Cu}(\text{Bpy})_2^+ \text{Br}^-$  is the predominant catalyst species. At 61.1% TEGDME in acetonitrile, the maximum  $k_a$  value was 10 fold lower than in acetonitrile, and resulted at Bpy/Cu(I)Br = 1:1, indicating a switch to  $\text{Cu}(\text{Bpy})_2^+ \text{CuBr}_2^-$  catalytic species. The  $k_a$  value of EBriB in acetonitrile at 35 °C using Cu(I)Br/PMDETA is four times larger than that using Cu(I)Br/*bis*(2-dimethylaminoethyl)ether (BDMAEE) (see Figure 1 for structure).<sup>43</sup> This indicates that some displacement of nitrogen atom coordination by oxygen in oxyethylene containing solvents may be responsible for the observed lower  $k_a$  values.

### *1.2.6 ATRP in aqueous suspension/emulsion conditions*

The success of the ATRP reaction depends upon the absence of side reactions and the presence of appropriate concentrations of activating and deactivating catalyst species in the polymerization medium. Thus, in heterogeneous suspension or emulsion conditions, the added surfactants/stabilizers must be inert towards ATRP initiator, catalyst, monomer, and polymer as well as the initiating and polymeric radicals. In addition, the partitioning of the catalyst between the disperse organic phase and the aqueous continuous phase must be such that it is present in sufficient concentrations at the site of polymerization.

In the presence of sodium dodecyl sulfate, an anionic surfactant commonly used in emulsion polymerizations, the ATRP of (meth)acrylates using copper based catalysts

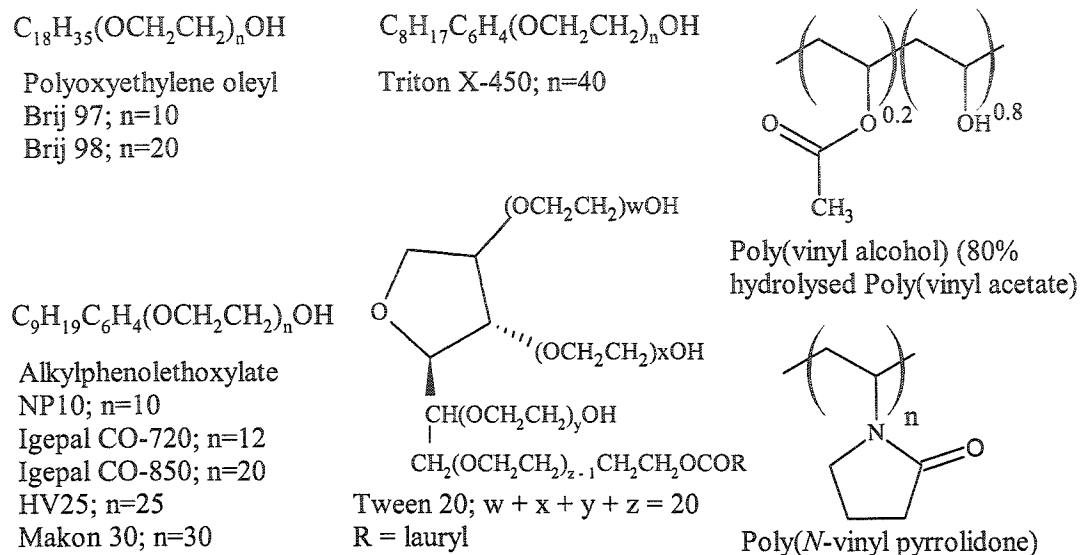
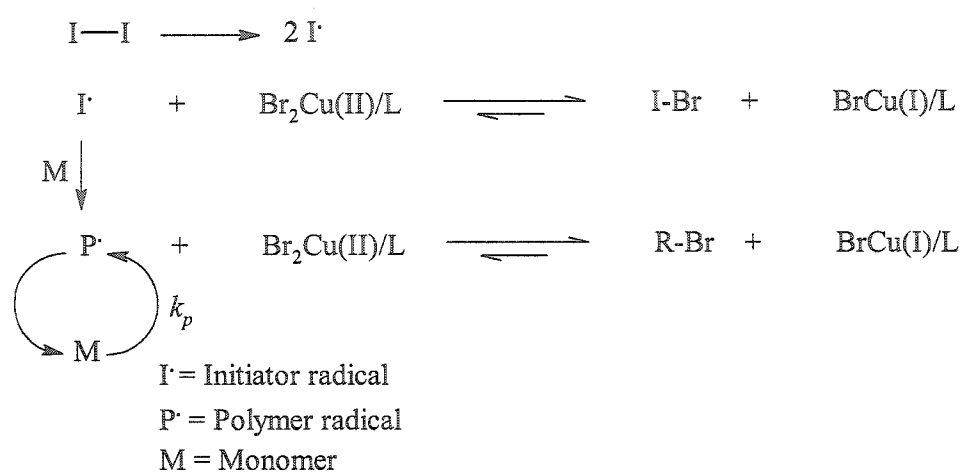


Figure 5. Structures of commonly used surfactants and stabilizers for suspension and emulsion ATRP.

and initiated by EBriB in suspension conditions, yields high molecular weight polymers with high polydispersities.<sup>58</sup> This is attributed to the reaction of Cu(II)Br<sub>2</sub> (or Cu(II)Cl<sub>2</sub>) with the sulfate anion to form CuSO<sub>4</sub> and NaBr. Thus, the growing radicals cannot be deactivated, as the sulfate group is not capable of being transferred to the growing radical, and the polymerization behaves like a conventional, redox-initiated radical polymerization. Use of non-ionic surfactants<sup>58</sup> or stabilizers (Figure 5) as exemplified by our recent work,<sup>59</sup> avoids this side reaction resulting in successful ATRP of methyl methacrylate, butyl methacrylate, butyl acrylate and styrene.

In addition to “direct” ATRP, where initiator radicals form upon transfer of halide from the alkyl halide to the low valent form of the catalyst species (Cu(I)Br/L), “reverse”



Scheme 11. Mechanism of “reverse” ATRP.

ATRP has also been conducted in aqueous dispersions.<sup>60</sup> “Reverse” ATRP starts with a conventional radical initiator and the high valency form of the catalyst species ( $\text{Cu(II)Br}_2/\text{L}$ ), and the ATRP equilibrium between dormant species and free radicals is reached through the mechanism illustrated in Scheme 11.

The formed radicals can initiate polymerization and/or react with deactivator ( $\text{Cu(II)Br}_2/\text{L}$ ). The net result is that the alkyl halide initiator and the lower oxidation state catalyst species ( $\text{Cu(I)Br}/\text{L}$ ) are generated *in situ*. In “direct” ATRP experiments, an oil soluble initiator such as EBriB is usually employed and in mechanistic terms the system resembles a conventional suspension polymerization. That is, surfactant stabilized oil droplets as well as surfactant micelles act as individual micro-reactors for solution polymerization. “Reverse” ATRP experiments on the other hand employ water soluble initiators (see examples in Figure 6) and the system resembles a conventional emulsion polymerization. Here, initiator dissociation in the aqueous phase yields free radicals that

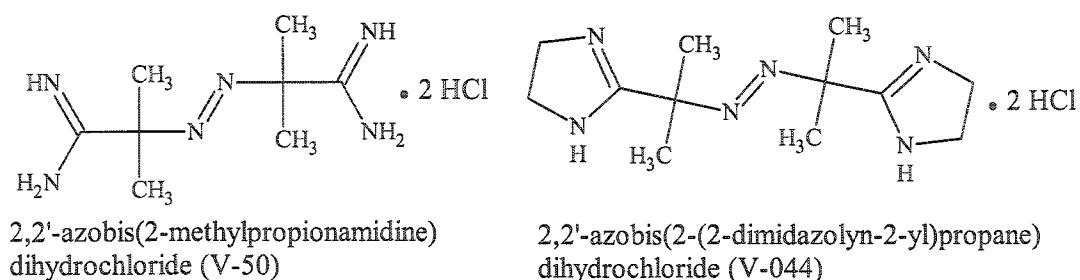


Figure 6. Water soluble azo-based initiators used in “reverse” ATRP. Half lives at 90 °C in water are about 7 -10 minutes.<sup>62</sup>

propagate by reaction with dissolved monomer. When the resulting oligomers attain a critical molecular weight, they partition into the surfactant micelles where polymerization continues. Thus, in the following discussion, experiments employing “direct” ATRP are referred to as suspension polymerizations, and those that employ “reverse” ATRP as emulsion polymerizations.

Controlled polymerization of (meth)acrylates in aqueous disperse systems is only achieved when hydrophobic ligands such as dNBpy, dnNBpy, or BPMODA are used. On the other hand, ligands such as Bpy, PMDETA, and Me<sub>6</sub>TREN that function very well in bulk or solution polymerizations lead to uncontrolled polymerization. This is ascribed to the favorable partitioning of hydrophobic ligand based catalysts into the organic phase in the aqueous dispersion.<sup>61</sup> Measurement of the partitioning of Cu(I)Br/2dNBpy and Cu(II)Br/2dNBpy between butyl methacrylate (BMA) and a water phase under conditions similar to those used in the emulsion polymerization of BMA except for the absence of surfactant, revealed that at the polymerization temperature (90°C), < 20% Cu(II) species and > 70% Cu(I) species remains in the BMA phase.<sup>62</sup> Despite the low concentration of

deactivator in the organic phase, polymer molecular weight increased linearly with conversion and polydispersity remained low ( $<1.4$ ), indicating that the number of chains remains constant and irreversible terminations are negligible. The polymerization exhibited an induction period of 30 minutes during which time the emulsion turned from green (color of  $\text{Cu(II)Br}/2\text{dNBpy}$ ) to brown (color of  $\text{Cu(I)Br}/2\text{dNBpy}$ ), indicating that the radicals generated by thermal decomposition of the conventional azo initiator were capped by halogen transfer from the catalyst. Poor initiator efficiency ( $\sim 30\%$ ), indicating irreversible termination of radicals by coupling and/or termination of radicals by uncomplexed  $\text{Cu(II)Br}_2$  present in the aqueous phase, was observed. However, initiator efficiency was independent of initial  $\text{Cu(II)Br}_2$  concentration in the aqueous phase, indicating that radical coupling is the major cause of initiator inefficiency.

Initiator efficiency in the suspension ATRP of MMA using EBriB- $\text{Cu(I)Br}/2\text{dNBpy}$  system was nearly quantitative as determined by the ratio of experimental ( $M_n(\text{exp})$ ) to theoretical molecular weights ( $M_n(\text{theo})$ ) at reaction end. In contrast, emulsion ATRP using the VA-044- $\text{Cu(II)Br}/2\text{dNBpy}$  system under otherwise similar conditions gave low  $M_n(\text{exp})$  values.<sup>63</sup> In the suspension experiment,  $M_n(\text{exp})$ 's were up to 50% higher than  $M_n(\text{theo})$  values at low conversion but the two coincided at high conversion. The discrepancy could result from slow initiation of EBriB and the presence of fewer polymer chains at low conversion. However, kinetic plots did not show an increase in radical concentration with conversion, excluding this possibility. Low concentration of deactivator due to its partitioning into the water phase resulting in termination of polymer radicals is also unlikely because in this case the  $M_n$  discrepancy

should have remained at high conversion as well. The authors speculated that the effects of low initiator efficiency caused by irreversible radical terminations may have been cancelled by side reactions at high conversions. The conclusion that low initiator efficiency results from irreversible radical terminations is supported by the observation that initiator efficiency varied inversely with Cu(I)Br/PMDETA concentration in the suspension polymerization of styrene using EBriB initiator and an oil phase comprised of toluene/styrene mixtures.<sup>64</sup> That is, at higher concentrations of Cu(I)Br/PMDETA, even in the presence of added Cu(II)Br<sub>2</sub>, initiator efficiencies were lower, because more significant termination reactions occurred during the early stages of ATRP because of a higher concentration of radicals and a limited concentration of deactivator in the organic phase. Reducing the Cu(I)Br/PMDETA concentration led to slower rates of radical generation, and consequently to less significant radical termination and higher initiator efficiencies.

In the former study mentioned above,<sup>63</sup> the poly(methyl methacrylate) particles formed in the suspension polymerization are large (up to 2  $\mu\text{m}$ ) and their size distribution is broad while those from emulsion polymerization were small (40 – 50 nm) and monodisperse. This indicates that the suspension ATRP proceeds by polymerization in monomer droplets, while emulsion polymerization involves micellar or homogeneous nucleation.

In a recently reported suspension polymerization of MMA using EBriB initiator, the Cu(I) and Cu(II) species were quantitatively confined to the MMA phase using hexylated triethylenetetramine ligands.<sup>65</sup> However, initiator efficiency was low ( $\sim 0.7$ )

and polydispersity was broad (1.3 – 1.6) presumably due to high radical concentration resulting from the high value of the ATRP equilibrium constant using aliphatic amine ligands. Low concentration (0.3 wt. %) of PVP was used as a suspension stabilizer and stirring the suspension at 500 rpm yielded large 500 – 700  $\mu\text{m}$  size polymer particles.

### 1.3 Statement of Problem, Research Proposal and Thesis Summary

Encapsulation by *in situ* polymerization of vinyl monomers has been developed to the extent that with careful selection of experimental conditions, capsules containing a range of core oils have been prepared. Critical experimental parameters include the polarity of the oil droplets versus that of the polymer, type and amount of surfactant and/or water miscible organic solvent in the water phase employed to modify the oil-water and polymer-water interfacial tensions, and the viscosity of the oil droplets. While the former two variables determine the thermodynamically favored morphology under a given set of experimental conditions, the latter affects the kinetics of polymer diffusion, and hence final morphology of the suspension polymer particles. In practice, viscosity is controlled by the amount and molecular weight of polymer forming in the oil phase. Chain transfer agents are employed to reduce molecular weight while an optimum polymer concentration is used to obtain mechanically stable capsule walls while avoiding high viscosity resulting from high polymer concentrations. Thus, the need to match the kinetics of *in situ* polymerization with the kinetics of polymer diffusion and development of the particle morphology within the experimental time frame, calls for extensive optimization for individual systems.

This research aims to investigate an alternative technique where the rate of *in situ* polymerization is significantly slower than that of polymer diffusion and the molecular weight of the forming polymer increases gradually with conversion imparting low viscosity conditions within the oil droplets. We propose that these aims can be met by employing *in situ* Atom Transfer Radical Polymerization (ATRP) for polymer preparation within the oil droplets. We anticipate that the living nature of ATRP will also provide access to polar copolymers based on oil and water soluble comonomers under suspension polymerization conditions despite partitioning of the water soluble monomer into the water phase. In addition, capsule walls exhibiting a compositional gradient across their thickness with hydrophilic comonomer occupying an outer shell may be accessible.

Two model systems were used to test the above hypotheses. Diphenyl ether was used as a common solvent in both systems to fix the polarity of the oil phase, while copolymers of differing polarity were chosen. The first system involved copolymers based on a pair of oil soluble comonomers, one non-polar (methyl methacrylate, MMA) and the other polar (poly(ethylene glycol) monomethyl ether methacrylate, MPEGMA), which partially partitions into the aqueous phase. The solution ATRP of the copolymers at several comonomer compositions was first developed followed by ATR copolymerizations in suspension conditions. The success of ATRP reactions in heterogeneous suspension conditions was evaluated by comparison with results obtained in solution polymerization conditions. Stable suspension polymer particles were prepared by adding a crosslinking monomer, diethylene glycol dimethacrylate (DEGDMA) to the suspension polymerizations, and the particle morphology was compared to that of

analogous particles prepared using conventional free radical polymerization (CFRP). In a second system, copolymers based on an oil soluble comonomer (MMA) and a polar monomer (poly(ethylene glycol methacrylate), PEGMA), which partitions extensively into water, were prepared by both solution and suspension polymerization and the ability of ATRP to incorporate the water soluble monomer into the copolymer forming within the oil droplets was evaluated. The morphology of crosslinked polymer particles was compared to that of CFRP particles as in the MPEGMA system described above. In both systems, *p*-toluene sulfonyl chloride was used as ATRP initiator with an ATRP catalyst system based on copper (I) bromide and 4,4'-dinonyl-2,2'-dipyridine ligands. The justification for the choice of ATRP system and experimental conditions are presented at appropriate locations in the following chapters.

## References:

- (1) Arshady, R. *Microspheres, Microcapsules and Liposomes* **1999**, *1*, 1461-1732.
- (2) Uhrich, K. E.; Cannizzaro, S. M.; Langer, R. S.; Shakesheff, K. M. *Chem. Rev.* **1999**, *99*, 3181-3198.
- (3) Trogolo, J. A.; Rossitto, F. C.; Welch, E. K. U. S. Patent 2003118664, 2003.
- (4) Torchilin, V. P. *Eur. J. Pharm. Sci.* **2000**, *11* (Suppl. 2), S81-S91.
- (5) Lohr, M.; Hummel, F.; Faulman, G.; Ringel, J.; Saller, R.; Hain, J.; Gunzburg, W. H.; Salmons, B. *Cancer Chemotherapy and Pharmacology* **2002**, *49*(Suppl. 1) S21-S24.
- (6) Bubbell, J. A.; Pathak, C. P.; Sawhney, A. S.; Desai, N. P.; Hill-West, J. L.; Hossainy, S. F. A. U. S. Patent 5,573,934, 1996.
- (7) Bubbell, J. A.; Pathak, C. P.; Sawhney, A. S.; Desai, N. P.; Hill-West, J. L.; Hossainy, S. F. A. U. S. Patent 6,632,446, 2003.
- (8) Bodmer, J. R.; Kendall, D. P.; Long, J. D.; Balster, L. A. U. S. Patent 2003022789, 2003.
- (9) David, R. F. *J. Microencapsulation* **1992**, *9*, 469-480.
- (10) Scarpelli, J. A.; Soper, J. C. U. S. Patent 5043161, 1991.
- (11) Berg, J.; Sundberg, D.; Kronberg, B. *J. Microencapsulation* **1989**, *6*, 327-337.
- (12) Torza, S.; Mason, S. G. *J. Colloid Interface Sci.* **1970**, *33*, 67-83.
- (13) Wang, J. -S.; Matyjaszewski, K. *J. Am. Chem. Soc.* **1995**, *117*, 5614-5615.
- (14) Patten, T. E.; Matyjaszewski, K. *Acc. Chem. Res.* **1999**, *32*, 895-903.
- (15) Oiu, J.; Charleux, B.; Matyjaszewski, K. *Prog. Polym. Sci.* **2001**, *26*, 2083-2134.
- (16) Arshady, R. *J. Microencapsulation* **1989**, *6*, 13-28.

- (17) Arshady, R. *Polym. Engn. Sci.* **1990**, *30*, 905-914.
- (18) Nixon, J. R.; Khalil, S. M. A.; Careless, J. E. *J. Pharm. Pharmacol.* **1966**, *18*, 409-416.
- (19) Jizomoto, H. *J. Pharm. Sci.* **1984**, *73*, 879-882.
- (20) Arshady, R. *Polym. Engn. Sci.* **1989**, *29*, 1746-1758.
- (21) Ishizaka, T.; Endo, K.; Koishi, M. *J. Pharm. Sci.* **1981**, *70*, 358-363.
- (22) Levy, M. C.; Rambuorg, P.; Levy, J. Porton, J. *J. Pharm. Sci.* **1982**, *71*, 759-762.
- (23) Arshady, R. *Polym. Engn. Sci.* **1990**, *30*, 915-924.
- (24) Linko, P.; Linko, Y. *Meth. Enzymol.* **1987**, *135*, 268-282.
- (25) Cowsar, D. R.; Tice, T. R.; Gilley, R. M.; English, J. P. *Meth. Enzymol.* **1985**, *112*, 101-116.
- (26) Sundberg, D. C.; Casassa, A. P.; Pantazopoulos, J.; Muscato, M. R. *J. Appl. Polym. Sci.* **1990**, *41*, 1425-1442.
- (27) Van Zyl, A. J. P.; Sanderson, R. D.; de Wet-Roos, D.; Klumperman, B. *Macromolecules* **2003**, *36*, 8621-8629.
- (28) Cho, I.; Lee, K. -W. *J. Appl. Polym. Sci.* **1985**, *30*, 1903-1926.
- (29) Chen, Y, -C; Dimonie, V.; El-Aasser, M. S. *Macromolecules* **1991**, *24*, 3779-3787.
- (30) Jönsson, J. -E.; Hassander, H.; Törnell, B. *Macromolecules* **1994**, *27*, 1932-1937.
- (31) Muscato, M. R.; Sundberg, D. C. *J. Polym. Sci.: Part B: Polym. Phys.* **1991**, *29*, 1021-1024.
- (32) McDonald, C. J.; Bouck, K. J.; Chaput, A. B. *Macromolecules* **2000**, *33*, 1593-1605.

- (33) Landfester, K.; Bechthold, N.; Tiarks, F.; Antonietti, M. *Macromolecules* **1999**, *32*, 5222-5228.
- (34) Tiarks, F.; Landfester, K.; Antonietti, M. *Langmuir* **2001**, *17*, 908-918.
- (35) Wang, J. -S.; Matyjaszewski, K. *J. Am. Chem. Soc.* **1995**, *117*, 5614-5615.
- (36) Szwarc, M. *Nature* **1956**, *178*, 1168-1169.
- (37) Pintauer, T.; Zhou, P.; Matyjaszewski, K. *J. Am. Chem. Soc.* **2002**, *124*, 8196-8197.
- (38) Matyjaszewski, K. *Macromol. Symp.* **1996**, *111*, 47-61.
- (39) Matyjaszewski, K.; Xia, J. *Chem. Rev.* **2001**, *101*, 2921-2990.
- (40) Luo, Y.-R. *Handbook of Bond Dissociation Energies in Organic Compounds*; CRC Press: Boca Raton, FL, 2003.
- (41) Gillies, M. B.; Matyjaszewski, K.; Norrby, P. -O.; Pintauer, T.; Poli, R.; Richard, P. *Macromolecules* **2003**, *36*, 8551-8559.
- (42) Nanda, A. J.; Matyjaszewski, K. *Macromolecules* **2003**, *36*, 599-604.
- (43) Nanda, A. J.; Matyjaszewski, K. *Macromolecules* **2003**, *36*, 1487-1493.
- (44) Qiu, J.; Matyjaszewski, K.; Thouin, L.; Amatore, C. *Macromol. Chem. Phys.* **2000**, *201*, 1625-1631.
- (45) Xia, J.; Matyjaszewski, K. *Macromolecules* **1997**, *30*, 7697-7700.
- (46) Matyjaszewski, K.; Woodworth, B. E.; Zhang, X.; Gaynor, S. G.; Metzner, Z. *Macromolecules* **1998**, *31*, 5955-5957.
- (47) Skene, W. G.; Belt, S. T.; Connolly, T. J.; Hahn, P.; Scaiano, J. C. *Macromolecules* **1998**, *31*, 9103-9105.

- (48) Matyjaszewski, K.; Göbelt, B.; Paik, H. -J.; Horwitz, C. P. *Macromolecules* **2001**, *34*, 430-440.
- (49) Skene, W. G.; Scaiano, J. C.; Listigovers, N. A.; Kazmaier, P. M.; Georges, M. K. *Macromolecules* **2000**, *33*, 5065-5072.
- (50) Beckwith, A. L.; Bowry, V. W.; Ingold, K. U. *J. Am. Chem. Soc.* **1992**, *114*, 4983-4992.
- (51) Mercier, C. L.; Lutz, J. -F.; Marque, S.; Moigne, F. L.; Tordo, P.; Lacroix-Desmaze, P.; Boutevin, B.; Couturier, J.-L.; Guerret, O.; Martschke, R.; Sobek, J.; Fischer, H. In *Controlled/Living Radical Polymerization: Progress in ATRP, NMP and RAFT*; Matyjaszewski, K., Ed.; ACS Symp. Ser. 768; American Chemical Society; Washington, DC, 2000; p.108.
- (52) Gromada, J.; Matyjaszewski, K. *Macromolecules* **2002**, *35*, 6167-6173.
- (53) Matyjaszewski, K. Paik, H. -J.; Zhou, P.; Diamanti, S. J. *Macromolecules* **2001**, *34*, 5125-5131.
- (54) Goto, A.; Fukuda, T. *Macromol. Rapid Commun.* **1999**, *20*, 633-636.
- (55) Matyjaszewski, K.; Shipp, D. A.; Wang, J. -L.; Grimaud, T.; Patten, T. E. *Macromolecules* **1998**, *31*, 6836-6840.
- (56) Pintauer, T.; Braunecker, W.; Collange, E.; Poli, R.; Matyjaszewski, K. *Macromolecules* **2004**, *37*, 2679-2682.
- (57) Haddleton, D. M.; Perrier, S.; Bon, S. A. F. *Macromolecules* **2000**, *33*, 8246-8251.
- (58) Gaynor, S. G.; Qiu, J.; Matyjaszewski, K. *Macromolecules* **1998**, *31*, 5951-5954.
- (59) Ali, M. M.; Stöver, H. D. H. *Macromolecules* **2003**, *36*, 1793-1801.

- (60) Qiu, J.; Gaynor, S. G.; Matyjaszewski, K. *Macromolecules* **1999**, *32*, 2872-2875.
- (61) Qiu, J.; Shipp, D.; Gaynor, S. G.; Matyjaszewski, K. *Am. Chem. Soc., Polym. Prepr.* **1999**, *40(2)*, 418-419.
- (62) Qiu, J.; Pintauer, T.; Gaynor, S. G.; Matyjaszewski, K.; Charleux, B.; Vairon, J. -P. *Macromolecules* **2000**, *33*, 7310-7320.
- (63) Jousset, S.; Qiu, J.; Matyjaszewski, K. *Macromolecules* **2001**, *34*, 6641-6648.
- (64) Sarbu, T.; Pintauer, T.; McKenzie, B.; Matyjaszewski, K. *J. Polym. Sci.: Part A: Polym. Chem.* **2004**, *42*, 1362-1366.
- (65) Bicak, N.; Gazi, M.; Tunca, U.; Kucukkaya, I. *J. Polym. Sci.: Part A: Polym. Chem.* **2004**, *42*, 1362-1366.

## CHAPTER 2

In this chapter, the Atom Transfer Radical Copolymerization of methyl methacrylate (MMA) and poly(ethylene glycol) monomethyl ether methacrylate (MPEGMA) is developed first in solution conditions and then in suspension condition. The objective of conducting suspension polymerization is to prove that a controlled/living copolymerization of these monomers can be carried out in the two phase system, with the ATRP catalyst confined to the suspended oil phase.

Also described is the crosslinking suspension ATR terpolymerization of MMA and MPEGMA using diethylene glycol dimethacrylate as crosslinking monomer. The morphology of the resulting suspension polymer particles is compared to those formed using conventional radical polymerization (CFRP) under analogous experimental conditions. Using ATRP, capsules are formed, while CFRP under analogous conditions gives matrix or solid polymer particles. The results are explained in terms of the slower kinetics of ATRP.

A summary of preliminary experiments aimed at the development of the ATRP of MA and MMA in a number of organic solvents is presented in Appendix II. These preliminary experiments played a role in the choice of the monomers, solvent, ATRP initiator and catalyst system used in this chapter.

**Polymeric Capsules Prepared by in situ Synthesis and Crosslinking of Amphiphilic Copolymer by Atom Transfer Radical Polymerization**

(Mir Mukkaram Ali and Harald D. H. Stöver, *Macromolecules* **2003**, 36(6), 1793-1801)

**ABSTRACT**

A technique for encapsulation of polar organic solvents using Atom Transfer Radical Polymerization (ATRP) by suspension polymerization was developed and used to encapsulate diphenyl ether (solubility parameter,  $\delta = 20.9 \text{ MPa}^{1/2}$ ) for the first time. An amphiphilic terpolymer was prepared by suspension polymerization, by first preparing poly(methyl methacrylate-*co*-poly(ethylene glycol) monomethyl ether methacrylate) P(MMA-*co*-MPEGMA) oligomers in solution conditions, followed by addition of a crosslinking monomer, diethylene glycol dimethacrylate to the polymerization solution, and then transfer of this oil phase to a stirred aqueous phase. The thermodynamic requirement for encapsulation of polar core-oils is that the polymer has low interfacial tensions with both the oil phase and the water phase. Therefore, increasing the polarity of the copolymer by increasing its MPEGMA content (from 0 to 31 mol%) led to a transition in suspension particle morphology from matrix to multi-hollow and hollow particles. Furthermore, particles prepared with similar monomer feed ratios by conventional free radical polymerization (CFRP) did not exhibit a multi hollow structure. We attribute this difference in ATRP and CFRP suspension particle morphology to the slow rate of the ATRP reaction that allows sufficient time for diffusion of the forming

polymer chains to the oil water interface, resulting in the thermodynamically favored hollow particle morphology.

## 2.1 Introduction

Polymeric capsules and hollow particles can be prepared both from monomeric starting materials as well as from oligomers and pre-formed polymers.<sup>1</sup> In most cases, the process involves a disperse oil phase in an aqueous continuous phase, and the precipitation of polymeric material at the oil – water interface causing each oil droplet to be enclosed within a polymeric shell. Interfacial polycondensation is used to prepare poly(urea),<sup>2</sup> poly(amide), or poly(ester) capsules,<sup>3</sup> for instance, by reaction between an oil soluble monomer and a water soluble monomer. As well, vinyl polymers based on styrenes, acrylates and methacrylates prepared by free radical polymerization under suspension<sup>4</sup> or emulsion polymerization<sup>5,6</sup> conditions have been used to prepare hollow or capsular polymer particles. In both approaches, the dispersed oil phase usually serves as the polymerization medium. The oil phase is a good solvent for the monomeric starting materials but a non-solvent for the product polymer. Therefore, upon polymerization the system is comprised of three mutually immiscible phases. Over the past three decades, several groups have studied the factors governing the morphologies that two immiscible phases can adopt when they are brought together and confined by a third immiscible phase.<sup>7-9</sup>

Torza and Mason<sup>7</sup> studied the phase behavior of low viscosity, immiscible organic liquids dispersed in an aqueous phase as the drops were subjected to varying shear and electric fields. They defined the spreading coefficient,  $S_i = \gamma_{jk} - (\gamma_{ij} + \gamma_{ik})$ ,

where  $i, j,$  and  $k$  represent the three immiscible phases and  $\gamma$ , the interfacial surface tension. For the premise that,  $\gamma_{12} > \gamma_{23}$ , it follows that  $S_1 < 0$ . The definition of  $S_i$ , leads to only three possible sets of values of  $S_i$ :  $S_1 < 0, S_2 < 0, S_3 > 0$  [1];  $S_1 < 0, S_2 < 0, S_3 < 0$  [2];  $S_1 < 0, S_2 > 0, S_3 > 0$  [3]. For interfacial conditions of equation [1] the core-shell morphology is preferred, while for equation [2] the hemispherical morphology is preferred.<sup>7</sup> The theoretical predictions agree well with the experimental results. Torza and Mason used low viscosity oils that are able to diffuse rapidly and assume the lowest interfacial energy morphology within the time frame of the experiment. Sundberg et al.<sup>8</sup> published a theoretical model based on the Gibbs free energy change of the process of morphology development. Starting with three immiscible phases (oil, polymer and water) they showed that the Gibbs free energy change per unit area for the process leading to a core shell morphology (with oil encapsulated within the polymer phase) is  $\Delta G = \gamma_{op} + \gamma_{pw} (1 - \phi_p)^{-2/3} - \gamma_{ow}$ ; where  $\gamma_{op}$ ,  $\gamma_{pw}$ , and  $\gamma_{ow}$  are the oil-polymer, polymer-water and oil-water interfacial tensions and  $\phi_p$  is the volume fraction of the polymer (in polymer plus oil “combined phase”). In the limit as  $\phi_p$  tends to zero,  $\Delta G = (\gamma_{op} + \gamma_{pw}) - \gamma_{ow}$ . Thus, when  $\gamma_{ow} > (\gamma_{op} + \gamma_{pw})$ , the core shell morphology with the core oil being engulfed by the polymer is the thermodynamically stable morphology. Analogous expressions were derived for the hemispherical, inverse core shell and distinct particle morphologies. The authors used these expressions to successfully predict the morphologies expected for a given set of interfacial conditions.

In earlier work, Berg *et.al.*<sup>9</sup> showed that the above analysis is equally valid when the polymer is synthesized *in situ* by free radical polymerization. Poly(methyl

methacrylate) was prepared *via* free radical polymerization by dispersing *n*-decane or hexadecane, methyl methacrylate and an oil soluble initiator in water containing a surfactant or stabilizer. The resultant morphology critically depended on the type of emulsifier used. The authors concluded that this was related to the minimization of interfacial energy for the particles as they are dispersed in water. In summary, the particle morphology that results from *in situ* polymer synthesis in suspension/emulsion polymerization conditions is predominantly driven by interfacial energy criteria.

The available studies in this area by the groups of Kasai,<sup>10,11</sup> Okubo,<sup>12-18</sup> McDonald,<sup>5,6</sup> and Sundberg,<sup>8,9</sup> all focus on encapsulation of relatively hydrophobic solvents. McDonald *et al.* and Sundberg *et al.* have encapsulated highly non-polar core oils such as decane and octane. Kasai *et al.* and Okubo *et al.* have encapsulated slightly more polar materials such as benzene, toluene and xylene. Since these groups set out to synthesize hollow polymer particles, the nature of the core oil has not been of relevance beyond its role in forming the capsules. However, if core-shell particles are intended for encapsulation of the core material, the technique should allow encapsulation of both hydrophobic and hydrophilic core materials.

Core-shell particles, with polymer engulfing an oil core, only form if the sum of the oil/polymer and polymer/water interfacial tensions is less than the oil/water interfacial tension. Furthermore, the polymerization conditions must permit the thermodynamic morphology dictated by the interfacial conditions to form within the time frame of the experiment. Consequently, encapsulation of more hydrophilic material demands the ability to synthesize sufficiently amphiphilic polymers that will satisfy this

interfacial requirement, as well as experimental conditions that allow sufficient time for the thermodynamic morphology to be reached.

We describe here, the *in situ* ATRP synthesis of a crosslinked amphiphilic terpolymer designed to migrate to the oil-water interface yielding hollow polymer particles. The terpolymer, poly(methyl methacrylate-*co*-poly(ethylene glycol) monomethyl ether methacrylate-*co*-diethylene glycol dimethacrylate) P(MMA-*co*-MPEGMA-*co*-DEGDMA) was prepared by suspension polymerization by first preparing a prepolymer P(MMA-*co*-MPEGMA) in solution conditions, followed by addition of the crosslinking monomer, DEGDMA to the polymerization solution and transfer of this oil phase to a stirred aqueous phase. In our work, use of ATRP as the polymerization method is expected to affect both the copolymer composition and the rate of at which polymer precipitates in the oil phase due to crosslinking. In addition to the usual properties of ATRP,<sup>19-20</sup> polymerization of crosslinking monomers by ATRP avoids auto acceleration and when crosslinker is added to preformed oligomers, higher conversion at gel point is observed in ATRP compared to typical crosslinking CFRP.<sup>21,22</sup> The living nature of the ATRP polymerization and its slow rate of polymerization should have two interesting consequences when a crosslinked terpolymer based on oil soluble and water soluble monomers is prepared by suspension polymerization. First, ATRP should allow more time for polymer in the oil droplets to diffuse from the core to the oil water interface, compared to polymer made by CFRP. Second, even if one of the monomers partitions significantly into the water phase, it would ultimately be incorporated into forming polymer chains. The incorporation of the polar monomer into the forming polymer is

important in order to satisfy the thermodynamic requirement for formation of capsular particles. Thus the use of ATRP may have both a kinetic and a thermodynamic advantage as compared to conventional free radical polymerization.

## 2.2 Results and Discussion

### 2.2.1 Copolymer synthesis in diphenyl ether.

The ATRP synthesis of poly(methyl methacrylate-*co*-poly(ethylene glycol) monomethyl ether methacrylate) P(MMA-*co*-MPEGMA) was first developed in solution conditions. PMMA and a series of copolymers of MMA and 9.5, 18, and 39 mol% MPEGMA were prepared by solution ATRP. A copolymer containing 18 mol% MPEGMA was also prepared by suspension polymerization and the molecular weights, polydispersity and kinetics of solution and suspension ATRP were compared.

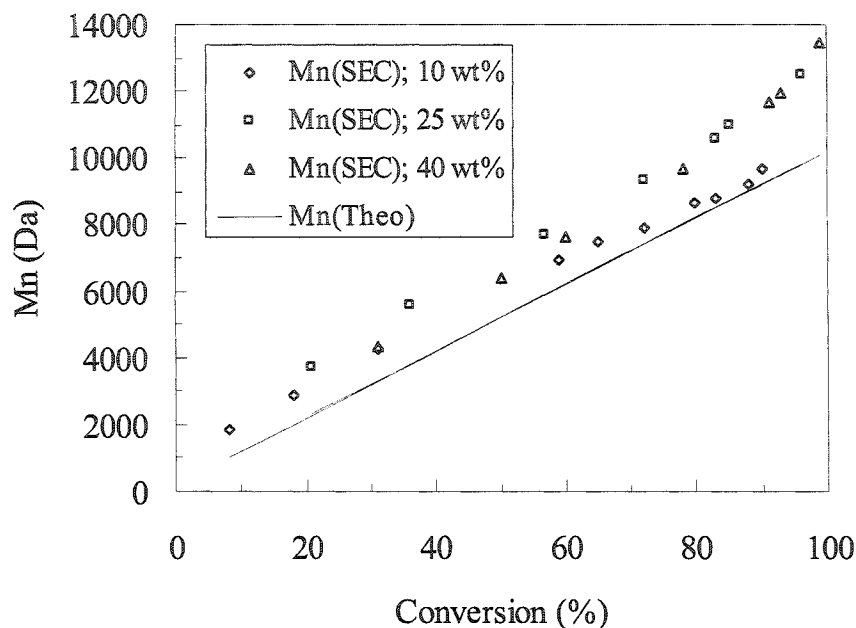
The suspension copolymerization involved the ATRP synthesis of P(MMA-*co*-MPEGMA) oligomers under solution conditions and subsequent transfer of the oligomer solution to a stirred aqueous phase. Diphenyl ether (DPE) was used as a model polar solvent (Table 1). It is a good ATRP solvent owing to its low chain transfer constant and its use for the ATRP of methyl methacrylate has been previously reported.<sup>23</sup> Toluene sulfonyl chloride (TSC) was used as initiator together with a catalyst based on Cu(I)Br and 4,4'-dinonyl-2,2'-bipyridine (dNBpy). The modified bipyridine ligand ensures homogeneous catalyst solubility in diphenyl ether as well as favorable partitioning of the catalyst into the oil phase during suspension polymerizations.<sup>24</sup>

Table 1. Solubility characteristics of some organic solvents

Solvent	Solubility parameter / MPa <sup>1/2</sup>	Solubility of solvent in water / % v/v	Solubility of water in solvent / % v/v
Ethyl acetate	18.2 / 18.6 <sup>a</sup>	9 (25 °C)	4 (25 °C)
n-butyl acetate	17 / 17.4 <sup>a</sup>	0.78 (25 °C)	2.9 (25 °C)
Hexyl acetate	17.3	Insoluble	Insoluble
Xylene	18.0 <sup>a</sup>	Insoluble	Insoluble
Anisole	19.4 <sup>b</sup>	Insoluble	Insoluble
Diphenyl ether	20.9 <sup>a</sup>	Insoluble	Insoluble
Dimethyl phthalate	22.1 / 21.9 <sup>a</sup>	Insoluble	Insoluble

<sup>a,b</sup> Source: Eric A. Grulke in “Solubility parameter values”, Polymer Handbook, Fourth Edition, John Wiley and Sons, Inc.(1999), , Table 7, pp. VII/688 and Table 9, pp. VII/698.

Both the solution polymerizations and the suspension polymerizations were run at 70 °C. The aim here was to develop the ATRP synthesis of P(MMA-co-MPEGMA) for use in the encapsulation reaction and thus the copolymerizations were carried out at low monomer loadings of 10 – 40 wt. %. The range of interest from the encapsulation viewpoint is between 10 and 25 weight percent as this amount of polymer is sufficient for constructing the capsular wall. For development of the ATRP reaction we chose a monomer feed composition of 82 mol% MMA and 18 mol% MPEGMA. Provided both comonomers are incorporated quantitatively into the copolymer, this comonomer ratio



**Figure 1.** Plots of experimental molecular weight ( $M_n(\text{SEC})$ ) vs conversion for copolymerization of MMA and MPEGMA in DPE at 10, 25 and 40 wt % total monomer loading.  $[\text{MMA}]_0:[\text{MPEGMA}]_0:[\text{TSC}]_0: [\text{Cu}(\text{dNBpy})_2\text{Br}]_0 = 60:14:1:1$  at 70 °C.  $M_n$  values are relative to poly(styrene) standards and errors of  $\pm 200$  Da are expected.

would yield copolymers exhibiting a hydrophilic lipophylic balance<sup>a</sup> (HLB) of 8 (considering MPEGMA as the hydrophilic portion). Such copolymers (HLB < 10) are expected to exhibit greater oil solubility than water solubility and hence be retained in the oil phase of oil-water suspensions.

<sup>a</sup> Hydrophilic lipophilic balance,  $\text{HLB} = (\text{Wt.}\% \text{ of hydrophilic portion}) / 5$

The experimental molecular weight,  $M_n(\text{SEC})$  of the copolymers was found to increase linearly with conversion at 10, 25 and 40 wt.% monomer loadings (Figure 1). The SEC traces of the three polymerizations at 90, 96 and 99 % conversion, respectively reveal a slight high molecular weight shoulder in the 10 wt% case, while the 25, and 40 wt% polymerization give bimodal molecular weight distributions (Figure 2).

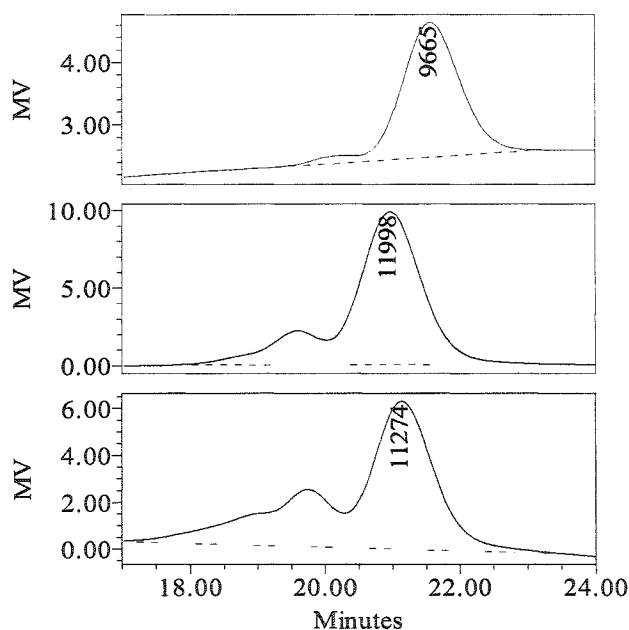


**Figure 2.** Size exclusion chromatographs showing the molecular weight profile of P(MMA-*co*-MPEGMA) containing 18 mol% MPEGMA at 10 wt% (90% conversion), 25 wt% (96% conversion), and 40 wt% (99% conversion) total monomer loading, respectively (top to bottom of stack) in diphenyl ether at 70°C. The reaction conditions are those presented in Figure 1.

The larger discrepancy between Mn(SEC) and Mn(Theo) in the 25 and 40 wt% cases relative to the 10 wt% case is attributed to the high molecular weight material formed in these cases. At 25 and 40 wt% monomer loading, the polydispersity narrowed with conversion up to about 50% conversion and then broadened continuously at higher conversions to finally give the observed bimodal molecular weight distributions. On the other hand, in the case of 10 % monomer loading, polydispersity decreased continuously with conversion as expected for a typical ATRP<sup>19</sup> (Figure 3). Figure 4 shows curvature in the  $\ln[M_0]/[M_t]$  versus time plots indicating that the free radical concentration diminished with conversion in all three cases. The 10 wt% experiment showed the strongest curvature and it is proposed that the polymerization kinetics are diffusion controlled at such low monomer loading leading to the observed non-linearity. The polymerization rate increased with monomer loading as expected (Figure 4). Results of the ATRP synthesis of PMMA and copolymers of MMA and MPEGMA at constant total monomer loading of 25 wt% and containing 9.5, 18 and 39 mol% MPEGMA are shown in Figures 5, 6 and 7. Polymerizations proceeded to high conversions in each case and the experimental number average molecular weights, Mn(SEC), matched the calculated molecular weights, Mn(Theo) (Figure 5). Figure 6 shows the polydispersity profile with conversion for each of the four polymerizations. While the polydispersity decreased with conversion in the polymerization of MMA, in the copolymerizations it decreased to about 50% conversion and increased thereafter.

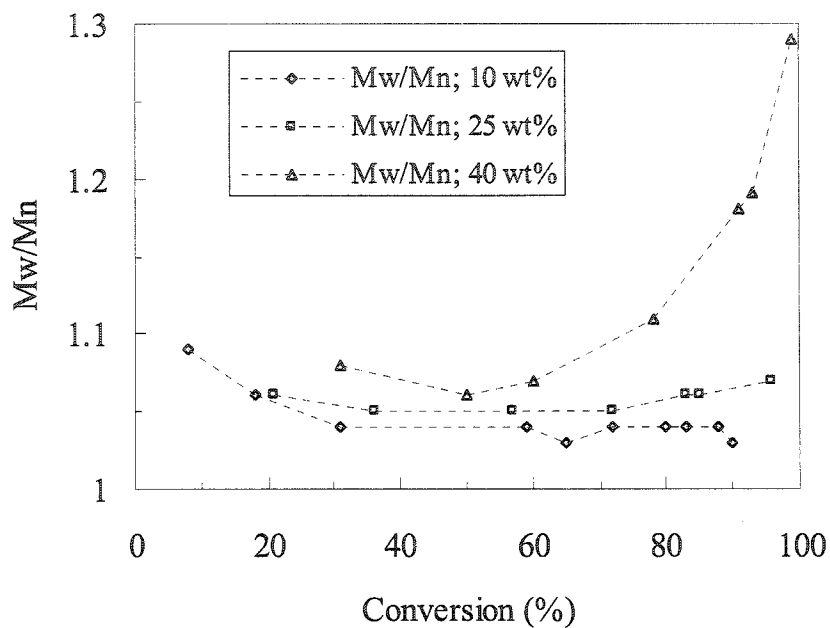


**Figure 3.** Plots of Polydispersity Index (Mw/Mn) vs conversion for copolymerization of MMA and MPEGMA in DPE at 10 25 and 40 wt % total monomer loading.  $[MMA]_0:[MPEGMA]_0:[TSC]_0:[Cu(dNBpy)_2Br]_0 = 60:14:1:1$  at 70 °C. Error expected in Mw/Mn measurements is  $\pm 0.02$ .

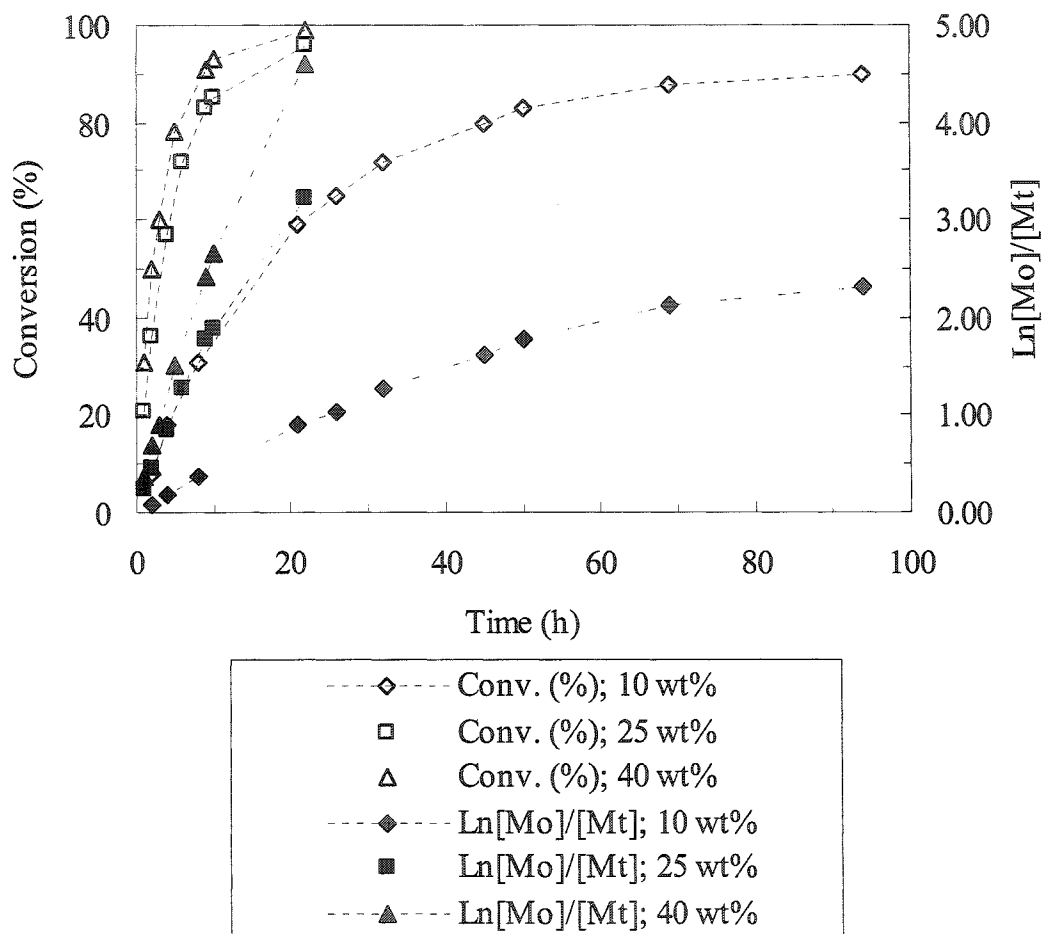
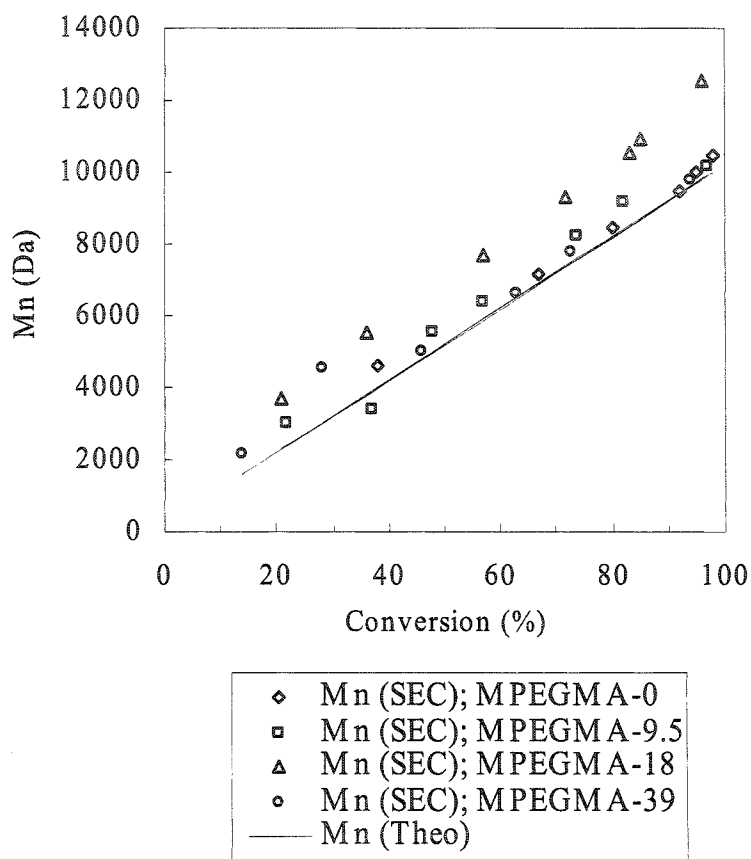
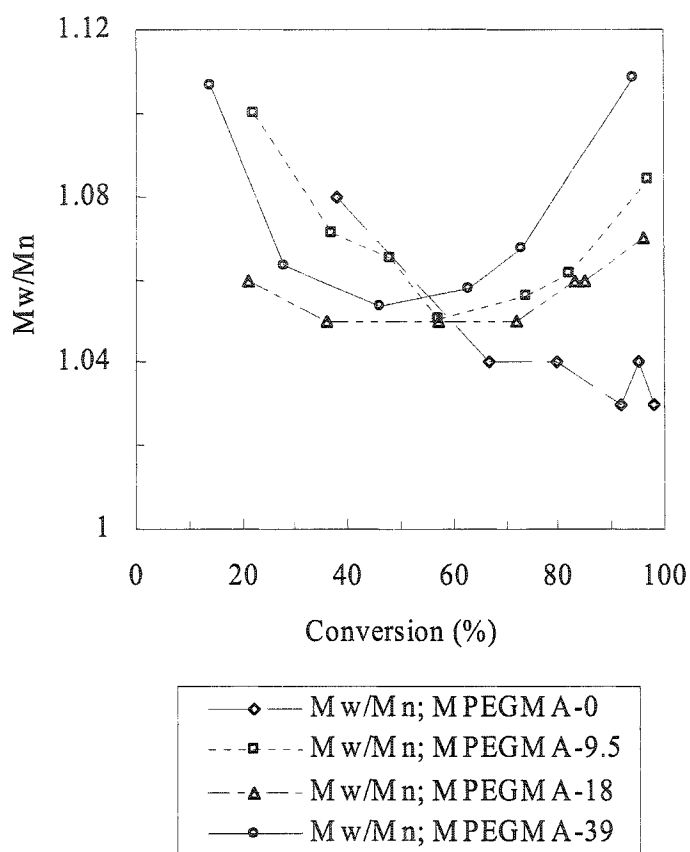


Figure 4. Kinetic profiles for copolymerization of MMA and MPEGMA in DPE at 10, 25 and 40 wt % total monomer loading.  $[MMA]_0:[MPEGMA]_0:[TSC]_0:[Cu(dNBpy)_2Br]_0 = 60:14:1:1$  at 70 °C. The dotted lines are only meant to guide the eye.



**Figure 5.** Plots of experimental ( $M_n(\text{SEC})$ ) and theoretical ( $M_n(\text{Theo})$ ) molecular weight vs conversion for copolymerization of MMA and MPEGMA (%MPEGMA = 0.0, 9.5, 18 and 39) in DPE at 25 wt%. $[\text{TSC}]_0$ :  $[\text{Cu}(\text{dNBpy})_2\text{Br}]_0 = 1:1$  at 70 °C.  $M_n$  values are relative to poly(styrene) standards and errors of  $\pm 200$  Da are expected.



**Figure 6.** Polydispersity vs conversion for copolymerization of MMA and MPEGMA (mol% MPEGMA = 0, 9.5, 18 and 39) in DPE at 25 wt%.  $[TSC]_0$ :  $[Cu(dNBpy)_2Br]_0 = 1:1$  at 70 °C. Error expected in Mw/Mn measurements is  $\pm 0.02$ .

As seen in Figure 7, the plot of  $\ln[M_0]/[M_t]$  is linear in the homopolymerization but exhibits a curvature in the copolymerizations indicating a decrease of the radical concentration with conversion. In all three copolymerizations the polymerization medium progressively turned from brown (color of  $Cu(I)(dNBpy)_2Br$ ) to green (color of

Cu(II)(dNBpy)<sub>2</sub>Br<sub>2</sub>, caused by accumulation of Cu(II) species. Both these observations suggest irreversible termination of polymeric radicals during polymerization. Again, the SEC's show that while the molecular weight distribution remains mono-modal throughout the homopolymerization of MMA, it becomes bimodal in the copolymerizations (Figure 8) and the fraction of the high molecular weight copolymer increases with increasing MPEGMA content. This high molecular weight copolymer may result from coupling of polymeric radicals as suggested by the observed accumulation of Cu(II) species as well as by the drop in radical concentration with conversion indicated by the curvature in the  $\ln[M_0]/[M_t]$  versus time plots.

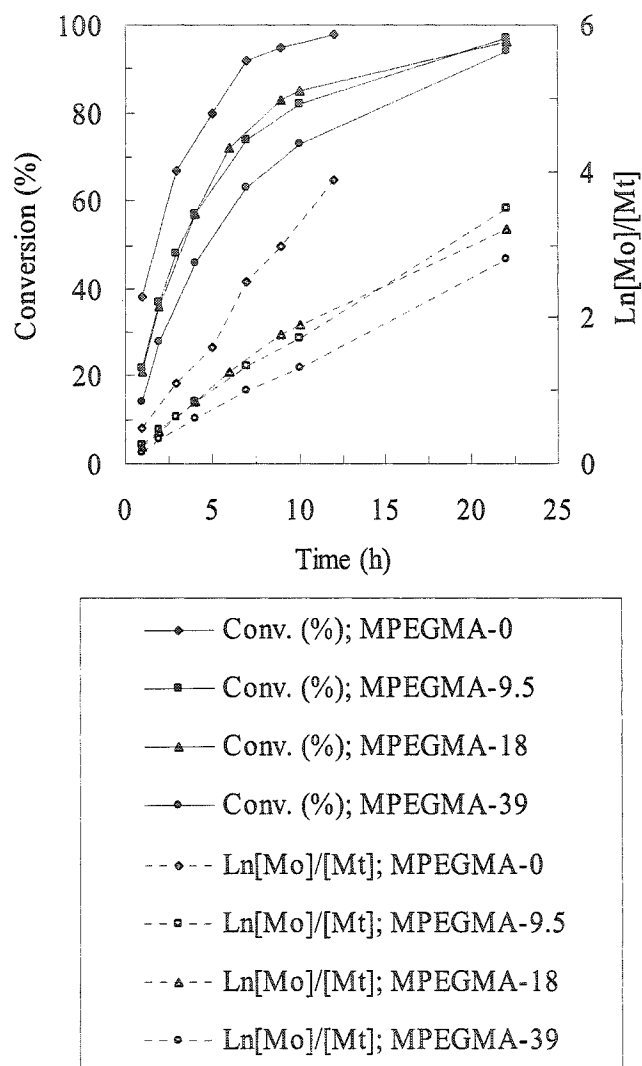
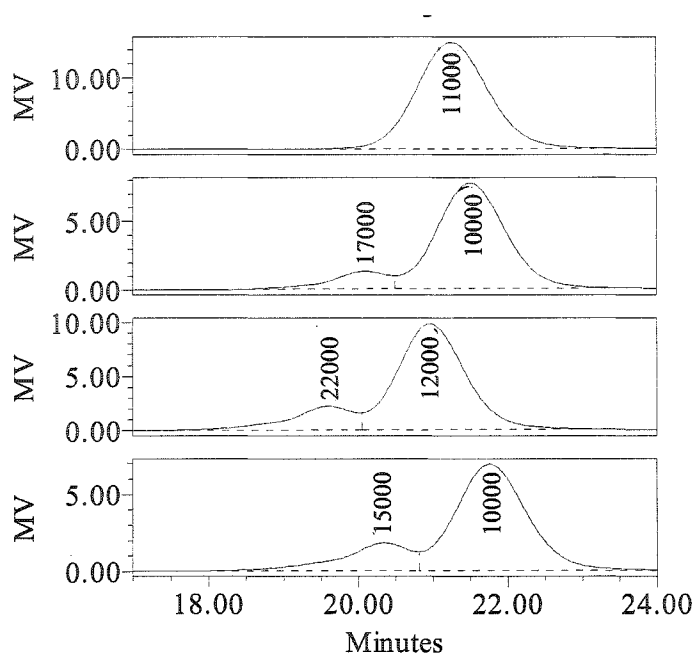


Figure 7. Kinetics of copolymerization of MMA and MPEGMA (mol% MPEGMA = 0, 9.5, 18 and 39) in DPE at 25 wt%. $[TSC]_0$ :  $[Cu(dNBpy)_2Br]_0 = 1:1$  at 70 °C.



**Figure 8.** Size exclusion chromatographs of, A. PMMA at 98% conversion; P(MMA-co-MPEGMA) containing, B. 9.5% MPEGMA at 97% conversion, high molecular weight peak (HMWP) is 12 % of total peak area; C. 18 mol% MPEGMA at 96% conversion, HMWP is 17 % of total peak area; D. 39 mol% MPEGMA at 94% conversion, HMWP is 20 % of total peak area. Chromatograms A – D are top to bottom of stack. The reaction conditions are those presented in Figure 5.

### *2.2.2 Partitioning of PegMA into the water phase.*

The encapsulation process involves partial synthesis of the amphiphilic terpolymer under suspension conditions. Monomer partitioning into the aqueous phase can alter the monomer concentration in the oil phase and directly affect the terpolymer composition and hence its polarity and morphology. MMA and DEGDMA have limited water solubility, while MPEGMA, containing ~5 ethylene glycol units is water soluble at room temperature. The partitioning of MPEGMA between oil and water phases at 70 °C in our experimental conditions was measured by equilibrating a 10% solution of MPEGMA in diphenyl ether with a four fold excess of water, separating the two phases while still at 70°C and determining the MPEGMA concentration in the water phase by aqueous size exclusion chromatography. Figure 9 shows the SEC of a 2% aqueous MPEGMA solution overlaid with an SEC of the aqueous phase of the partitioning experiment. Both chromatograms show five components. MPEGMA macromonomer ( $M_n \sim 300$  Da, Aldrich) consists of a mixture of compounds with an average of 4 to 5 ethylene oxide units in the pendant poly(ethylene glycol) monomethyl ether (MPEG) chain. Based on the retention time in aqueous size exclusion chromatography, we tentatively assigned the five component peaks at retention times (RT) of 47.9, 50.5, 53.8, 57.7 and 65.0 minutes to 7, 6, 5, 4, and 3 ethylene oxide units in the pendant MPEG chain. Electrospray mass spectrometry of the aqueous SEC fractions at RT = 50.5, 53.8, 57.7 and 65.0 minutes showed  $(M + Na)^+$  ion peaks at  $m/z = 387.2, 343.2, 299.1,$  and  $255.0$  respectively, confirming this assignment. Despite the difference in the length of the pendant MPEG chain, no significant difference in the partitioning of the MPEGMA components between

diphenyl ether and water was observed. Figure 10 therefore gives the combined MPEGMA calibration curve for 0.1% to 2% (w/w) MPEGMA in 0.1M NaNO<sub>3</sub> and 100 ppm NaN<sub>3</sub>.

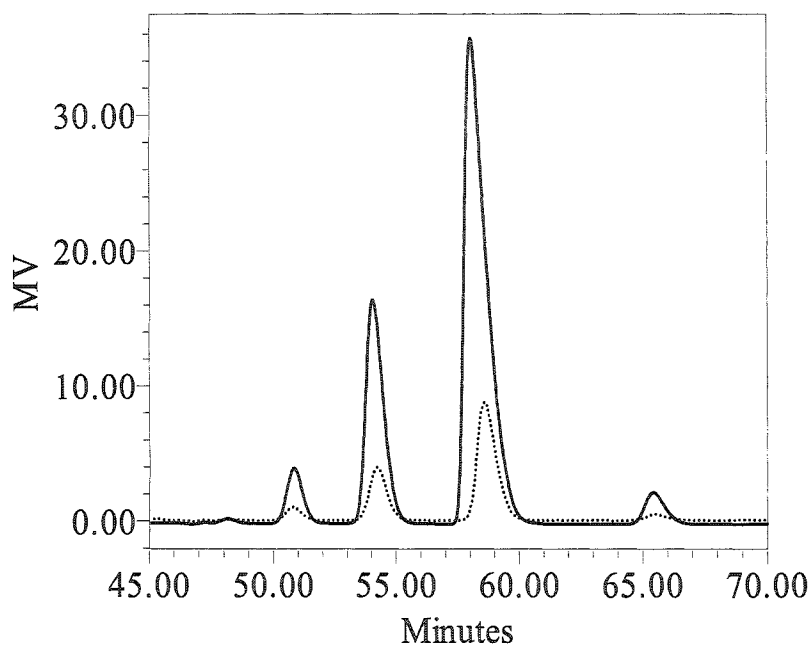


**Figure 9.** Aqueous Size Exclusion Chromatographs of (a) 2% (w/w) aqueous MPEGMA in 0.1M NaNO<sub>3</sub> and 100 ppm NaN<sub>3</sub> (solid line) (b) Aqueous phase of MPEGMA partitioning experiment done at 70 °C between 80 mL distilled water and 20 mL 10% (w/w) MPEGMA solution in diphenyl ether (dotted line). Injection volume: 30 µL. Elution solvent: Aqueous 0.1M NaNO<sub>3</sub> and 100 ppm NaN<sub>3</sub>; Flow rate: 0.8 mL/min; Column Temperature: 35 °C; Refractive Index detector temperature: 30 °C.

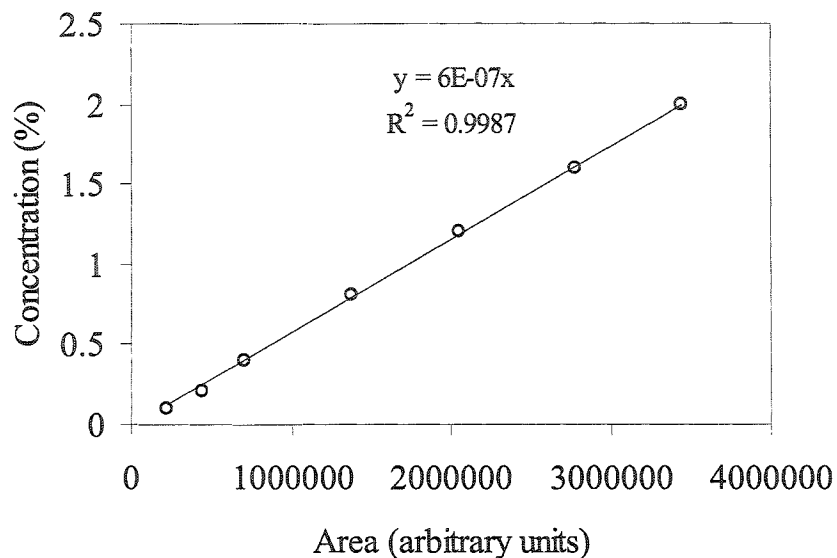


Figure 10. Aqueous Size Exclusion Chromatography calibration curve for MPEGMA based on total area under the five component peaks. Chromatographic conditions as in Figure 9.

This gave a combined MPEGMA partition coefficient,  $K_{oil/water} = 0.05$ , i.e., 18 % (w/w) MPEGMA partitions into the water phase in the suspension polymerizations using an oil : water ratio of 1:4.

### 2.2.3 Copolymer synthesis in suspension conditions.

Next, the ATRP synthesis of P(MMA-co-MPEGMA) was conducted, in part, in suspension conditions. The purpose of this experiment was first to show that P(MMA-co-MPEGMA) can be prepared by ATRP in suspension polymerization conditions and

secondly, to test to what degree copolymer composition would reflect the comonomer feed ratio. P(MMA-co-MPEGMA) containing 18 mol% MPEGMA was chosen for this experiment. The copolymer synthesis was initiated in DPE solution at 70 °C and allowed to proceed to a number average molecular weight of about 2500 Da, corresponding to about 25% conversion. At this point, the solution polymerization mixture was transferred under argon to a four-fold excess of water (containing 1% (w/w) PVA) at 70 °C and mechanically stirred yielding an oil in water suspension.

Results of this sequential solution-suspension polymerization for 25% monomer loading are presented in Figures 11 and 12. Figure 11 shows a slight enhancement of reaction rate in the suspension polymerization compared to the solution polymerization. This is attributed to the higher partitioning of Cu(II) catalyst species into the water phase relative to Cu(I) species.<sup>25</sup> Plots of  $\ln ([M_0]/[M_t])$  versus time are non-linear in both cases for reasons discussed above. The molecular weight increased linearly with conversion in both cases, however the polydispersity was significantly higher in the suspension polymerization (Figure 12). Higher polydispersity is consistent with higher radical concentration as this leads to more irreversible termination via radical coupling and disproportionation reactions. Like the solution polymerization product, the suspension polymerization product also contains high molecular weight material. In addition, the low molecular weight fraction itself has a higher polydispersity (Figure 13). This is consistent with higher radical concentrations in the suspension system. <sup>13</sup>C NMR was used to confirm that the water soluble comonomer, MPEGMA continues to be incorporated into the growing polymer chains in the oil phase even during the suspension

polymerization. NMR spectra of samples taken prior to, during and at the end of the suspension polymerization were recorded.

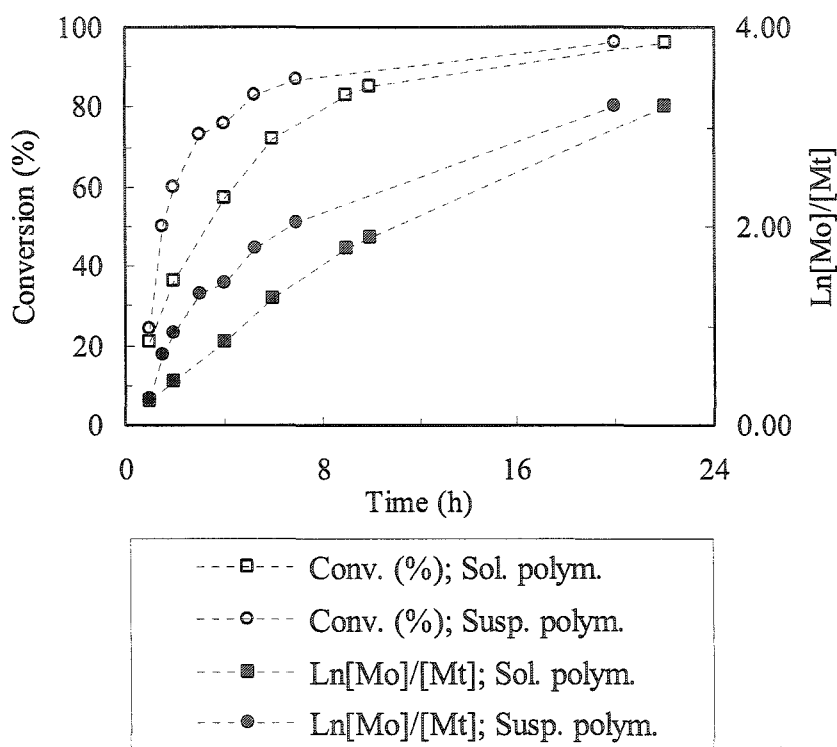


**Figure 11.** Kinetics of solution and suspension copolymerization of MMA and MPEGMA (18 mol% MPEGMA).  $[MMA]_0:[MPEGMA]_0:[TSC]_0:[Cu(dNBpy)_2Br]_0 = 60:14:1:1$ ; 25% total monomer in DPE; oil (monomers + DPE) /water ratio in suspension = 1:4; both polymerizations at 70 °C. The dashed lines are meant only as a guide.

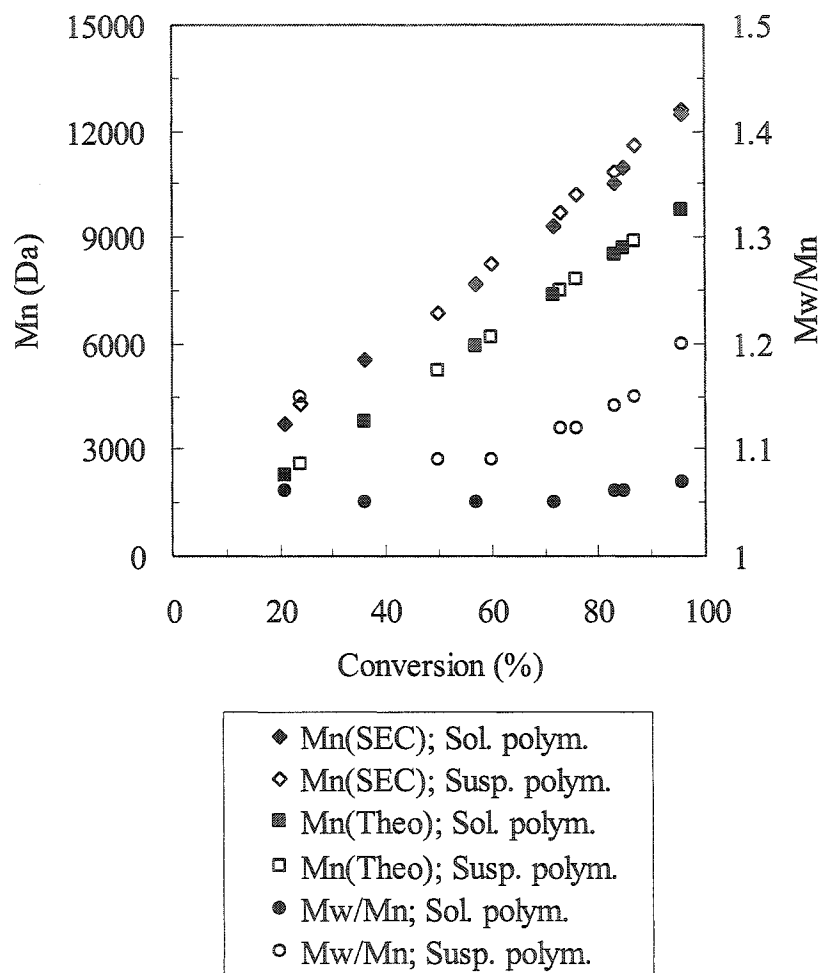


**Figure 12.** Plots of molecular weight and polydispersity versus conversion for solution and suspension copolymerization of MMA and MPEGMA (18 mol% MPEGMA).  $[MMA]_0:[MPEGMA]_0:[TSC]_0: [Cu(dNBpy)_2Br]_0 = 60:14:1:1$ ; 25% total monomer in DPE; oil (monomers + DPE) /water ratio in suspension = 1:4; both polymerizations at 70 °C.

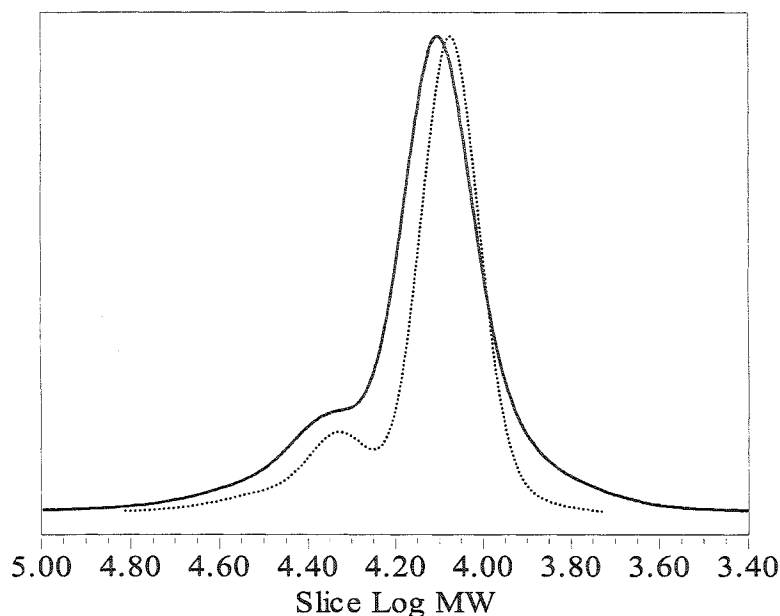


**Figure 13.** Molecular weight distributions of P(MMA-*co*-MPEGMA) (18 mol% MPEGMA) prepared by solution polymerization (dashed line) and solution-suspension polymerization (solid line) both at 96% conversion. Reaction conditions as in Figure 11.

Figure 14 shows the carbon-13 spectrum and the J-modulated spin sort spectra of the copolymer. The methoxy group of the MMA comonomer was assigned to  $\delta_C = 51.9$  ppm, while that of the MPEGMA comonomer was assigned to  $\delta_C = 59.2$  ppm based on the expected chemical shift values.  $^{13}\text{C}$  NMR spectra of a sample drawn just prior to transferring the organic reaction mixture to the aqueous phase, of samples from the end of the suspension polymerization and that of the corresponding copolymer prepared by solution polymerization (conversion = 100 %) were recorded.

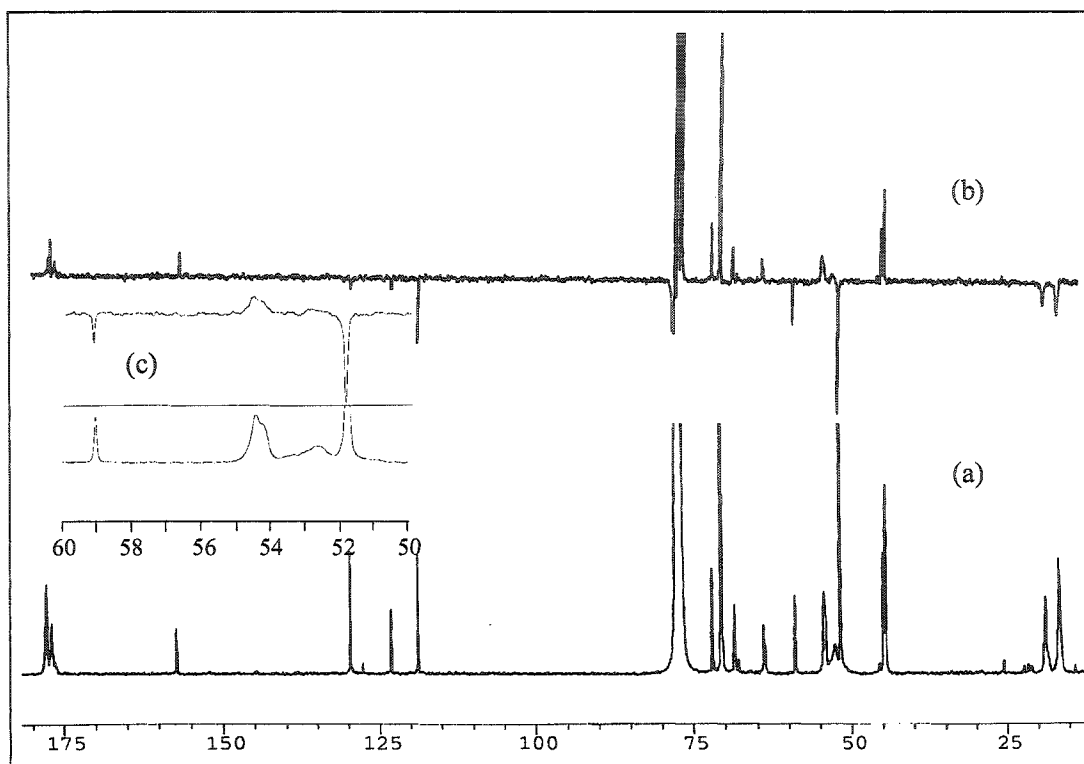


**Figure 14.** (a) Carbon-13 NMR of final P(MMA-*co*-MPEGMA) (18 mol% MPEGMA) in CDCl<sub>3</sub> at 125 MHz; (b) J-modulated spin sort spectrum of P(MMA-*co*-MPEGMA); (c) Expansion ( $\delta_C = 50 - 60$  ppm) of spectra (a) and (b).

Integration of the relevant peaks indicated only 12% MPEGMA content in all of the spectra, while the monomer feed in both the solution and suspension polymerizations contained 18.8 % MPEGMA. Addition of a paramagnetic relaxation agent, Cr(acac)<sub>3</sub>, yielded a MPEGMA content of 14% in both the solution polymerization and suspension polymerization samples. Finally, a gated decoupling experiment was run to reduce possible enhancement of the MMA methoxy carbon due to the nuclear Overhauser effect

and this indicated a MPEGMA content of 17 % for both the solution polymerization and suspension polymerization samples (Figure 15). This confirms that MPEGMA was indeed incorporated into the copolymer to the same extent in the suspension polymerization as it was in the solution polymerization.

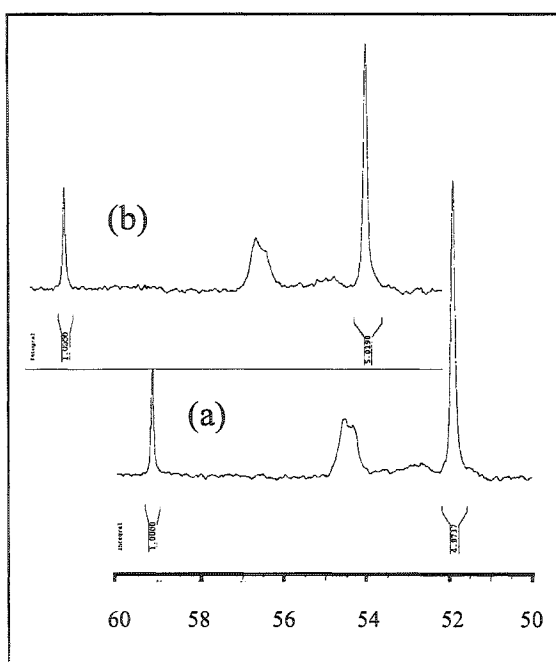


**Figure 15.** Carbon-13 spectra ( $\delta_C = 50 - 60$  ppm) of P(MMA-*co*-MPEGMA) in  $CDCl_3$  with  $Cr(acac)_3$  in a gated decoupling experiment; (a) prepared by solution polymerization at quantitative conversion; (b) 2 hour in suspension polymerization at 82 % conversion.

#### *2.2.4 Encapsulation of diphenyl ether.*

The encapsulation process consisted of three steps: synthesis of low molecular weight amphiphilic copolymers by solution ATRP; addition of the cross-linking monomer to the reaction solution followed by a 10 minute mixing period to ensure homogeneous distribution of the crosslinking monomer; and transfer of this oil phase to four times excess of 1% aqueous poly(vinyl alcohol) (PVA) in a baffled reactor. The resulting suspension was mechanically stirred with a propeller type mixer. A series of encapsulation experiments were performed to study the effect of the polymer composition on the internal morphology of the resultant polymer particles. Table 2 gives details of these formulations. In entries 1 – 4, the water soluble monomer was varied from 0 – 31 mol % while the crosslinker and the total polymer loading in the oil phase were held constant. The total polymer loading in the oil phase was held constant at  $30 \pm 4$  % (w/w) so that differences in particle morphology at a given conversion to polymer can be related directly to the interfacial properties of the forming polymer in the oil phase.

ATRP was used as the polymerization method in entries 1 to 4 while conventional free radical polymerization (CFRP) was used in control experiments (entries 5 and 6). Figure 16 shows an Environmental Scanning Electron Micrograph (ESEM) of the suspension polymer particles PegMA-15. The ESEM image showed that while most polymer particles maintained their spherical shape some were deflated and assumed a red blood cell like shape under the high vacuum in an ESEM sample preparation step. This suggests that the polymer particles have a hollow or less dense interior and a dense surface shell. Transmission Electron Microscopy (TEM) was conducted to determine the

internal morphology of the particles. Figure 17 presents the internal morphology of the ATRP particles and the CFRP particles. In the ATRP particles a clear transition in morphology is observed upon increasing the fraction of water soluble monomer in the oil phase from 0 mol % to 31 mol %. ATRP-MPEGMA-0 (Figure 17B) particles exhibit a matrix morphology. This suggests that PMMA crosslinked with DEGDMA has no tendency to migrate to the oil water interface as it precipitates from DPE. The ATRP-MPEGMA-8 particles also exhibit matrix morphology but a few hollow particles are observed.

Table 2. Reaction conditions for encapsulation of diphenyl ether using 20 mol% crosslinking monomer and an increasing MPEGMA:MMA ratio.<sup>a</sup>

Sample Code	Poly. phase (% w/w)	Mole % water sol. mon. MPEGMA	Conv. at transfer to susp. (% w/w)	Final conv. to polymer (% w/w)	Conv. to polymer of particle (% w/w)	Particle morph. (TEM) <sup>b</sup>
MPEGMA-0	32	0	57	100	82	Matrix
MPEGMA-8	34	8	35	98	83	Matrix
MPEGMA-15	33	15	57	100	98	Matrix
MPEGMA-31	31	31	46	99	92	Capsule
MPEGMA-0-C <sup>c</sup>	30	0	0	93	93	Matrix
MPEGMA-31-C <sup>d</sup>	28	31	0	98	79, 97	Matrix

<sup>a</sup> All suspension polymerizations were carried out using a 1:4 oil/water ratio at 70 °C using 1% PVA as suspension stabilizer (unless specified otherwise); <sup>b</sup> Transmission Electron Microscopy; <sup>c</sup> 3% methyl cellulose was used as suspension stabilizer; <sup>d</sup> 3% PVA was used as suspension stabilizer.

This suggests some tendency to migrate to the oil water interface but the predominant morphology still remains the matrix morphology (Figure 17C). ATRP-

MPEGMA-15 particles exhibit a macroporous interior suggesting a decrease in solubility of the crosslinked terpolymer in the DPE oil phase and the resulting tendency to yield macroporous structures.

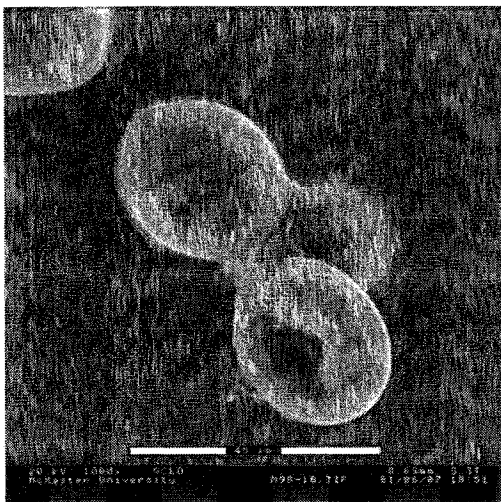


**Figure 16.** ESEM micrograph showing suspension polymer particles of P(MMA-co-MPEGMA) crosslinked with DEGDMA.  $[MMA]_0:[MPEGMA]_0:[DEGDMA]_0:[TSC]_0:[Cu(dNBpy)_2Br]_0 = 30 : 7 : 9 : 1 : 1$ ; 32% total monomer in DPE; suspension = 11% monomers + DPE and 1% PVA (rel. to water) at 70 °C.

In this case, the crosslinked terpolymer fills the entire volume of the suspension polymer particles, however, a macroporous interior characterized by internal voids and a relatively high density surface skin are observable. This morphology suggests that some amphiphilic terpolymer migrates to the oil water interface; the rest remains kinetically and enthalpically trapped in the interior of the particle to form a lower density matrix.

Upon further increasing the MPEGMA content to 31 mol% (ATRP-MPEGMA-31) the particles exhibit a matrix morphology characterized by large internal voids. The transition in particle morphology was monitored by determining the fraction of matrix (M), multi-hollow (MH) and capsular (C) particles in a population of 100 particles from four TEM sections for each of the MPEGMA-0, 8, 15 and 31 samples. At PEGMA-0, M:MH:C = 93:0:7; upon increasing the MPEGMA content to 8, 15 and 31 mol%, the ratios (M:MH:C = 78:16:6; 0:71:29; 0:53:47) showed increasing proportions of multi-hollow and capsular particles. To study the effect of having used a living polymerization, control experiments using conventional free radical polymerization were conducted. CFRP-MPEGMA-0 particles and CFRP-MPEGMA-31 (entries 5 and 6, Table 2) particles were prepared using similar monomer compositions and polymerization conditions as the analogous ATRP particles. In these experiments, initiator, monomers and solvent were mixed at room temperature and degassed by a stream of Argon for 30 minutes. This oil phase was then transferred to a four fold excess of water containing 3% stabilizer (PVA or methyl cellulose) at 70 °C in a reactor. The colloidal suspension in CFRP-MPEGMA-31 experiment was stable only when 3% PVA was used. Similarly, the CFRP-MPEGMA-0 suspension was stable only when 3% methyl cellulose was used. Thus, relative to the ATRP experiments, the CFRP suspension polymerizations needed higher viscosity of the water phase (obtained either through higher levels of PVA or through a more viscous stabilizer, methyl cellulose) to yield stable suspensions. This may be due to the additional stability of the ATRP suspension caused by the presence of

performed amphiphilic copolymer in the oil droplets. The suspension was mixed at 1000 rpm for 30 minutes and at 500 rpm thereafter.

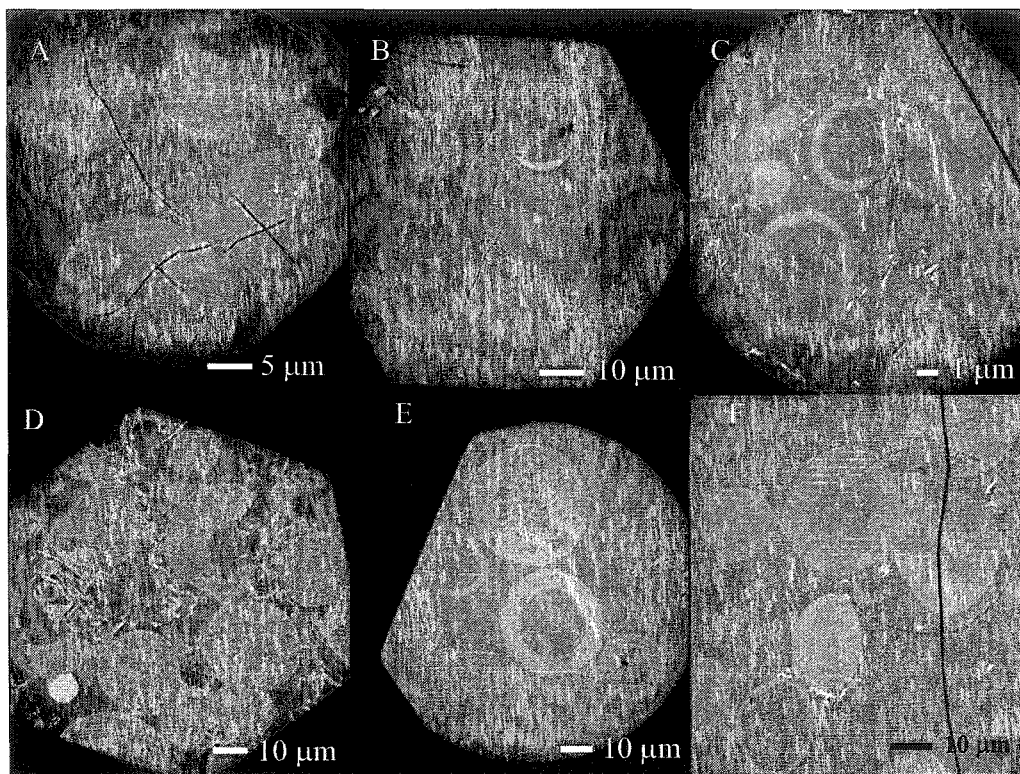


**Figure 17.** TEM micrographs showing internal morphology of suspension particles using DPE as oil phase: A. MPEGMA-0 particles (conv.= 90%) prepared by CFRP. B. MPEGMA-0 particles (conv.= 99%) prepared by ATRP. C. MPEGMA-8 particles (conv.= 98%) prepared by ATRP. D. MPEGMA-15 particles (conv.= 98%) prepared by ATRP. E. MPEGMA-31 particles (conv.= 92%) prepared by ATRP. F. MPEGMA-31 particles (conv.= 100%) prepared by CFRP.

Figure 17A and 17F show the internal morphology of the suspension particles obtained. Both compositions give similar predominantly matrix type particles (M:MH:C = 95:0:5 and 93:0:7 for CFRP-MPEGMA-0 and CFRP-MPEGMA-31, respectively). Thus, there is a clear difference in morphology between the ATRP particles and the CFRP particles.

ATRP of crosslinking monomers is characterized by low rates of polymerization, no observable auto acceleration, and higher conversion at gel point compared to conventional free radical crosslinking polymerization.<sup>21,22</sup> Since the crosslinking reaction is slow in ATRP, the forming gels phase separate from the core oil at a relatively slow rate. Thus, when the thermodynamically favored morphology is one in which the polymer engulfs the core oil, then there is more time for polymer in the oil to diffuse from the core to the oil water interface compared to gels made by the conventional free radical polymerization. Thus the use of ATRP has a kinetic advantage as compared to conventional free radical polymerization, yielding the observed hollow particles when ATRP is used, but matrix particles when CFRP is used.

### 2.3 Conclusions

In this work, increasing the polarity of the copolymer by increasing its MPEGMA content from 0 to 31 mol% led to a transition in suspension particle morphology from matrix to multi-hollow and capsular particles. In contrast, comparable suspension particles prepared by conventional free radical polymerization (CFRP) only showed matrix structure. Thus, we have shown that the use of a living/controlled polymerization characterized by slow rate of polymerization relative to polymer migration allows the thermodynamically favored morphology to be achieved (within the time frame of the

encapsulation experiment). This finding is particularly important for encapsulation of polar core oils because the driving force for polymer migration to oil water interface is relatively weak unless the polymer forming in the oil phase is highly polar. Preparing polar polymer in the oil phase by suspension polymerization is challenging because polar monomers are water soluble and therefore inherently not easily adaptable to polymerization by a suspension polymerization. As well, ATRP permits preparing suspension copolymers comprised of water soluble and oil soluble comonomers. In ATRP the majority of the polymer chains remain alive throughout the polymerization and so incorporation of water soluble monomer into the forming chains continues until all monomer is consumed. In our present work because only about 20% of the MPEGMA comonomer was found to partition into the water phase. The described advantage of living polymerization would be even more useful in case of larger or more polar MPEGMA analogs. In the following chapters we will explore this concept using a similar water soluble monomer that would partition more strongly into the water phase. Since the incorporation of water soluble monomer into the forming polymer in the oil phase is important in the encapsulation of polar core oils, the use of ATRP may then have both a kinetic and a thermodynamic advantage as compared to conventional free radical polymerization. We recognize that the presence of copper catalyst in the final suspension particles may be undesirable for certain applications. In future, use of lower concentrations of a more active catalyst or use of iron-based ATRP catalysts would address this concern. Also, our finding may be extended to any living free radical polymerization such as RAFT or nitroxide mediated polymerizations.

## 2.4 Experimental Section

**Materials.** Toluene sulfonyl chloride (TSC) (99+%), 4,4'-dinonyl-2,2'-dipyridyl (dNBpy) (97%), diphenyl ether (DPE) (99%) and poly(vinyl alcohol) (PVA) (80% hydrolyzed,  $M_w = 9000 - 10,000$  Da) were purchased from Aldrich and used as received. Methyl cellulose (Viscosity of 2% solution, 4000 cps) was purchased from Matheson Coleman and Bell and used as received. Copper (I) bromide (98%, Aldrich) was purified according to a published procedure.<sup>26</sup> Methyl methacrylate (99%), poly(ethylene glycol) monomethyl ether methacrylate ( $M_n \sim 300$  Da) and diethylene glycol dimethacrylate (95%) were obtained from Aldrich and passed over a basic alumina column to remove inhibitor. Neutral Alumina and basic Alumina (both Brockman Activity 1, mesh 60-325) were purchased from Fisher Scientific and used as received. Tetrahydrofuran (99%, Caledon Laboratories Limited) and pentane (98%, Caledon Laboratories Limited) were used as received.

**Solution ATRP in diphenyl ether.** CuBr (72.8 mg, 0.5 mmol), dNBpy (408.8 mg, 1.0 mmol), MMA (2.06 g, 21 mmol), MPEGMA (2.00 g, 7 mmol), and DPE (15.00 g) were placed in a 50 mL round bottom flask in a nitrogen filled glove bag and closed with a septum. TSC (95.3 mg, 0.5 mmol) was dissolved in a portion of MMA (940 mg, 9 mmol) in a vial equipped with a septum inside a nitrogen filled glove bag. The monomer and catalyst solution was degassed in a stream of argon for 30 minutes and then transferred to an oil bath at 70 °C. The initiator solution (1 mL) was introduced in one aliquot via a syringe that had been previously degassed with a stream of argon for 3 minutes. Samples (1 mL) for Size Exclusion Chromatography (SEC) and conversion

measurements were drawn periodically via a syringe that had been previously degassed with a stream of argon for 3 minutes. SEC samples (0.2 mL) were prepared by diluting with THF (1 mL) and passing over a neutral alumina column to remove catalyst. Conversion was determined gravimetrically. This involved precipitation (twice) of 0.8 mL samples in 18-19 mL cold pentane in 20 mL vials; the vials were then centrifuged at 3500 rpm, the supernatant decanted and the precipitate vacuum dried at 60 °C to constant weight. The polymerization proceeded to quantitative conversion (see Figures 1, 2 and 3), with 17 mol% PegMA (by  $^{13}\text{C}$  NMR) incorporated in the copolymer.

**Suspension ATRP.** A solution polymerization having the same composition as described above was initiated at 70 °C with addition of initiator solution at once in one aliquot. At 1 hour reaction time (~25% conversion) this prepolymer solution was transferred via canula to a Büchi Miniclave Drive 100 mL glass reactor containing distilled, deionised water (80 mL, 1% (w/w) PVA) that had been previously degassed in a stream of argon for 1 hour and heated to 70 °C. The reactor was equipped with appropriate baffles to break the vortex caused by mixing. The suspension was stirred mechanically at 1000 rpm for 30 minutes and at 500 rpm subsequently until the end of suspension polymerization, using a propeller type mixer. Aqueous suspension samples (5 mL) for conversion measurement and SEC analysis were drawn periodically *via* syringe. These samples were then centrifuged at 3500 rpm giving an organic bottom layer and aqueous supernatant that was carefully decanted. The wet organic layer was then freeze dried. The freeze dried samples, now containing diphenyl ether, unreacted monomer, and copolymer were dissolved in THF (5 mL) by rolling the vials gently in a modified hot

dog roller at room temperature for 24-48h. The THF solutions were precipitated in pentane (15 mL), centrifuged at 3500 rpm, decanted (this sequence was carried out twice) and vacuum dried at 70 °C to constant weight. The polymerization proceeded to 96% conversion (see Figures 7 and 8) with 17 mol% MPEGMA ( $^{13}\text{C}$  NMR) incorporated in copolymer.

**Encapsulation of diphenyl ether in crosslinked terpolymer.** A solution copolymerization comprised of the same composition was initiated as described above. At 57% conversion the crosslinking monomer, DEGDMA (2.22 g, 9 mmol) was added and the mixture was stirred for 10 minutes before being transferred via canula to a 100 mL glass reactor containing distilled, deionised water (80 mL, 1% PVA) that had been previously degassed in a stream of argon for 1 hour. The reactor was equipped with a set of baffles to prevent vortexing. The suspension was stirred mechanically at 1000 rpm for 30 minutes and at 500 rpm subsequently until the end of suspension polymerization using a propeller type mixer. Aqueous suspension samples (5 mL) for conversion measurement were drawn periodically by syringe. The suspension samples were freeze dried. The freeze dried samples, now containing diphenyl ether, unreacted monomer, and crosslinked terpolymer were swollen in THF (5 mL) by rolling the vials gently in a modified hot dog roller at room temperature for 24-48h. The swollen particles were precipitated in pentane (15 mL), centrifuged at 3500 rpm, decanted (this sequence was done twice) and vacuum dried at 70 °C to constant weight. The conversion to crosslinked polymer was quantitative. The morphology of the crosslinked particles is shown in Figure 16. To determine conversion to particles, the precipitated polymer particles that

contain both sol and gel fractions were swollen in 18-19 mL THF by rolling in a hot dog roller for 12-24 hours and then centrifuged at 3500 rpm. The supernatant was decanted. This procedure was repeated twice before the gel fraction was vacuum dried to constant weight at 60 °C. Conversion to gel fraction was 98%.

**Measurements.** The identities of the components in poly(ethylene glycol) monomethyl ether methacrylate macromonomer were confirmed by positive ion Electrospray Mass Spectrometry using a triple quadrupole Micromass Ultima instrument. Polymer molecular weight was determined by size exclusion chromatography using a Waters 515 HPLC Pump connected to three Waters 5  $\mu\text{m}$  (7.8 X 300 mm) Styragel (HR2, HR3 and HR4) linear columns (exclusion limits 500-20,000 Da, 500-30,000 Da, and 5000-600,000 Da) and a Waters 2414 Refractive Index Detector. The HPLC pump was equipped with a Water 717 plus Autosampler and computer controlled using the Millennium 32 Chromatography Manager. The column and detector temperature were set at 40.0 °C and 35.0 °C, respectively. Tetrahydrofuran was used as elution solvent (flow rate = 1 mL/min), and narrow disperse linear polystyrene standards were used for calibration. The surface and internal morphologies were determined using a Phillips-2020 Environmental Scanning Electron Microscope (ESEM) and a JEOL 1200EX Transmission Electron Microscope (TEM), respectively. ESEM samples were prepared by depositing dilute aqueous dispersions of polymer particles on cover glass slips fixed to aluminum stubs, drying at room temperature and sputter coating with a 5 nm layer of gold. For TEM analysis, polymer particles were embedded in Spurr epoxy resin and microtomed to ~ 100 nm thickness. Optical microscopy was performed using an Olympus

BH-2 microscope, equipped with a Kodak DC 120 Digital Camera. The  $^1\text{H}$  and  $^{13}\text{C}$  NMR spectra were recorded in  $\text{CDCl}_3$  at 300 MHz and 75 MHz respectively on a Bruker AV-300 Instrument.

**Acknowledgement.** We acknowledge NSERC and 3M Canada for funding this research and Dr. Nicholas Burke and Wen Hui Li for valuable suggestions. We also thank Lisa M. Croll and Anna Shulkin for their help with Electron Microscopy.

## References

- (1) Arshady, R. *Microspheres, Microcapsules Liposomes* **1999**, *1*, 1461-1732.
- (2) Beestman, G. B.; Deming, J. M. U.S. Patent 4,417,916, 1983.
- (3) Arshady, R. *J. Microencapsulation* **1989**, *6* (1), 13-28.
- (4) Kasai, K.; Hattori, M.; Takeuchi, H.; Sakurai, N. U.S. Patent 4,908,271, 1990.
- (5) McDonald, C; Chonde, Y.; Cohrs, W. E.; MacWilliams, D. C. U.S. Patent 4,973,670, 1990.
- (6) McDonald, C. J.; Bouck, K. J.; Chaput, A. B.; Stevens, C. J.; *Macromolecules* **2000**, *33*, 1593-1605.
- (7) Torza, S.; Mason, S., G. *J. Colloid and Interface Sci.* **1970**, *33* (1), 67.
- (8) Sundberg, D. C.; Casassa, A. P.; Pantazopoulos, J.; Muscato, M.R. *J. Appl. Polym. Sci.* **1990**, *41*, 1425.
- (9) Berg, J.; Sundberg, D.; Kronberg, B. *J. Microencapsulation* **1989**, *6* (3), 327.
- (10) Kasai, K.; Hattori, M.; Takeuchi, H.; Sakurai, N. US Patent 4,798,691, 1989.
- (11) Itou, N.; Masukawa, T.; Ozaki, I.; Hattori, M., Kasai, K.; *Colloids Surf. A: Physiochem. Eng. Aspects* **1999**, *153*, 311-316.
- (12) Okubo, M.; Minami, H.; Yamashita, T. *Macromol. Symp.* **1996**, *101*, 509-516.
- (13) Okubo, M.; Minami, H.; *Colloid Polym. Sci.* **1996**, *274*, 433-438.

- (14) Okubo, M.; Minami, H. *Colloid Polym. Sci.* **1997**, *275*, 992-997.
- (15) Okubo, M.; Konishi, Y.; Minami, H. *Colloid Polym. Sci.* **1998**, *276*, 638-642.
- (16) Okubo, M.; Konishi, Y.; Minami, H. *Colloid Polym. Sci.* **2000**, *278*, 659-664.
- (17) Okubo, M.; Konishi, Y.; Minami, H. *Colloid Polym. Sci.* **2001**, *279*, 519-523.
- (18) Okubo, M.; Konishi, Y.; Inohara, T.; Minami, H. *Macromol. Symp.* **2001**, *175*, 321-328.
- (19) Patten, T. E.; Matyjaszewski, K.; *Acc. Chem. Res.* **1999**, *32*, 895-903.
- (20) Patten, T. E.; Xia, J.; Abernathy, T.; Matyjaszewski, K.; *Science* **1996**, *272*, 866-868.
- (21) Yu, Q.; Zeng, F.; Zhu, S.; *Macromolecules* **2001**, *34*, 1612-1618.
- (22) Jiang, C.; Shen, Y.; Zhu, S.; Hunkeler, D.; *J. Polym. Sci., Part A: Polym. Chem.* **2001**, *39*, 3780-3788.
- (23) Wang, J.; Grimaud, T.; Matyjaszewski, K.; *Macromolecules* **1997**, *30*, 6507-6512.
- (24) Gaynor, S. G.; Qiu, J.; Matyjaszewski, K.; *Macromolecules* **1998**, *31*, 5951-5954.
- (25) Qiu, J.; Pintauer, T.; Gaynor, S. G.; Matyjaszewski, K.; Charleux, B.; and Vairon, J. P.; *Macromolecules* **2000**, *33*, 7310-7320.
- (26) Keller, R. N.; Wycoff, H. D. *Inorg. Synth.* **1946**, *2*, 1-4.

## CHAPTER 3.

In this chapter, analysis and purification of commercially available poly(ethylene glycol) monomethacrylate (PEGMA) is described. Unlike poly(ethylene glycol) monomethyl ether methacrylate (MPEGMA), described in Chapter 2, the pendant PEG chain of PEGMA bears a hydroxyl end group. The Atom Transfer Radical homopolymerization of PEGMA and its copolymerization with methyl methacrylate (MMA) is developed in solution conditions. The copolymers were found to be water soluble and to exhibit Lower Critical Solution Temperatures. The broader objective here is to prepare copolymers of oil soluble MMA and water soluble PEGMA in solution conditions. These results would then form the basis of evaluation of suspension copolymerizations that are described in Chapter 4.

**Well defined Amphiphilic Thermosensitive Copolymers based on Poly(ethylene glycol) monomethacrylate and Methyl methacrylate prepared by Atom Transfer Radical Polymerization**

(Mir Mukkaram Ali and Harald D. H. Stöver, *Macromolecules* 2004, 37 (14), 5219-5227)

**ABSTRACT**

Amphiphilic homopolymers of the hydroxy-functional macromonomer poly(ethylene glycol) monomethacrylate (PEGMA) and its copolymers with methyl methacrylate (MMA) were prepared by Atom Transfer Radical Polymerization. Commercially available PEGMA (Aldrich) contains non-functional poly(ethylene glycol) (PEG), mono-functional PEGMA, and di-functional poly(ethylene glycol) dimethacrylate (PEGDMA) in a 1:3:1 ratio as analyzed by HPLC. A solvent extraction procedure yielded a PEGMA enriched mixture (PEG : PEG-MA : PEGDMA = 5:92:3) with PEGMA  $M_n$  values of 480 Da and 410 Da based on HPLC and  $^1\text{H}$  NMR respectively. ATRP homopolymerization of this purified PEGMA in the hydroxyl bearing solvents, cyclohexanol and ethanol ( $\epsilon = 16.4$  and  $25.3$ , respectively) yielded well defined homopolymers ( $M_w/M_n < 1.1$ ). On the other hand, ATRP copolymerizations of MMA with content 10, 18, 24, 30, 40 mol % PEGMA yielded best results in non-hydrogen bonding diphenyl ether ( $\epsilon = 3.37$ ). The homopolymers, and copolymers containing more than 24 mol% (57 wt.%) PEGMA, were water-soluble and exhibited sharp lower critical solution temperatures (LCST) that increased with increasing PEGMA content as expected. Unlike similar PEGMA based amphiphilic copolymers prepared by

conventional free radical polymerizations, the ATR polymerizations reported here proceeded to high conversions (60 – 100%) and yielded well-defined polymers ( $M_w/M_n = 1.1 - 1.15$ ) with no gel fraction that remained linear and water-soluble after storage in ambient conditions for several months.

### 3.1 Introduction

Atom Transfer Radical Polymerization (ATRP) is a recent living/controlled radical polymerization method<sup>1,2</sup> that has been developed extensively owing to its tolerance of a wide range of functional groups, and to the relatively non-stringent experimental conditions required.<sup>3,4</sup> In ATRP radicals are formed by a redox transfer of a halide atom from a initiator halide to a transition metal based catalyst. The formed radicals add monomer and react with the oxidized metal catalyst to reform a halogen-capped dormant species. The resulting active radical/dormant species equilibrium lies predominantly on the side of the dormant species, thereby maintaining a very low equilibrium radical concentration, which minimizes chain termination. Furthermore, a fast dynamic equilibrium between the active radical and halide capped dormant species ensures that all growing chains get an equal opportunity to add monomer units, resulting in low polydispersity polymer. While ATRP is usually employed for the preparation of well defined polymers and block copolymers, immobilizing ATRP initiators on substrates allows growth of polymer chains from surfaces via the “grafting from” approach, thereby imparting desirable properties to the substrate. Immobilization of conventional free radical polymerization initiators yields high graft densities, but results in poor control of

molecular weight and polydispersity.<sup>5,6</sup> ATRP grafting offers better control over these properties<sup>7,8,9</sup> and enables block copolymer grafting.<sup>10</sup>

One particularly interesting class of polymers to be grafted from surfaces are thermally responsive polymers (TRP's). The development of ATRP to form novel TRPs in solution conditions is a necessary precursor for a myriad of potential surface grafting applications and is the subject of this work. TRPs have been the subject of intensive research in recent years<sup>11</sup> due to their potential in diverse areas such as controlled drug delivery,<sup>12,13</sup> reversible surfactants,<sup>14,15</sup> chromatography<sup>16</sup> and the development of new methods of fighting microbial and other bio-fouling of surfaces.<sup>17</sup> Temperature induced swelling and shrinking of drug-loaded TRP macrogels may be used to absorb/release drugs.<sup>18</sup> Similarly, release from microcapsules may be thermally modulated by either surface coating the capsule<sup>19</sup> or by filling the cavities in the capsule with TRPs.<sup>20</sup> As well, surface grafting of TRP's on porous membranes using living polymerization techniques has been explored.<sup>21</sup>

Brush shaped copolymers based on poly(ethylene glycol) monomethyl ether methacrylates exhibiting soft elastomeric properties have recently been prepared by ATRP.<sup>22,23</sup> Also, similar methoxy capped oligoethylene glycol methacrylates were polymerized by living anionic polymerization yielding well-defined thermoresponsive comb shaped polymers.<sup>24</sup> However, well defined hydroxyl-bearing oligoethylene glycol analogues have only been prepared via ionic polymerization of hydroxyl-protected monomers.<sup>25</sup>

We report the solution Atom Transfer Radical homopolymerization of hydroxyl-bearing poly(ethylene glycol) monomethacrylate and its copolymerization with methyl methacrylate in organic solvents, using toluene sulfonyl chloride as initiator and Cu(I)Br/alkyl bipyridine as catalyst. The polymerizations yielded narrow disperse polymers ( $M_w/M_n < 1.15$ ) with molecular weights reflecting the monomer to initiator ratio. Unlike conventional free radical polymerizations of PEGMA which yield crosslinked gels in the absence of added chain transfer agents and typically crosslink during storage,<sup>26</sup> the ATRP products remained linear and soluble over several months of storage. The homopolymer, and copolymers containing more than 57 mol% PEGMA, are water-soluble. The water-soluble copolymers exhibit lower critical solution temperatures that could be varied with the comonomer ratio. This work has potential for the development of smart materials based on substrates bearing surface grafted thermo-responsive polymer.

## 3.2 Results and discussion

### 3.2.1 HPLC analysis of PEGMA macromonomer.

PEGMA is commercially available from Aldrich and Polysciences Inc., and is quoted as having a  $M_n$  of 360 Da and 285 Da ( $n = 200$ ; where “n” is the molecular weight of the pendant poly(ethylene glycol) chain), respectively. As PEGMA is commonly prepared by methacrylate functionalization of poly(ethylene glycol) (PEG), we anticipated that the macromonomer would be comprised of the non-functional PEG, mono-functional poly(ethylene glycol) monomethacrylate (PEG-MA) and di-functional, poly(ethylene glycol) dimethacrylate (PEG-DMA). This is in contrast to poly(ethylene

glycol) monomethyl ether methacrylate (MPEGMA) which is prepared by reaction of PEG oligomers (bearing a non-reactive methoxy terminus on one end and a reactive hydroxyl group on the other) with methacryloyl chloride in a quantitative reaction, and hence only contains the mono-functional homologues.<sup>27</sup> PEGMA was analyzed using a reverse phase C-18 HPLC column and methanol : water (1:1) as mobile phase. The peaks in the overlaid chromatograms (Figure 1) were analyzed by LC-MS and those in the 5 – 8 minute retention time region were assigned to zero-functional PEG containing 2 to 21 ethylene oxide units (Z2 - Z21), 8 to 30 minute range to mono-functional PEG-MA containing 1 to 27 ethylene oxide units (M1 – M27), and 30 to 150 minute range to di-functional PEG-DMA containing 2 – 30 ethylene oxide units (D2 –D30). The mass spectral data is presented in Table 1.

Table 1. LC-MS data for crude PEGMA

	Mono-func.	Compds.	Di-func.	Compds.	Non-func.	Compds.
n	FW	M+1*	FW**	M+1*	FW**	M+1*
1	130.14	<b>131.14</b>	<i>198.21</i>	199.21	<i>62.07</i>	63.07
2	174.19	<b>175.19</b>	242.26	<b>243.26</b>	106.12	<b>107.12</b>
3	218.24	219.24	286.31	<b>287.31</b>	150.17	<b>151.17</b>
4	262.29	<b>263.29</b>	330.36	<b>331.36</b>	194.22	<b>195.22</b>
5	306.34	<b>307.34</b>	374.41	<b>375.41</b>	238.27	<b>239.27</b>
6	350.39	<b>351.39</b>	418.46	<b>419.46</b>	282.32	<b>283.32</b>
7	394.44	<b>395.44</b>	462.51	<b>463.51</b>	326.37	<b>327.37</b>
8	438.49	<b>439.49</b>	506.56	<b>507.56</b>	370.42	<b>371.42</b>

9	482.54	<b>483.54</b>	550.61	<b>551.61</b>	414.47	<b>415.47</b>
10	526.59	<b>527.59</b>	594.66	<b>595.66</b>	458.52	<b>459.52</b>
11	570.64	<b>571.64</b>	638.71	<b>639.71</b>	502.57	<b>503.57</b>
12	614.69	<b>615.69</b>	682.76	<b>683.76</b>	546.62	<b>547.62</b>
13	658.74	<b>659.74</b>	726.81	<b>727.81</b>	590.67	<b>591.67</b>
14	702.79	<b>703.79</b>	770.86	<b>771.86</b>	634.72	<b>635.72</b>
15	746.84	<b>747.84</b>	814.91	<b>815.91</b>	678.77	<b>679.77</b>
16	790.89	<b>791.89</b>	858.96	<b>859.96</b>	722.82	<b>723.82</b>
17	834.94	<b>835.94</b>	903.01	904.01	766.87	<b>767.87</b>
18	878.99	<b>879.99</b>	947.06	948.06	810.92	<b>811.92</b>
19	923.04	<b>924.04</b>	991.11	992.11	854.97	<b>855.97</b>
20	967.09	<b>968.09</b>	1035.16	1036.16	899.02	<b>900.02</b>
21	1011.14	1012.14	1079.21	1080.21	943.07	<b>944.07</b>
22	1055.19	1056.19	1123.26	1124.26		
23	1099.24	1100.24	1167.31	1168.31		
24	1143.29	1144.29	1211.36	1212.36		
25	1187.34	1188.34	1255.41	1256.41		
26	1231.39	1232.39	1299.46	1300.46		
27	1275.44	1276.44	1343.51	1344.51		
28			1387.56	1388.56		
29			1431.61	1432.61		
30			1475.66	1476.66		

\* Components shown in bold were detected in the mass spectrum while the others were assigned by extrapolation;

\*\* Components in italics are not present in the LC-MS but have been retained here for reference.

The chromatograms in Figure 1 were acquired using a refractive index detector. Since the refractive index of the zero, mono, and di-functional homologs are similar (Table 2), the areas under the peaks were used to quantitatively determine the composition of PEGMA. This indicated that the composition of crude PEGMA is PEG : PEGMA : PEGDMA = 19 : 60 : 21, and yielded a number average molecular weight ( $M_n$ ) of 453 Da for mono-functional components and 466 Da for the mixture of mono- and di- functional components. The  $M_n$  assigned by the supplier (~360 Da) therefore significantly differs from the average values obtained here from HPLC.

Table 2. Refractive indices of some oligo ethylene glycols and dimethacrylate derivatives

Compound	Refractive Index (Aldrich)
Ethylene glycol	1.431
Diethylene glycol	1.446
Triethylene glycol	1.455
Poly(ethylene glycol)	1.454
Ethylene glycol dimethacrylate	1.454
Diethylene glycol dimethacrylate	1.458
Triethylene glycol dimethacrylate	1.46
Poly(ethylene glycol) dimethacrylate ( $M_n = 330$ Da)	1.463

### *3.2.2 Isolation and analysis of mono-functional PEG-MA.*

PEG-MA was isolated from the mixture by extraction of its aqueous solution with diphenyl ether (DPE) to selectively remove the PEG-DMA followed by an extraction of the resulting aqueous phase with a 3:1 mixture of methylene chloride and hexanes ( $\text{CH}_2\text{Cl}_2/\text{C}_6\text{H}_{14}$ ) following a literature procedure<sup>28</sup> to partition the PEG-MA almost entirely into the organic phase from which it was recovered by solvent evaporation. Integration of the area under the peaks in the chromatograms of crude and purified PEGMA (Figure 1) showed that purified PEGMA is composed of PEG : PEG-MA : PEG-DMA = 5 : 92 : 3 (19 : 60 : 21 in crude PEGMA). The area under the component peaks was also used to calculate the number average molecular weight of purified PEGMA; and yielded a  $M_n$  of 480 Da for mono-functional components and 510 Da for the mixture of mono- and di- functional components. The  $M_n$  values were further verified by  $^1\text{H}$  NMR. The ratio of the peak areas of the vinyl protons ( $\delta_{\text{H}} = 6.1$  and  $5.6$  ppm) to that of the methylene protons in the pendant PEG chain ( $\delta_{\text{H}} = 4.3$  and  $3.6$  ppm) in the  $^1\text{H}$  NMR spectrum of purified PEGMA indicated an average of 7.3 ethylene oxide units in the pendant PEG chain or a formal  $M_n$  of 410 Da.

### *3.2.3 ATRP synthesis of poly(poly(ethylene glycol) monomethacrylate) (P(PEGMA)).*

Good control over polymer molecular weight and polydispersity in ATRP depends upon fast initiation relative to propagation, a low radical concentration and a fast dynamic equilibrium between the active and dormant radicals. In general, arenesulfonyl

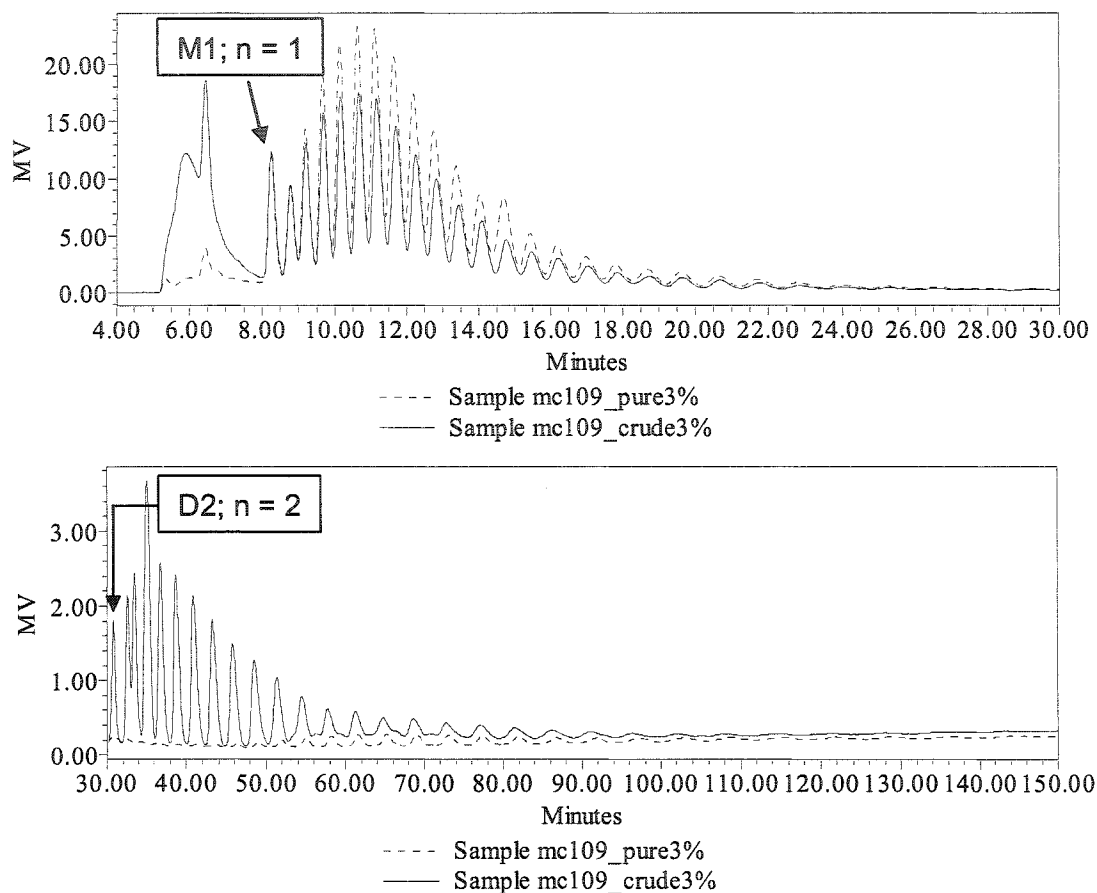


**Figure 1.** Overlaid HPLC chromatograms of crude (solid line) and purified (dotted line) PEGMA (Aldrich). Chromatographic conditions as follows: reverse phase C-18 column; mobile phase: methanol/water = 1:1; flow rate = 0.5 mL/minute; column temp.= 35 °C; refractive index detector temp.= 30 °C; sample conc. = 3 wt.%; injection vol. = 20  $\mu$ L; run time = 150 minutes. Non-functional PEG components (Z2–Z21), mono-functional PEG-MA components (M1–M27) and di-functional PEG-DMA (D2–D30) elute in the 5-8, 8 – 30 and 30 – 150 minute ranges respectively.

Table 3. Dielectric constants and solubility parameters of some ATRP solvents

Solvent	Solubility Parameter <sup>a</sup> /MPa <sup>1/2</sup>	Dielectric constant ( $\epsilon$ ) <sup>b</sup> (T / K)
p- xylene	18	2.27 (293.2)
Diphenyl ether	20.9	3.73 (283.2)
n-Butyl acetate	17.4	5.07 (293.2)
Cyclohexanol	22.5	16.4 (293.2)
Ethanol	26.6	25.3 (293.2)

<sup>a</sup> Source: Grulke, E.A. In Solubility Parameter values. *Polymer Handbook*, 4<sup>th</sup> edition.; John Wiley and Sons: New York, 1999; Table 7, p VII/688. <sup>b</sup> Source: Wohlfarth, C. In *CRC Handbook of Chemistry and Physics*, 76<sup>th</sup> edition.; CRC Press: Boca Raton, 1995-1996; p 6-159.

halides in conjunction with Cu (I) halide / bipyridine catalysts serve as efficient ATRP initiators for methacrylates,<sup>29</sup> with initiation rates being four orders of magnitude higher than the propagation rate and near 100% initiation efficiency. We have previously demonstrated the efficacy of this system for the copolymerization of MMA with poly(ethylene glycol) monomethyl ether methacrylate (MPEGMA).<sup>27</sup>

Thus toluene sulfonyl chloride (TSC) was used as the ATRP initiator with a catalyst based on copper (I) bromide and 4,4'-dinonyl-2,2'-dipyridyl. The solvent polarity can significantly affect the position of the active radical - dormant species equilibrium and is therefore a key parameter in determining the success of an ATRP reaction.<sup>30,31,32</sup> Accordingly, we studied the ATR homopolymerization of PEGMA in a series of organic solvents of varying polarity and hydrogen bonding characteristics (Table 3). Bo *et al.*<sup>26</sup> studied the conventional free radical copolymerization of PEGMA (Mn ~ 400 Da) with

MMA and ethyl hexyl acrylate and reported that the formation of crosslinked gels could be avoided only by conducting the polymerizations below 30 % monomer loading and in the presence of chain transfer agents. Crosslinking was attributed to chain transfer to polymer. In view of Bo's report, we conducted all homopolymerizations and copolymerizations at 25 wt.% monomer loading. We believe the crosslinking observed by Bo *et al.* was in part due to chain transfer to pendant PEG moieties as concluded by the authors but may also have been due to significant quantities of difunctional crosslinking monomer present in their polymerizations.

Diphenyl ether (DPE) and xylene (XYL) provide a pair of aprotic solvents that differ significantly in their overall polarity (solubility parameters,  $\delta_{\text{XYL}} = 18.0 \text{ MPa}^{1/2}$  and  $\delta_{\text{DPE}} = 20.9 \text{ MPa}^{1/2}$ ; dielectric constants,  $\epsilon_{\text{XYL}} = 2.27$ ;  $\epsilon_{\text{DPE}} = 3.73$ ). Furthermore, we have previously shown that DPE and XYL are good solvents for ATRP of methyl methacrylate.<sup>33</sup> Hence, the ATRP homopolymerization of PEGMA was first attempted in these two solvents. Both MMA and PEGMA are methacrylates, but with three key differences. First, PEGMA being a macromonomer, suffers from having a low concentration of polymerizable groups in the system, plus possibly steric hindrance during the monomer addition as well as the atom transfer reactions with the catalyst. The former could lower the polymerization rate and the latter could alter the position of the active radical / dormant species equilibrium. Second, PEGMA is a more polar macromonomer than MMA and bears a hydroxyl group, both properties that are known to increase the activation rate constant in ATRP.<sup>3,5</sup> Third, PEGMA bears a pendant ether moiety that imparts it coordination ability. Haddleton *et al.*<sup>34</sup> observed an unusually high

rate of polymerization of methoxy terminated poly(ethylene glycol) methacrylate and attributed it to complexation of the oxyethylene groups to the copper in a dynamic competition with the alkyl-2-pyridylmethanimine ligand, resulting in a more active catalyst. Thus, although we have previously demonstrated that ATRP of MMA in DPE and XYL is successful, the PEGMA system may behave differently.

Figures 2 and 3 give the molecular weight and molecular weight distribution, and the kinetic results for the ATRP results of PEGMA in DPE and XYL. In both polymerizations, the reaction mixture turned bright green upon initiator addition indicating that TSC initiation is fast. However, we observed a significant difference in the post initiation equilibrium concentration of Cu(I)/Cu(II) species in the polymerization medium, with green Cu(II) species being more predominant in the DPE case. This indicates that the deactivation rate constant in DPE is lower than that in XYL, possibly due to a change in the redox potential of the catalyst in more polar DPE ( $\epsilon_{\text{XYL}} = 2.27$  and  $\epsilon_{\text{DPE}} = 3.73$ ). In even more polar butyl acetate ( $\epsilon_{\text{BuAc}} = 5.07$ ), the polymerization mixture turned bright green upon initiation and remained bright green with no polymer forming after 24 hours. We attribute this to a very low deactivation rate constant that leads to high radical concentration and consequent irreversible radical-radical termination as evidenced by the permanent green color of the reaction medium. Thus, we conclude that the deactivation rate constant is inversely related to the polarity of the reaction solvent. The lower deactivation rate constant in DPE leads to fast polymerization, but low final conversion to polymer due to irreversible radical-radical termination as evidenced by the significant curvature in the kinetic plot (Figure 3). The molecular weight increased

linearly with conversion after an initial exponential growth and prior to establishment of the Cu(I)/Cu(II) equilibrium (Figure 2). The conversion profile was as expected. On the other hand, in XYL, molecular weight increased exponentially between 10 and about 30% conversion to polymer. This unusual behavior was accompanied by broadening polydispersity (Figure 2) and an unusual positive deviation in the kinetic and conversion profiles (Figure 3).

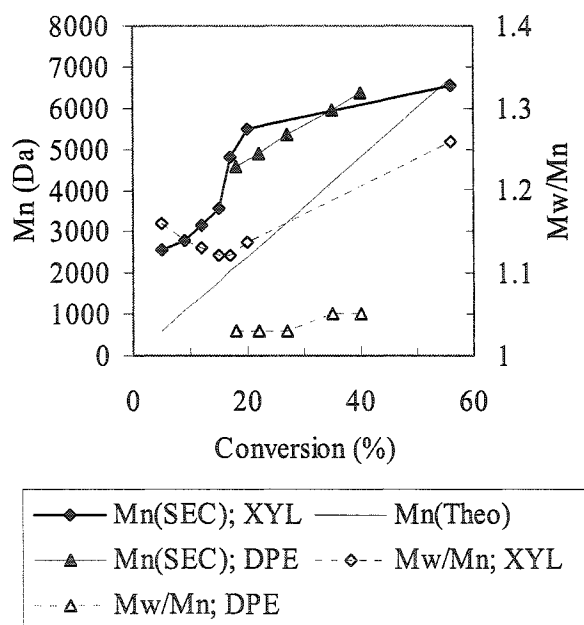


**Figure 2.** Molecular weight and polydispersity profiles for polymerization of PEGMA in DPE and XYL at 25 wt% monomer loading.  $[TSC]_0: [Cu(dNBpy)_2Br]_0 : [PEGMA] = 1:1:30$  at 70 °C.

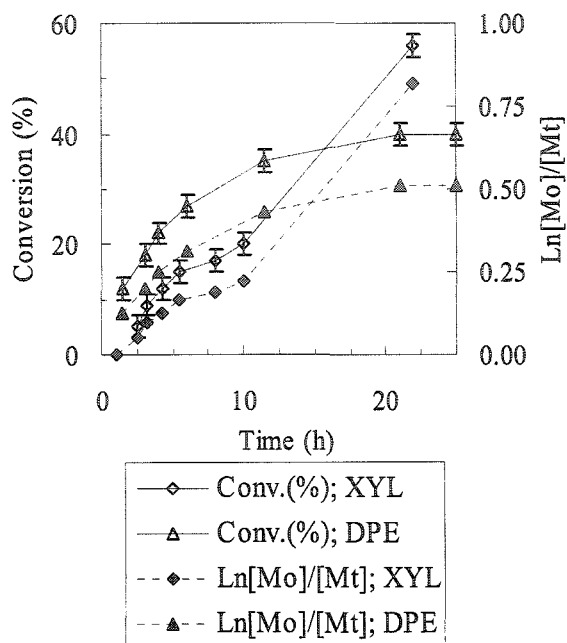


**Figure 3.** Conversion and kinetic profiles for polymerization of PEGMA in DPE and XYL. Conditions as in Figure 2.

The SEC of the 22 hour sample was bimodal indicating that a significant amount of high molecular weight material formed in the latter part of the reaction. This high molecular weight polymer may result from coupling of methacrylate polymer radicals and radicals resulting from chain transfer to polymer, forming branched polymer with molecular weights 2 –3 times higher than the peak average. While this explains the exponential increase in molecular weight, it contradicts the upward trends in the conversion and kinetic profiles because radical-radical coupling should lower radical

concentrations and decrease polymerization rates. We propose that the forming PEGMA microphase separates in non polar xylene and that Cu(I)/Cu(II) catalyst species within these polymer-rich domains favors higher radical concentrations and faster polymerization rates causing the observed exponential increase in polymer molecular weight and broadening polydispersity. This is consistent with the higher rate of polymerization observed in the more polar solvent DPE.

The subsequent set of experiments involved cyclohexanol (CXL) and ethanol (ETH) as a pair of strongly hydrogen bonding protic solvents that also differ in their overall polarity ( $\delta_{\text{CXL}} = 22.5 \text{ MPa}^{1/2}$ ,  $\delta_{\text{ETH}} = 26.6 \text{ MPa}^{1/2}$ ;  $\epsilon_{\text{CXL}} = 16.4$ ;  $\epsilon_{\text{ETH}} = 25.3$ ). In both solvents, the reaction mixture turned bright green upon initiation, and then gradually regained its deep red brown color in 1 and 2 hours respectively, indicating that the Cu(I) species predominates in the post initiation Cu(I)/Cu(II) equilibrium. In both cases, the molecular weight increased non-linearly up to ~25 wt.% conversion, beyond which point linear behavior was observed and the polydispersity remained low (Figure 4). Unlike the XYL system, in ETH and CXL, the conversion profile (Figure 5) exhibited the expected steady initial polymerization rate that leveled off at about 50 wt.% final conversions to polymer. However, in both cases radical concentrations diminished significantly beyond 30 % conversion as indicated by the curvature in kinetic profiles (Figure 5). Since poly(ethylene glycol) monomethacrylate (PEGMA) comprises a mixture of monomers of varying PEG chain lengths, monomer incorporation into poly(poly(ethylene glycol) monomethacrylate) (P(PEGMA)) could be biased towards low molecular weight species. HPLC analysis of residual monomer showed that the homolog distribution in residual

monomer is identical to that in the feed indicating that monomer incorporation is independent of the macromonomer molecular weight.

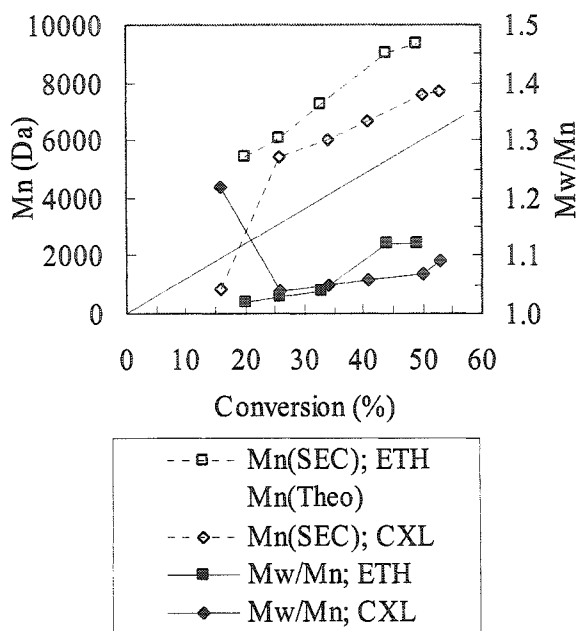


**Figure 4.** Molecular weight and polydispersity profiles for polymerization of PEGMA in CXL and ETH at 25 wt% monomer loading.  $[\text{TSC}]_0 : [\text{Cu}(\text{dNBpy})_2\text{Br}]_0 : [\text{PEGMA}] = 1:1:30$  at 70 °C.

### 3.2.4 ATRP copolymerization of PEGMA and MMA.

Amphiphilic copolymers exhibiting a range of hydrophilic-lipophilic balance (HLB) were prepared by copolymerization of hydrophobic MMA with water soluble PEGMA (Table 4). Since the ATRP of PEGMA was relatively successful in CXL, we anticipated

that copolymerization with MMA might also be successful in this solvent. First, the homopolymerization of MMA in CXL was attempted prior to extending these solvent conditions to the copolymerization. In this experiment the forming PMMA phase separated in the solvent mixture yielding a distinctly viscous polymer phase and a low viscosity solvent phase. The polymerization however proceeded to quantitative conversion in this biphasic mixture. The product polymer was bimodal with 98% polymer exhibiting the theoretically expected molecular weight and low polydispersity ( $M_n = 8900$  Da,  $M_w = 9400$  Da,  $M_w/M_n = 1.06$ ). The small amount (2%) of high molecular weight polymer ( $M_n = 65,000$  Da,  $M_w = 83,000$  Da,  $M_w/M_n = 1.28$ ) could result from a Trommsdorff type effect in the viscous polymer phase. Having proved that both MMA and PEGMA can be homopolymerized by ATRP in CXL, copolymers were prepared in this solvent and in DPE (a good solvent for ATRP copolymerization of methyl methacrylate and poly(ethylene glycol) monomethyl ether methacrylate.<sup>27</sup> The polymerization in CXL proceeded in a controlled manner as evidenced by the linear increase in molecular weight, and decrease in polydispersity, with conversion (Figure 6). The high polydispersity at reaction end ( $M_w/M_n = 1.5$ ) could result from slow initiation (relative to propagation), from irreversible termination events during the polymerization, or from a slow dynamic equilibrium between the active and dormant chains. Upon initiation, the polymerization mixture turned bright green and then turned back to a deep red-brown color indicating fast initiation followed by establishment of the Cu(I) / Cu(II) equilibrium in which the Cu(I) species is predominant. Thus slow initiation is unlikely to be the cause of the observed broad polydispersity. Also, the linearity of the kinetic plot

(Figure 7) indicates no loss of radical concentration suggesting that irreversible radical termination was insignificant.

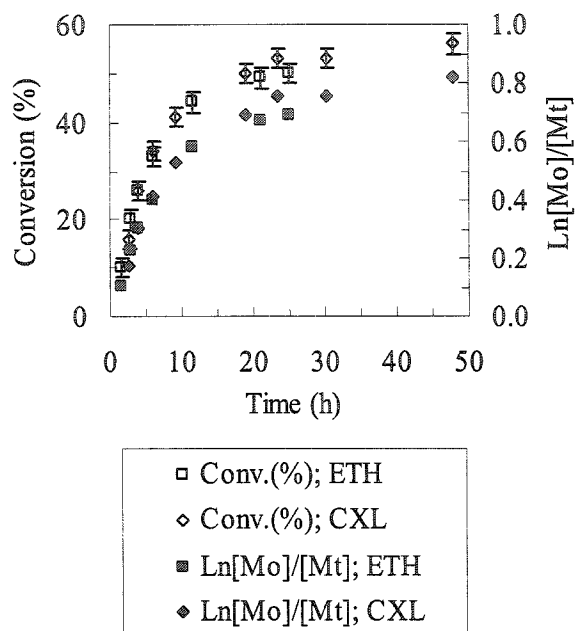


**Figure 5.** Conversion and kinetic profiles for polymerization of PEGMA in CXL and ETH at 25 wt% monomer loading.  $[\text{TSC}]_0 : [\text{Cu}(\text{dNBpy})_2\text{Br}]_0 : [\text{PEGMA}] = 1:1:30$  at 70 °C.

While slow dynamic equilibrium between the dormant and active polymer chains remains a plausible explanation, we believe the broad polydispersity is due to some uncontrolled polymerization in the early stages of the reaction. The SEC chromatograms of polymer at 27, 55, 77 and 99 % conversion showed that the molecular weight of a minor (high

molecular weight) peak in the bimodal distribution did not increase with conversion indicating that these polymer chains were irreversibly terminated early in the reaction.

Table 4. Hydrophilic lypophilic balance of P(PEGMA) and P(PEGMA-co-MMA)

(Co)polymer	Mol % PEGMA	Wt.% PEGMA	HLB* (based on PEGMA content)	HLB* (based on PEG content)	Water solubility (LCST/°C)
PEGMA-10	10	32	6.4	5	no
PEGMA-18	18	49	9.8	7.6	no
PEGMA-24	24	57	11.4	8.9	yes (42.7)
PEGMA-30	30	64	12.8	10	yes (49.8)
PEGMA-40	40	74	14.8	11.5	yes (55.8)
PEGMA- 100 <sup>#</sup>	100	100	20	15.6	yes (no)

\* The Hydrophilic lypophilic balance,  $HLB = (\text{Wt.\% of hydrophilic portion}) / 5$

<sup>#</sup> PEGMA-100 is PEGMA homopolymer so its HLB based on PEGMA content is 20 by definition.

This “dead” polymer was likely formed by uncontrolled polymerization prior to establishment of the required Cu(I)/Cu(II) equilibrium via the persistent radical effect and is responsible for the observed high polydispersity. The major peak (low molecular weight) peak shifted to higher molecular weights with conversion as expected in an ATRP reaction. Due to the poor polydispersity observed in the ATRP of P(MMA-co-PEGMA) in CXL, further copolymerizations containing 10, 18, 24, 30, and 40 mol% (i.e., 32, 49, 57, 64, and 74 wt. %) PEGMA in the feed were conducted in DPE.

The copolymer molecular weights increased linearly with conversion and are in good agreement with the theoretical molecular weight (solid line in Figure 8). Increasing the PEGMA content of the comonomer feed from 10 to 40 mol% led to loss of control in the ATRP reaction. This trend is apparent from lower conversion at reaction end (Figure 9), higher polydispersities at a given conversion (Figure 10), and greater curvature in the kinetic plots (Figure 11) with increasing amounts of PEGMA. The increasing curvature in the kinetic plots suggests diminishing radical concentrations indicating irreversible termination either by coupling or disproportionation of polymeric radicals.

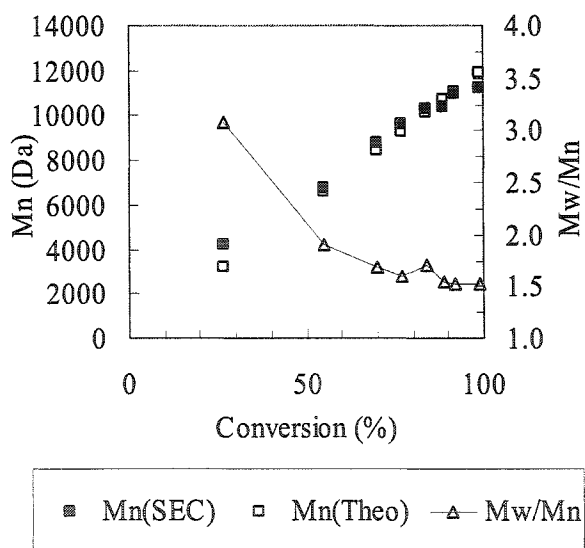


**Figure 6.** Molecular weight and polydispersity profiles for copolymerization of MMA with PEGMA (mol% PEGMA = 18) in CXL at 25 wt%.  $[TSC]_0$ :  $[Cu(dNBpy)_2Br]_0$ :  $[MMA] : [PEGMA] = 1:1:60:14$  at 70 °C.

The SEC chromatograms in all copolymerizations were bimodal beyond ~30 % conversion to polymer with a small high molecular weight peak comprising a quarter of the product (at reaction end) in the copolymerization containing 10 mol % PEGMA and about a third in other cases. This indicates that loss of radical concentration was predominantly due to radical-radical coupling. PEGMA copolymers are known to yield crosslinked gels in conventional free radical polymerizations.<sup>26</sup> The authors attributed the observed crosslinking to relatively high (of the order of  $10^{-3}$  –  $10^{-4}$ ) chain transfer constants of the oxyethylene units in PEG and PEG derivatives in the polymerization of methacrylates,<sup>35</sup> acrylonitrile<sup>36</sup> and vinyl acetate.<sup>37</sup> It is probable that the presence of PEG chains in PEGMA macromonomer and in the forming copolymers causes chain transfer to polymer. This would lead to chain branching and to crosslinking *via* radical coupling. In ATRP polymerizations, we believe the carbon radicals on the pendant PEG moieties (formed via chain transfer to polymer) as well as methacrylate radicals on chain branches arising thereof are reversibly terminated by atom transfer reaction with the ATRP catalyst, thereby maintaining low radical concentrations characteristic of ATRP (of the order of  $10^{-9}$  -  $10^{-10}$  mol/L as apposed to  $10^{-5}$  –  $10^{-7}$  mol/L in conventional free radical polymerization).

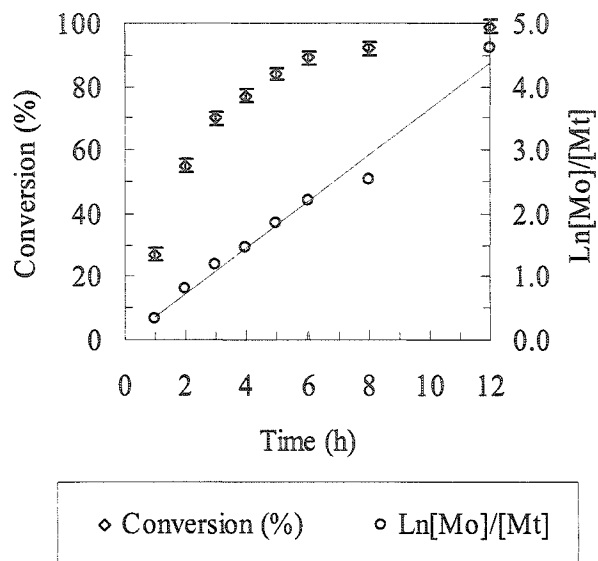


**Figure 7.** Conversion and kinetic profiles for copolymerization of MMA with PEGMA (mol% PEGMA = 18) in CXL. Conditions as in Figure 6.

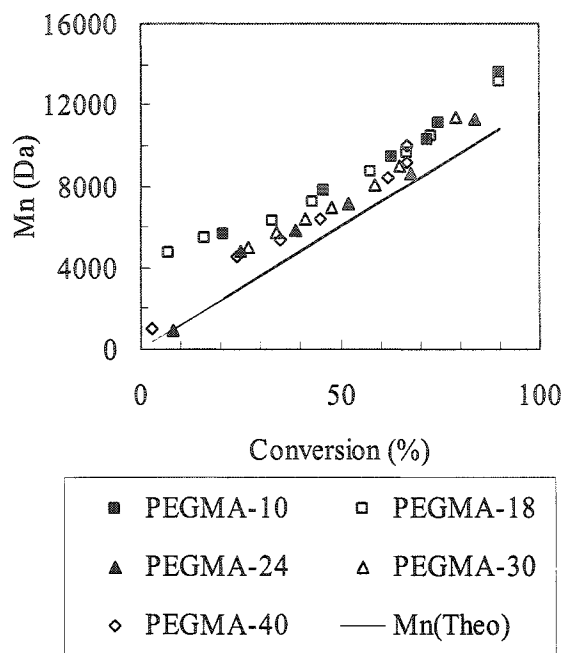


**Figure 8.** Plots of experimental ( $M_n(\text{SEC})$ ) and theoretical ( $M_n(\text{Theo})$ ) molecular weight vs conversion for copolymerization of MMA with PEGMA (%PEGMA = 10, 18, 24, 30 and 40 mol % PEGMA) in DPE at 25 wt%. $[\text{TSC}]_0$ :  $[\text{Cu}(\text{dNBpy})_2\text{Br}]_0 = 1:1$  at 70 °C.

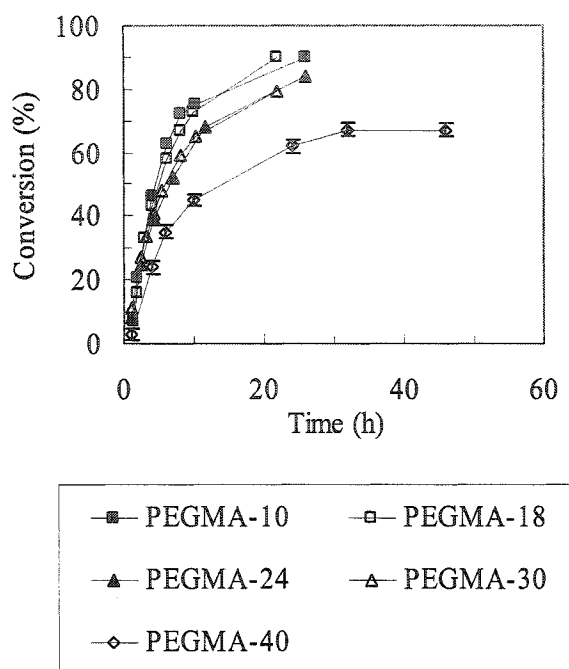


**Figure 9.** Conversion profiles for polymerization of P(MMA-*co*-PEGMA) (%PEGMA = 10, 18, 24, 30 and 40 mol % PEGMA) in DPE using conditions of Figure 8. Errors in conversion measurements at 10, 18, 24, and 30 mol% PEGMA are similar to those shown for the 40 mol% PEGMA copolymerization, but are omitted for clarity.

Hence the extent of radical-radical coupling reactions is significantly lower in ATRP leading to less cross-linking and network formation. This explains the absence of gel-formation during polymerization and the improved shelf life of ATRP polymers indicating that ATRP is a better means of preparing perhaps branched but soluble polymers of polyethylene oxide based macromonomers.

### 3.2.5 Copolymer composition and microstructure

The composition of P(MMA-co-PEGMA) copolymers should reflect the comonomer feed ratio at quantitative conversion. However, the copolymer may be richer in the more reactive monomer in the early stages of the polymerization. Furthermore, since every polymer chain remains alive throughout an ATRP reaction, preferential incorporation of one monomer would yield gradient copolymers.

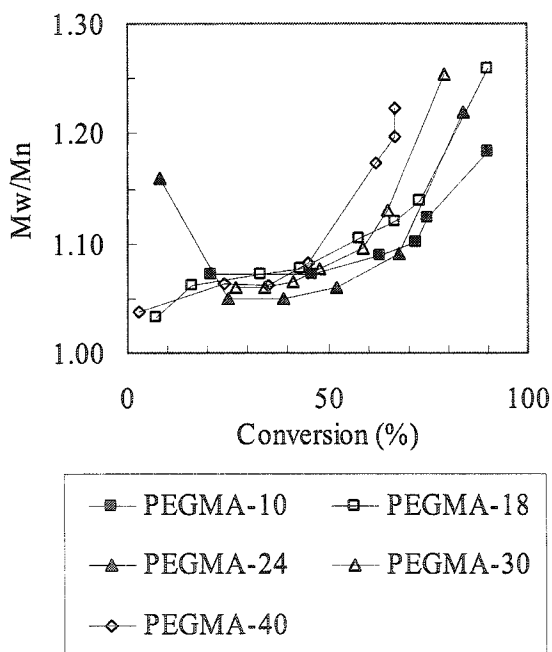
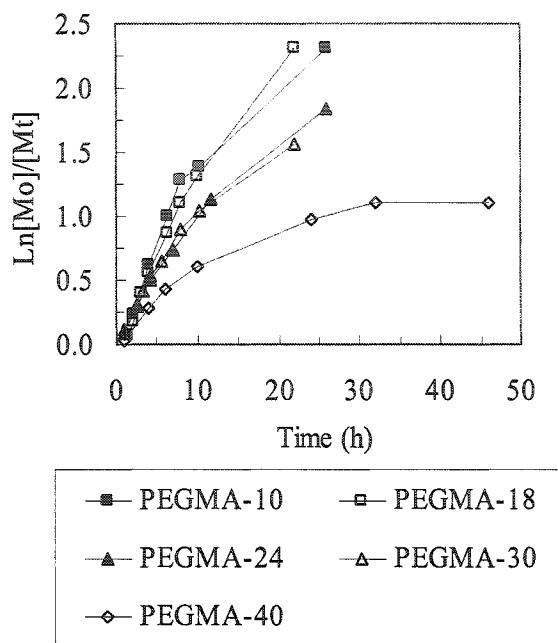


Figure 10. Polydispersity profiles for polymerization of P(MMA-co-PEGMA) (%PEGMA = 10, 18, 24, 30 and 40 mol % PEGMA) in DPE using conditions of Figure 8.



**Figure 11.** Kinetic profiles for polymerization of P(MMA-*co*-PEGMA) (%PEGMA = 10, 18, 24, 30 and 40 mol % PEGMA) in DPE using conditions of Figure 8.

In general, macromonomers are believed to have lower reactivity than the corresponding low molecular weight monomers due to the low concentration of polymerizable groups in the system as well as possible steric hindrance during monomer addition to the growing polymer chain.

The composition of P(MMA-*co*-PEGMA) copolymers was monitored by  $^1\text{H}$  NMR (Figure 12). The methoxy protons of methyl methacrylate monomer ( $\delta\text{CH}_3\text{O} = 3.58$  ppm) overlap with all the methylene protons of the pendant PEG chain in the

PEGMA monomer ( $\delta\text{CH}_2\text{O} = 3.61$  ppm) except the methylene protons next to the ester functionality ( $\delta\text{CH}_2\text{OCO} = 4.09$  ppm).

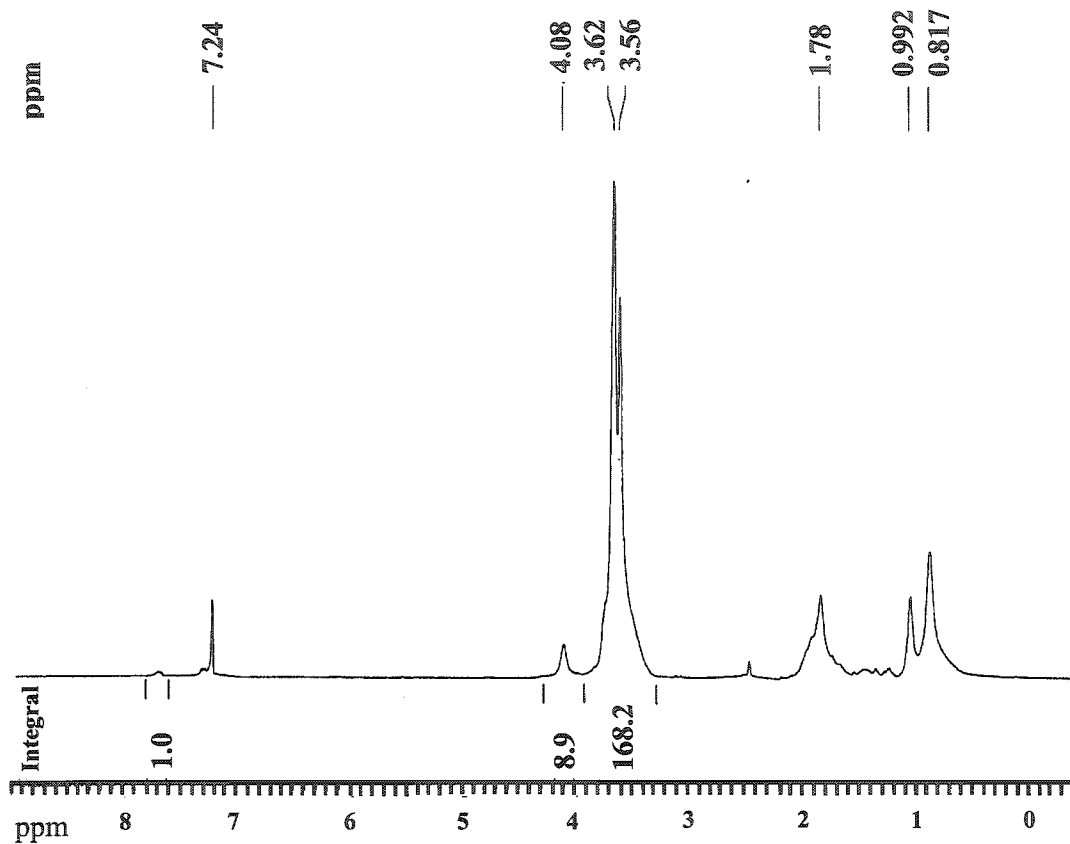
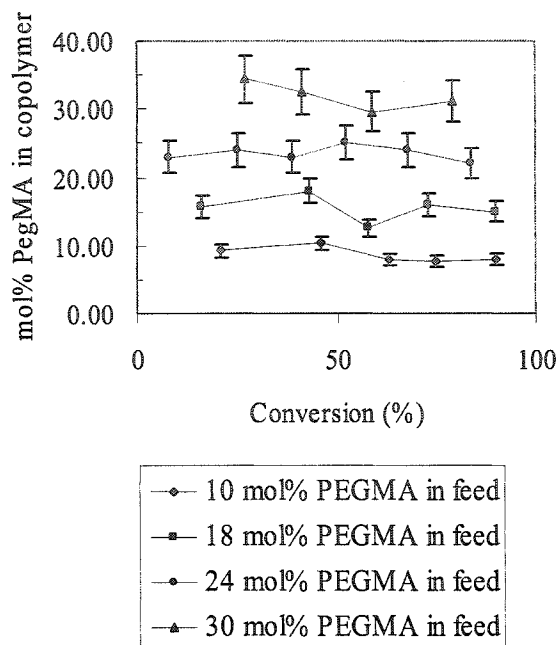


Figure 12.  $^1\text{H}$  NMR spectrum of P(MMA-*co*-PEGMA) copolymer (in  $\text{CDCl}_3$ , 300 MHz) containing 18 mol% PEGMA.

Using an average pendant PEG chain length of 7 ethylene oxide units, the contribution of the methylene protons of the pendant PEG chain to the overlapped peaks at 3.58 ppm and 3.61 ppm was determined by multiplying the area under of the peak at 4.09 ppm by 13.



**Figure 13.** Evolution of PEGMA content in P(MMA-*co*-PEGMA) copolymer with conversion as determined by  $^1\text{H}$  NMR spectroscopy.

This allowed determination of the ratio of MMA to PEGMA in the copolymers. Figure 13 gives the evolution of copolymer composition with conversion. The copolymer composition reflected the comonomer feed ratio throughout the polymerization indicating no preferential incorporation of MMA over the PEGMA macromonomer. Thus, the copolymers prepared are random copolymers rather than gradient copolymers.

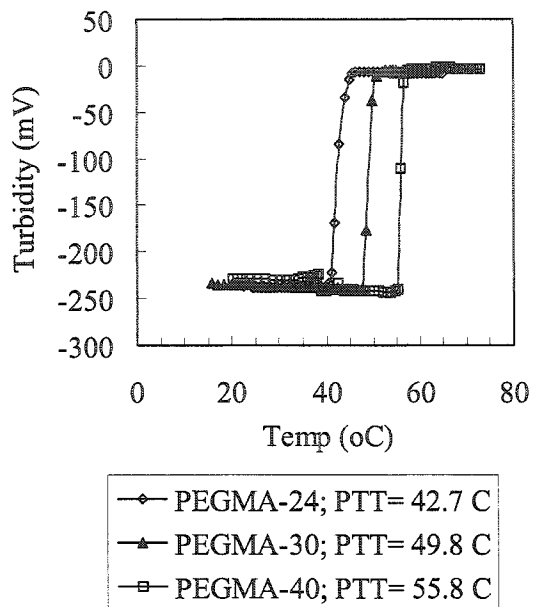


**Figure 14.** Turbidity versus temperature curves of 1 wt.% aqueous solutions of water soluble P(MMA-*co*-PEGMA) containing 24, 30, and 40 mol% PEGMA showing the phase transition temperatures (42.7, 49.8 and 55.8 °C, respectively) of the copolymers (as determined by location of the point of inflection).

### *3.2.6 Temperature induced phase transitions of aqueous homopolymer and copolymer solutions.*

P(PEGMA) and P(PEGMA-co-MMA) are polymers comprised of a hydrophobic methacrylate back bone and hydrophilic poly(ethylene glycol) pendant chains. The homopolymer and copolymers containing 57 wt.% and above PEGMA are water soluble (Table 3). The aqueous copolymer solutions exhibit phase transition temperatures that increased with increasing PEGMA content of the copolymer (Figure 14). The water solubility of the copolymers is based on hydrogen bonding interactions of the pendant PEG chains with water molecules. Increasing the temperature is expected to induce entropy driven desolvation of the PEG chains causing the inter- and intra-molecular polymer-polymer interactions to dominate thereby leading to polymer precipitation. Since polymer-water interactions are favored with increasing PEGMA content in the copolymers, the phase transition temperature increases with PEGMA content as observed.

### **3.3 Conclusion**

The atom transfer radical polymerization of macromonomer PEGMA was developed in organic solvents using toluene sulfonyl halide initiator and Cu(I)Br/alkyl bipyridine based catalyst. Commercially available PEGMA was analyzed by LC-MS and purified using a solvent extraction technique that largely removed cross-linking dimethacrylate impurities as well as non-functional poly(ethylene glycol). The polymerization rates of PEGMA macromonomer were comparable to those of methyl

methacrylate, however conversions to polymer at reaction end remained low (50 – 60 %). The ATRP reaction failed in polar n-butyl acetate. The failure is attributed to very high initial radical concentration (efficient initiation) coupled with slow deactivation which leads to irreversible radical-radical termination and the consequent irreversible build-up of Cu(II) catalytic species as evidenced from the color of the reaction mixture.

In less polar diphenyl ether, conversion to polymer was low (~30 %), however, the product polymer exhibited low polydispersity and a mono-modal molecular weight distribution indicating that the polymerization was controlled. We attribute the low conversion to irreversible termination of polymeric radicals *via* coupling and/or disproportionation. In even less polar xylene, a more favorable activator/deactivator concentration led to more controlled reaction in the early stages of the polymerization. However, the product polymer exhibited a bimodal molecular weight distribution. We propose this is caused by microphase separation of PEGMA in non-polar xylene, with the equilibrium concentration of Cu(I)/Cu(II) catalyst species within these polymer-rich domains favoring higher radical concentrations and faster polymerization rates. This caused the observed exponential increase in polymer molecular weight and broadening polydispersity in the latter stages of the polymerization. Polymerization in hydrogen bonding solvents, ethanol and cyclohexanol, yielded narrow disperse polymers of controlled molecular weight that exhibited mono-modal molecular weight distributions. The better ATRP control and higher conversion to polymer in these solvent was attributed to higher activator concentration coupled with a fast dynamic Cu(I)/Cu(II) equilibrium.

The ATRP copolymerizations yielded best results in diphenyl ether. Copolymers containing greater than 57 mol % PEGMA were water-soluble. The water-soluble copolymers exhibited sharp phase transition temperatures which increased with increasing PEGMA content as expected. Conventional free radical copolymerizations of PEGMA with hydrophobic monomers are known to yield gels unless chain transfer agents are used. Also, such materials are known to crosslink and become insoluble gels unless stored in solution.<sup>26</sup> Gel formation during polymerization has been attributed to chain transfer to polymer (or monomer) via its PEG moieties. In ATRP polymerizations, we believe the carbon radicals on the pendant PEG moieties (formed via chain transfer to polymer) as well as methacrylate radicals on chain branches arising thereof are reversibly terminated by atom transfer reaction with the ATRP catalyst, thereby maintaining low radical concentrations characteristic of ATRP (of the order of  $10^{-9}$  -  $10^{-10}$  as apposed to  $10^{-5}$  -  $10^{-7}$  in conventional free radical polymerization). Hence the extent of radical-radical coupling reactions is significantly lower in ATRP leading to hindered cross-linking and network formation. This explains the absence of gel-formation during polymerization and the improved shelf life of ATRP polymers indicating that ATRP is a better means of preparing perhaps branched but soluble polymers of polyethylene oxide based macromonomers.

### 3.4 Experimental Section

**Materials.** Toluene sulfonyl chloride (99+%) and 4,4'-dinonyl-2,2'-dipyridyl (97%), diphenyl ether (99%), cyclohexanol (99%), and *p*-xylene (99%) were purchased from Aldrich and used as received. Poly(ethylene glycol) monomethacrylate  $M_n \sim 360$  Da was

purchased from Aldrich (Lot # 04023BU) and Polysciences Inc. ( $n = 200$ ; where “n” is the molecular weight of the pendant PEG chain; Lot # 519486) and purified as described in this paper. Copper (I) bromide (98%, Aldrich) was purified according to a published procedure.<sup>38</sup> Methyl methacrylate (99%), was obtained from Aldrich and passed over a basic alumina column to remove inhibitor. n-Butyl acetate (reagent grade), *iso*-propyl ether (reagent grade), neutral Alumina and basic Alumina (both Brockman Activity 1, mesh 60-325) were purchased from Fisher Scientific and used as received. Tetrahydrofuran (99%), dichloromethane (reagent grade), hexanes (reagent grade), methanol (HPLC grade), and water (HPLC grade) were purchased from Caledon Laboratories Limited and used as received. Anhydrous ethanol (100%) was purchased from Commercial Alcohols Inc. (Brampton, Ontario). Methylene-D2 chloride (99.9%) and chloroform-d (99.8%) were purchased from Cambridge Isotope Laboratories and used as received.

**Isolation of PEG-MA by solvent extraction technique.** In a typical PEGMA isolation experiment, 50 mL PEGMA was dissolved in 200 mL distilled water and extracted with DPE (2 X 50 mL). The suspension was then separated by centrifugation at 5000 rpm for 5 minutes. The organic layer (containing the PEG-DMA components) was discarded and the aqueous phase was extracted with dichloromethane/ hexane (3:1) (2 X 250 mL). The suspension was separated as before, the aqueous phase (containing the PEG components) was discarded and PEG-MA was recovered from the organic phase by rotary evaporation at 40 °C.

ATRP homopolymerization of PEGMA in organic solvent (CXL, ETH, DPE, and BuAc, or XYL). CuBr (36.4 mg, 0.25 mmol), dNBpy (204.4 mg, 0.5 mmol), PEGMA (3206 mg, 7 – 8 mmol), and solvent (9621 mg) were placed in a 50 mL round bottom flask in a nitrogen filled glove bag and closed with a septum. TSC (47.7 mg, 0.25 mmol) was dissolved in a 1 g portion of either solvent or monomer in a vial equipped with a septum inside a nitrogen filled glove bag. The monomer and catalyst solution was degassed in a stream of argon for 30 minutes and then transferred to an oil bath at 70 °C. The initiator solution was introduced in one aliquot via a syringe that had been previously degassed with a stream of argon for 3 minutes. Samples (1 mL) were drawn periodically via a previously degassed syringe for Size Exclusion Chromatography (SEC) and conversion measurements. SEC samples (0.2 mL) were prepared by diluting with THF (1 mL) and passing over a neutral alumina column to remove catalyst. Conversion was determined gravimetrically. This involved dilution of 0.8 mL samples to 2 mL with THF, followed by precipitation in 18-19 mL *iso*-propyl ether in 20 mL vials; the vials were then centrifuged at 3500 rpm, the supernatant decanted and the precipitate vacuum dried (at 40 °C) in the dark to constant weight. The polymerizations typically proceeded to 50 – 70% conversion.

ATRP copolymerization in DPE (and CXL). The following is a description of the ATRP synthesis of poly(MMA-*co*-PEGMA) containing 18 mol% PEGMA and is typical of all other copolymerizations. CuBr (72.8 mg, 0.5 mmol), dNBpy (408.8 mg, 1.0 mmol), MMA (2000 mg, 20 mmol), PEGMA (2851 mg, 7 mmol), and solvent (17,533 mg) were placed in a round bottomed flask in a nitrogen filled glove bag and closed with a septum.

TSC (95.3 mg, 0.5 mmol) was dissolved in MMA (1000 mg, 10 mmol) in a vial equipped with a septum inside a nitrogen filled glove bag. The monomer(s) and catalyst solution was degassed in a stream of argon for 30 minutes and then transferred to an oil bath at 70 °C. The initiator solution was introduced in one aliquot via a syringe that had been previously degassed with a stream of argon for 3 minutes. Samples (1 mL) were drawn periodically via a previously degassed syringe for Gel Permeation Chromatography (GPC) and conversion measurements. GPC samples (0.2 mL) were prepared by diluting with THF (1 mL) and passing over a neutral alumina column to remove catalyst. Conversion was determined gravimetrically as described in the homopolymerization section above. The polymerizations typically proceeded to 60 – 100% conversion.

**Measurements.** Polymer molecular weight was determined by size exclusion chromatography using a Waters 515 HPLC Pump connected to three Waters 5 µm (7.8 X 300 mm) Styragel (HR2, HR3 and HR4) linear columns (exclusion limits 500-20,000 Da, 500-30,000 Da, and 5000-600,000 Da) and a Waters 2414 Refractive Index Detector. The HPLC pump was equipped with a Water 717 plus Autosampler and computer controlled using the Millennium 32 Chromatography Manager. The column and detector temperature were set at 40.0 °C and 35.0 °C, respectively. Tetrahydrofuran was used as elution solvent (flow rate = 1 mL/min), and narrow disperse linear polystyrene standards were used for calibration.

The identities of the components in poly(ethylene glycol) monomethacrylate macromonomer were confirmed by Liquid Chromatography Mass Spectrometry (LCMS). HPLC was performed using a Symmetry Shield Reverse Phase C-18 column and the

same autosampler, HPLC pump and refractive index detector as for the size exclusion chromatography (described above). HPLC parameters were: sample concentration = 3 wt.%; mobile phase: methanol / water = 1:1; injection volume = 30  $\mu\text{L}$ ; flow rate = 0.5 mL/minute; column temperature ( $^{\circ}\text{C}$ )/RI detector temperature ( $^{\circ}\text{C}$ )/run time (minutes) = 35/30/150. Liquid Chromatography Mass Spectrometry (LCMS) was performed using an HPLC coupled to a electrospray mass spectrometer (ESMS). Positive ion Electrospray Mass Spectrometry was performed using a triple quadrupole Micromass Ultima instrument.

The phase transition temperatures of the amphiphilic copolymer solutions were measured using the cloud point method. An automatic PC-Titrator (Mandel) equipped with a temperature probe and a photometer incorporating a 1 cm path length fiber optics probe (GT-6LD, MITSUBISHI) was used to trace the phase transition by monitoring the transmittance of a beam of white light. The turbidity of solution was recorded as photo induced voltage, where a reading of about  $-220$  mV corresponded to a transparent solution below the cloud point and a reading close to 0 mV for the system above the cloud point. The phase transition temperature was defined as the inflection point of the mV vs temperature curve, as determined by the maximum in the first order derivative. The concentration of the polymer solutions was 1.0 wt.%, and the heating rate was  $1.0$   $^{\circ}\text{C}$   $\text{min}^{-1}$ .

The  $^1\text{H}$  NMR spectra were recorded in  $\text{CD}_2\text{Cl}_2$  or  $\text{CDCl}_3$  at 300 MHz on a Bruker AV-300 Instrument.

**Acknowledgement.** We acknowledge NSERC and 3M Canada for funding this research and Dr. Nicholas Burke for valuable suggestions.

## References:

- (1) Wang, J. -S.; Matyjaszewski, K. *J. Am. Chem. Soc.* **1995**, *117*, 5614-5615.
- (2) Kato, M.; Kamigaito, M.; Sawamoto, M.; Higashimura, T. *Macromolecules* **1995**, *28*, 1721-1723.
- (3) Matyjaszewski, K.; Xia, J. *Chem. Rev.* **2001**, *101*, 2921-2990.
- (4) Kamigaito, M.; Ando, T.; Sawamoto, M. *Chem. Rev.* **2001**, *101*, 3689-3745.
- (5) Prucker, O.; R uhe, J. *Macromolecules* **1998**, *31*, 592-601.
- (6) Prucker, O.; R uhe, J. *Macromolecules* **1998**, *31*, 602-613.
- (7) Ejaz, M.; Ohno, K.; Tsujii, Y.; Fukuda, T. *Macromolecules* **2000**, *33*, 2870-2874.
- (8) Von Werne, T. A.; Germack, D. S.; Hagberg, E. C.; Sheares, V. V.; Hawker, C. J.; Carter, K. R. *J. Am. Chem. Soc.* **2003**, *125*, 3831-3838.
- (9) Chen, X.; Randall, D. P.; Perruchot, C.; Watts, J. F.; Patten, T. E.; Von Werne, T. A.; Armes, S. P. *J. Colloid Interface Sci.* **2003**, *257*, 56-64.
- (10) Holmberg, S.; Holmlund, P.; Wil n, C. -E.; Kallio, T.; Sundholm, G.; Sundholm, F. *J. Polym. Sci. : Part A: Polymer Chemistry* **2002**, *40*, 591-600.
- (11) Pelton, R. *Adv. Colloid Interface Sci.* **2000**, *85*, 1-33.
- (12) Jeong, B.; Kim, S. W.; Bae, Y. H. *Adv. Drug Delivery Rev.* **2002**, *54*, 37-51.
- (13) Kost, J.; Langer, R. *Adv. Drug Delivery Rev.* **2001**, *46*, 125-148.

- (14) Mathur, A. M.; Drescher, B.; Scranton, A. B.; Klier, J. *Nature* **1998**, *392*, 367-370.
- (15) Saunders, B. R.; Koh, A. Y. C. *Chem. Commun.* **2000**, 2461-2462.
- (16) Kanazawa, H.; Matsushima, Y.; Okano, T. *Adv. Chromatogr.* **2001**, *41*, 311-336.
- (17) Ista, L. K.; Perez-Luna, V. H.; López, G. P. *Appl. Environ. Microbiol.* **1999**, *65*, 1603-1609.
- (18) Hoffman, A.S.; Afrassiabi, A.; Dong, L. C. *J. Controlled Release* **1986**, *4*, 213-222.
- (19) Okahata, Y.; Lim, H. J.; Nakamura, G.; Hachiya, S. *J. Am. Chem. Soc.* **1983**, *105*, 4855-4859.
- (20) Kidchob, T.; Kimura, S.; Imanishi, Y. *J. Chem. Soc. Perkin Trans. 2* **1997**, 2195-2199.
- (21) Peng, T.; Cheng, Y. -L. *Polymer* **2001**, *42*, 2091-2100.
- (22) Neugebauer, D.; Zhang, Y.; Pakula, T.; Sheiko, S. S.; Matyjaszewski, K. *Macromolecules* **2003**, *36*, 6746-6755.
- (23) Neugebauer, D.; Zhang, Y.; Pakula, T.; Matyjaszewski, K. *Polymer* **2003**, *44*, 6863-6871.
- (24) Han, S.; Hagiwara, M.; Ishizone, T. *Macromolecules* **2003**, *36*, 8312-8319.
- (25) Ishizone, T.; Han, S.; Okuyama, S.; Nakahama, S. *Macromolecules* **2003**, *36*, 42-49.

- (26) Bo, G.; Wesslén, B.; Wesslén, K. B. *J. Polym. Sci. : Part A: Polymer Chemistry* **1992**, *30*, 1799-1808.
- (27) Ali, M. M.; Stöver, H. D. H. *Macromolecules* **2003**, *36*, 1793-1801.
- (28) Klier, J.; Scranton, A. B.; Peppas, N. A. *Macromolecules* **1990**, *23*, 4944-4949.
- (29) Percec, V.; Barboiu, B.; Kin, H.-J. *J. Am. Chem. Soc.* **1998**, *120*, 305-316.
- (30) Matyjaszewski, K.; Nanda, A. J. *Macromolecules* **2003**, *36*, 599-604.
- (31) Destarac, M.; Alric, J.; Boutevin, B.; *Macromol. Rapid Commun.* **2000**, *21*, 1337-1341.
- (32) Chambard, G.; Klumperman, B.; German, A. L. *Macromolecules* **2000**, *33*, 4417-4421.
- (33) Ali, M. M.; Stöver, H. D. H. in "Advances in Controlled/ Living Radical Polymerization"; Editor: Matyjaszewski, K.; *ACS Symposium Series* **854**, **2003**, *36*, 299-315.
- (34) Haddleton, D. M.; Perrier, S.; Bon, S. A. F. *Macromolecules* **2000**, *33*, 8246-8251.
- (35) Nandi, U. S.; Kumar, S.; Bhaduri, G. C. *Indian J. Chem.* **1981**, *20A*, 759-763.
- (36) Schneider, A.; Fritzsche, P. *Acta. Polym.* **1979**, *30*, 270-272.
- (37) Okamura, S.; Katagiri, K.; Motoyama, T. *J. Polym. Sci.* **1960**, *43*, 509-516.
- (38) Keller, R. N.; Wycoff, H. D. *Inorg. Synth.* **1946**, *2*, 1-4.

## CHAPTER 4

This chapter describes the suspension Atom Transfer Radical Polymerization (ATRP) copolymerization of methyl methacrylate (MMA) and poly(ethylene glycol) monomethacrylate (PEGMA). The results indicate that despite extensive partitioning of PEGMA into the water phase, suspension copolymerization conversions were comparable to those in solution conditions (Chapter 3). Also described is the crosslinking suspension ATR terpolymerization of MMA and PEGMA using diethylene glycol dimethacrylate and the morphology of the resulting suspension polymer particles. These particles are compared to those formed using conventional radical polymerization (CFRP) in analogous experiments. Using ATRP capsules are formed at lower PEGMA in feed than when CFRP is used under analogous conditions. These results are explained in terms of the slower kinetics of ATRP as well as the potentially higher polarity of ATRP derived gels. In addition, the formation of interesting composite walled polymer capsules is discussed.

**Interfacial Living Radical Copolymerization of Oil and Water Soluble Comonomers Yields Composite-walled Polymer Capsules**

Mir Mukkaram Ali and Harald D. H. Stöver, submitted for publication in *Macromolecules*, June 2004.

ABSTRACT

Suspension copolymerization of oil-soluble methyl methacrylate (MMA) and water-soluble poly(ethylene glycol) monomethacrylate (PEGMA) using ATRP yielded well-defined amphiphilic copolymers ( $M_w/M_n < 1.3$ ). Copolymers containing up to 30 mol% (63 wt.%) PEGMA were prepared despite the extensive partitioning (70%) of PEGMA into the water phase indicating that use of a living polymerization ensures incorporation of the water soluble monomer into the copolymers. Conversion to polymer by suspension polymerization was comparable to that obtained by solution polymerization (> 80% w/w). Copolymers with high PEGMA content contained a significant proportion of high molecular weight material formed via uncontrolled polymerization unless PVA was added to stabilize the oil droplets. Addition of diethylene glycol dimethacrylate DEGDMA gave capsules at as low as 17 mol% PEGMA using ATRP, while conventional radical polymerization (CRP) only led to capsules at 24 mol% PEGMA in the feed. ATRP causes particle-capsule transition at lower PEGMA levels, reflecting the slower ATRP kinetics and possibly higher polarity of ATRP-derived gels due to improved incorporation of PEGMA into the gels. Suspension ATRP using 24 mol% PEGMA in the feed gave two-layered capsule walls bearing a uniformly thick

TEM-visible inner layer and TEM/ESEM-visible irregular outer layer suggesting a compositional gradient across the capsule wall.

#### 4.1 Introduction

Polymer capsules ranging in size from a few tens of nanometers<sup>1</sup> to the meso-scale<sup>2</sup> have been vigorously developed in the recent past. Throughout the entire size range, these polymer shells, typically enclosing a liquid core, are prepared by the spontaneous assembly of polymers driven by the need to minimize interfacial energy. Shell crosslinked block copolymer micelles (known as shell crosslinked knedels, SCK's), pioneered by Wooley *et al.*,<sup>3</sup> and developed by Armes *et al.*,<sup>4</sup> are prepared by the self assembly of block copolymers in block selective solvents, followed by crosslinking of the shell forming block. SCK's are easily converted into nano-capsules by subsequent etching of the core forming block.<sup>5</sup> Block copolymers self assemble into micron sized vesicles and subsequent hardening of the vesicle wall by crosslinking polymerization gives polymer capsules called "polymersomes".<sup>6</sup> Unlike lipid vesicles, that typically exhibit ~4 nm thick walls, block copolymer vesicle walls are considerably thicker (4 nm to 20 nm or more, depending on the size of the vesicle membrane core forming block), and tougher.<sup>7,8</sup> Up to one micron thick vesicle walls, likely resulting from several self assembled block copolymer layers, that maintain their structural integrity upon drying have also been reported.<sup>9</sup> Furthermore, amphiphilic graft and block copolymer may be assembled at an oil-water interface and crosslinked via metathesis polymerization<sup>10</sup> or ionic reactions<sup>11</sup> to give polymer capsules of controllable size. While SCK-derived

nanocage and polymersome membranes are typically based on uni- and bi-molecular polymer layers, walls of such capsules derived from reactive graft and block copolymers are likely to be several molecular layers thick.

Conventionally, polymer capsules are prepared by precipitation of polymer at an oil-water interface. Typically, the wall forming polymer is derived from monomers and/or precursor polymers in either the oil or water phases or from interfacial reaction, and is insoluble in both the disperse oil phase and the continuous water phase. In addition, the forming polymer is amphiphilic such that interfacial energy of the three phase (polymer, oil and water) system is minimized by formation of a polymer shell that engulfs the oil droplet. Encapsulations based on coacervation,<sup>12</sup> suspension crosslinking<sup>13</sup> and solvent evaporation,<sup>14</sup> employ preformed polymers for capsule wall formation. On the other hand, interfacial polycondensation<sup>15,16</sup> and *in situ* radical polymerization of vinyl monomers<sup>17</sup> employ monomeric starting materials. The *in situ* radical polymerization technique is attractive as it allows access to the wide range of chemistries accessible through vinyl monomers. When conducted in aqueous miniemulsions,<sup>18,19</sup> emulsions<sup>20</sup> and suspensions,<sup>21,22</sup> this techniques yields nanometer to several micron size capsules. The governing thermodynamic and kinetic requirements for capsule formation are well understood,<sup>23,24</sup> but careful selection of the experimental conditions is necessary to obtain the desired capsules in a given system. McDonald *et al.*<sup>25</sup> showed that modifying the polarity of the water phase of an emulsion by adding a water miscible alcohol together with formation of low molecular weight polymer in the early stages of the polymerization, helps to form PMMA microcapsules. Also, Kasai *et al.*<sup>26</sup>

demonstrated that the presence of preformed polymer in the oil phase, different from the wall forming polymer, is beneficial for obtaining the capsular morphology presumably due to polymer-polymer de-mixing that drives the forming polymer to the interfacial region. Formation of capsular particles is therefore non-trivial, because in addition to the thermodynamic requirements for capsule formation, the kinetics of *in situ* polymerization must allow development of the thermodynamically favored morphology within the experimental time frame. In contrast, more recent encapsulation techniques employing highly amphiphilic block or graft copolymers described above,<sup>10,11</sup> promise to be more robust due to the strongly amphiphilic nature of the precursor polymers as well as the segregation of the assembly and crosslinking processes.

We recently demonstrated<sup>27</sup> that use of “living” Atom Transfer Radical Polymerization (ATRP) in suspension conditions gave capsular particles under conditions where conventional free radical polymerization (CFRP) gave solid or matrix particles. In that system, copolymers of methyl methacrylate (MMA) and poly(ethylene glycol) monomethyl ether methacrylate, both essentially oil soluble monomers, were crosslinked using oil soluble diethylene glycol dimethacrylate (DEGDMA) to yield suspension polymer particles. The capsular morphology of ATRP derived particles was attributed to the slow propagation rate of ATR polymerizations that allows the gels growing in the oil phase to migrate to the oil-water interface yielding the thermodynamically favored morphology. In contrast, analogous CFRP derived particles exhibited matrix morphology due to kinetic entrapment of the forming gels within the oil droplets. Here we report the synthesis of non-crosslinked well-defined copolymers of

MMA and a water soluble monomer, poly(ethylene glycol) monomethacrylate (PEGMA) by suspension ATRP polymerization. Polymer chains in ATRP switch between active and dormant states (dormant being the predominant state) thereby maintaining low radical concentrations and minimizing irreversible radical termination via coupling and disproportionation reactions. That is, ideally propagation continues until all monomer is incorporated into the forming polymer. This feature of ATRP promises to allow preparation of strongly amphiphilic copolymers based on oil and water soluble comonomers in suspension conditions despite partitioning of the water soluble monomer into the water phase. We also report crosslinking suspension terpolymerizations using oil soluble DEGDMA. The morphology transitions of ATRP derived suspension polymer particles caused by increasing the PEGMA level in the feed are compared with those of CFRP derived particles. In addition, the formation of interesting composite walled polymer capsules using ATRP at high PEGMA concentrations is discussed.

## 4.2 Results and discussion

### *4.2.1 Choice of monomers, solvents and ATRP initiator-catalyst system for suspension polymerization.*

This work has three objectives: first to develop suspension living radical copolymerizations of oil and water soluble comonomers to yield amphiphilic copolymers; to prepare crosslinked gels in suspension conditions by crosslinking amphiphilic copolymers using an oil soluble crosslinker and third to study the morphology of crosslinked suspension polymer particles formed with increasing amounts of water soluble monomer in the ternary comonomer feed. MMA and DEGDMA were

chosen as the oil soluble monomers and PEGMA as the water soluble monomer. PEGMA is miscible with water in all proportions at room temperature due to ether oxygen and the terminal hydroxyl group of the pendant PEG chain. Thus, in oil-water suspension, PEGMA partitioning between the oil and water phases is governed by the polarity and hydrogen bonding characteristics of the oil phase. A number of largely water immiscible solvents that differ in their polarity and hydrogen bonding characteristics were studied. Xylene, n-butyl acetate, diphenyl ether and cyclohexanone (XYL, BuAc, DPE, and CXN) are solvents of increasing polarity as indicated by their dielectric constants (see Table 1), and cyclohexanol (CXL) is a strongly hydrogen bonding, yet water immiscible solvent. Since we have earlier demonstrated that MMA/PEGMA copolymers can be prepared in DPE and CXL solutions at 70°C using *p*-toluene sulfonyl chloride (TSC) as ATRP initiator and 4,4'-dinonyl-2,2'-dipyridyl (dNBpy) / copper (I) bromide as ATRP catalyst,<sup>28</sup> this ATRP initiator-catalyst system was retained for the present suspension polymerizations. The hydrophobic alkyl chains on the dNBpy ligands yield homogeneous catalyst solutions in organic solvents. As well, hydrophobic ligands limit catalyst solubility in the aqueous phase in suspension polymerizations to a negligibly low level and thereby retain it in the oil phase for effective ATRP catalysis.<sup>29,30</sup>

#### ***4.2.2 PEGMA partitioning between water and oil phases.***

The partition coefficients of PEGMA between water and the five solvents shown in Table 1 were determined as follows: 5% (w/w) aqueous PEGMA solutions (containing 100 ppm NaN<sub>3</sub>) were mixed with half their weight of organic solvent by shaking the suspensions vigorously for 1 to 2 minutes by hand three times at 10 minute intervals. The

temperature was maintained at 25 °C and 70 °C using water baths and residual PEGMA concentration in the aqueous phase was determined using aqueous size exclusion chromatography (SEC). The individual SEC peaks (Figure 1) were identified by electrospray mass spectrometry (ESMS), analogous to earlier HPLC characterizations of PEGMA macromonomers.<sup>28</sup>

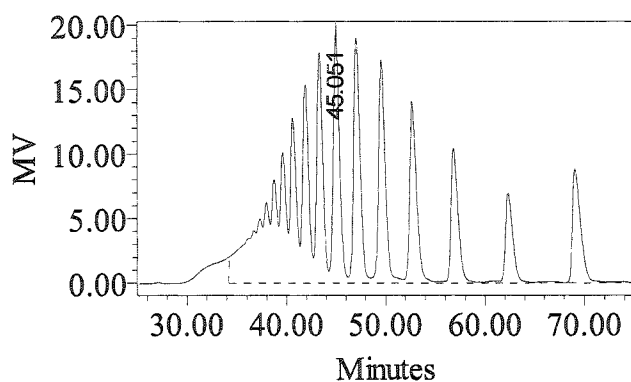


**Figure 1.** Size exclusion chromatogram of a 5% (w/w) solution of PEGMA in 100 ppm  $\text{NaN}_3$ .

In the SEC trace (Figure 1), the broad peak eluting at retention time below 34.6 minutes was assigned to poly(ethylene glycol) (PEG) oligomers while the peaks with longer retention times are PEGMA components bearing 1-27 ethylene glycol units in the pendant PEG chain. Since PEG oligomers are not incorporated into the desired copolymers, only partitioning of PEGMA components between the oil and water phases is of interest. Thus a calibration curve for PEGMA quantitation in the water phase was obtained by determining the total area under the peaks eluting above 34.6 minutes in

chromatograms of standards containing 1 to 8% (w/w) PEGMA in 100 ppm  $\text{NaN}_3$  (the SEC mobile phase).

Using the linear calibration obtained (Figure 2), PEGMA concentrations in the water phase after extraction with organic solvents was determined and used to calculate the partition coefficients presented in Table 1. The partition coefficients in organic solvents ( $K_{\text{SOLVENT}/\text{WATER}}$ ) increase with increasing solvent polarity as gauged by the solvent dielectric constant. At 25 °C, the partition coefficient in non-polar xylene ( $K_{\text{XYL}/\text{WATER}} = 0.04$ ) is an order of magnitude lower than that in the other, relatively polar solvents shown.

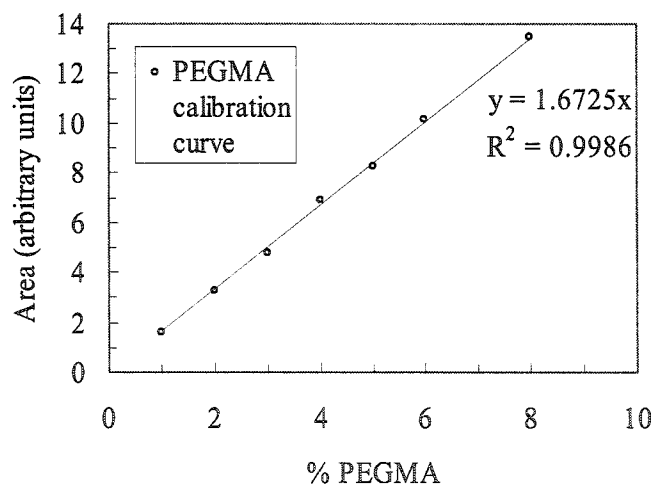


Figure 2. PEGMA calibration curve using SEC chromatograms of 1 to 8 % (w/w) standard aqueous PEGMA solutions. The total area under the SEC peaks representing PEGMA components bearing 1 to 27 ethylene oxide units in the pendant PEG chain was used as a measure of PEGMA concentration.

**Table 1.** Partition coefficients of PEGMA in selected organic solvents

Organic Solvent	Density <sup>a</sup> (g/mL)	Dielectric Constant <sup>b</sup> (T/Kelvin)	$K_{\text{SOLVENT}}$ at 25 °C	$K_{\text{SOLVENT}}$ at 70 °C	%PEGMA in water at 25 °C <sup>c</sup>	%PEGMA in water at 70°C <sup>c</sup>
XYL	0.866	2.274 (293.2)	0.04	0.44	97	82
DPE	1.073	3.726 (283.2)	0.38	0.82	84	71
BuAc	0.883	5.07 (293.2)	0.21	1.32	91	60
CXN	0.947	15 (293.2)	0.74	4.33	73	32
CXL	0.947	16.4 (293.2)	----	10.52	----	16

<sup>a</sup>Source: Aldrich Catalog, 2003-2004; <sup>b</sup> Source: CRC Handbook; <sup>c</sup> In an oil-water suspension using an oil:water ratio = 1:2. Symbols: XYL = Xylene; DPE = Diphenyl ether; BuAc = n-butyl acetate; CXN = Cyclohexanone; CXL = Cyclohexanone.

The highest value of  $K_{\text{CXN/WATER}}$  and  $K_{\text{CXL/WATER}}$  is attributed to their high polarity as well as the additional hydrogen bonding ability of CXL that is expected to increase the solubility of PEGMA in this solvent. For all solvents studied,  $K_{\text{SOLVENT/WATER}}$  values are higher at 70 °C than at 25 °C. This is expected as hydrated PEGMA molecules in water would suffer a larger entropic penalty upon heating than PEGMA in organic solvent.

Also presented in Table 1 are the amounts of PEGMA that would partition into the water phase at the 1:2 oil:water ratio used in the suspension polymerizations in this work. Since the objective of this work is to prepare amphiphilic copolymers based on an oil soluble monomer and a polar comonomer that partitions significantly into the water phase in suspension conditions, CXL does not serve as a suitable model solvent due to the high  $K_{\text{CXL}}$  value that leaves only 16% PEGMA in the water phase at 70 °C. Thus, the

ATR suspension copolymerization of MMA and PEGMA using CXL as oil phase was not developed any further.

#### *4.2.3 ATRP synthesis of Poly(MMA-co-PEGMA) in solution and suspension conditions.*

Suspension polymerizations were conducted by initiating the ATR copolymerization in solution conditions. At 7 – 15 % conversion, the oligomer solutions were transferred to a two fold excess of water under seclusion of air and the polymer continued under suspension conditions. The copolymerizations were first developed in solution conditions to determine reaction kinetics, and to provide a basis for evaluation of suspension copolymerization.

*Solution copolymerization of MMA and PEGMA in XYL, BuAc, CXN and DPE.* We recently reported the successful ATR copolymerization of MMA and PEGMA in DPE solution<sup>28</sup>. These results are reproduced here for comparison with the solution copolymerizations in XYL, BuAc and CXN reported below (Figures 3 to 7). All copolymerizations were carried out with 19 mol% PEGMA in the feed, using TSC as ATRP initiator, and dNBpy/Cu(I)Br as catalyst system. In XYL, BuAc and DPE, the copolymer molecular weight (MW) increased linearly with conversion and in good agreement with the theoretical MW based on the monomer to initiator ratio (Figure 3). As well, the polydispersity (PDI) increased slightly with conversion but remained reasonably low (Figure 4) ( $M_w/M_n < 1.25$ ) at the polymerization end, suggesting that the polymerizations were controlled. In CXN, however, the molecular weight distribution was bimodal (Figure 5) and the MW's and PDI's shown in Figure 3 and Figure 4 were

obtained by integration of only the low MW peak in Figure 5. High MW polymer ( $M_p = 93,500$  Da) forms at low conversion ( $\sim 25\%$ ) and its MW does not increase with conversion indicating that it forms upon ATRP initiation and before the Cu(II) concentration is sufficiently high for efficient capping of the growing polymer radicals and thereby lowering the radical concentration. Thus this polymer forms by uncontrolled radical polymerization and is terminated irreversibly by conventional coupling and/or disproportionation reactions.

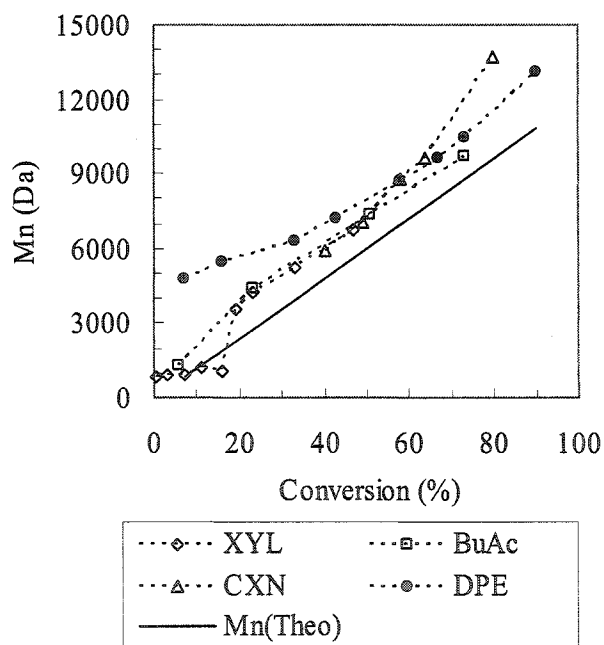


**Figure 3.** Molecular weight versus conversion plots for solution copolymerization of MMA with PEGMA (mol% PEGMA = 19) at 25 wt% monomer loading in the solvents shown.  $[TSC]_0$ :  $[Cu(dNBpy)_2Br]_0$ :  $[MMA]$ :  $[PEGMA]$  = 1:1:60:14 at 70 °C. DPE results are reproduced from Ref. 28.

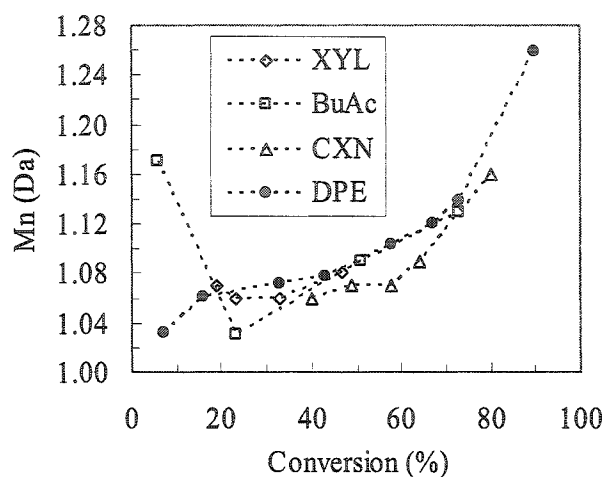


**Figure 4.** Polydispersity versus conversion for solution copolymerization of MMA with PEGMA (mol% PEGMA = 19) at 25 wt% monomer loading in the solvents shown. [TSC]<sub>0</sub>: [Cu(dNBpy)<sub>2</sub>Br]<sub>0</sub>: [MMA] : [PEGMA] = 1:1:60:14 at 70 °C. DPE results are reproduced from Ref. 28.

The linear increase in MW of the low molecular weight polymer and its low PDI (Figure 3 and 4) indicate that the polymerization in CXN was controlled except at this early stage. However, due to the presence of a significant proportion of dead polymer up to around 50% conversion to polymer, the copolymerization in CXN was not extended to suspension conditions. Final conversion to polymer at reaction end was high in DPE, CXN and BuAc (90, 80, and 73 %, respectively) indicating that irreversible termination was limited and that most polymer chains were living throughout the polymerization. In contrast, final conversion in XYL was low (47 %) indicating significant irreversible

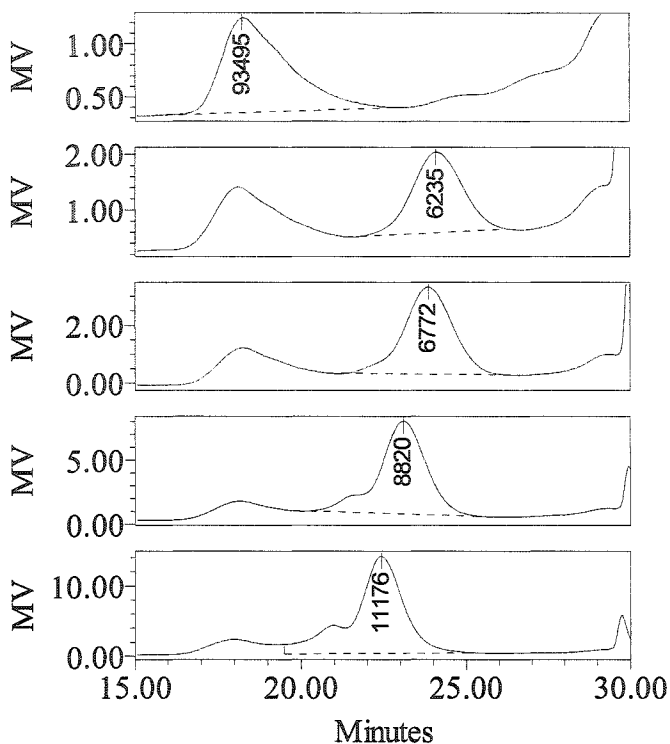


**Figure 5.** SEC chromatograms of P(MMA-co-PEGMA) (mol% PEGMA = 19) prepared in CXN at 25 wt% monomer loading at 28, 40, 49, 58, 64 and 80% conversion (top to bottom of stack).  $[\text{TSC}]_0 : [\text{Cu}(\text{dNBpy})_2\text{Br}]_0 : [\text{MMA}] : [\text{PEGMA}] = 1:1:60:14$  at 70 °C.

termination (Figure 6). The kinetic plots of copolymerization (Figure 7) were non-linear in all cases. The greatest and least deviation from linearity is observed in XYL and DPE, respectively, indicating that irreversible terminations (leading to diminishing radical concentrations) were most significant in XYL and least significant in DPE, in agreement with conclusions drawn from the conversion profiles in Figure 6.

The BuAc phase contains 2.9 % (v/v) water at saturation at 25 °C. Thus, to evaluate the ATR copolymerization in BuAc suspensions, a solution copolymerization was attempted in BuAc saturated with water. While the ATRP catalyst is soluble in it, MMA is only partially miscible with water-saturated BuAc. ATR copolymerization proceeded in this biphasic mixture, yielding copolymer with controlled MW and low PDI ( $M_n$  (SEC) = 11,300 Da;  $M_n$  (Theo) = 9,900 Da;  $M_w/M_n$  = 1.19). However, the polymerization was slower and final conversion to polymer was lower relative to DPE. Due to the limitations of ATR copolymerizations in CXN, XYL and BuAc, only suspension polymerizations using DPE as oil phase were investigated further.

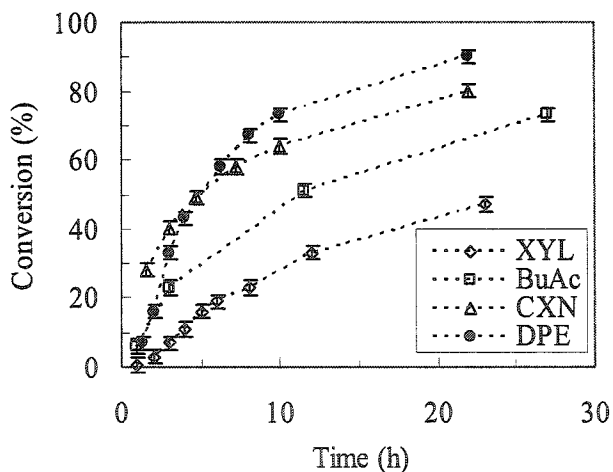


**Figure 6.** Conversion profiles for solution copolymerization of MMA with PEGMA (mol% PEGMA = 19) at 25 wt% monomer loading in the solvents shown.  $[TSC]_0$ :  $[Cu(dNBpy)_2Br]_0$ :  $[MMA]$  :  $[PEGMA]$  = 1:1:60:14 at 70 °C. DPE results are reproduced from Ref. 28.

*Suspension copolymerization of MMA and PEGMA using DPE as oil phase.*

Suspension polymerizations were conducted starting with ATRP initiation (at 70 °C) in solution, followed by transfer of the oligomer solution (at 7 to 15% conversion) to twice its weight of water (also at 70 °C) in a sealed reactor under argon. The resulting suspensions were stirred at a controlled rate using a three bladed propeller shaft magnetically coupled to an overhead mixer. Monomer feeds containing 10, 19 and 30 mol% PEGMA were used in the suspension polymerizations (Table 2). The copolymerizations were sensitive to the rate stirring. At 500 rpm, soluble polymers were obtained at all three comonomer feed compositions (Entries 1, 2 and 3, Table 2).

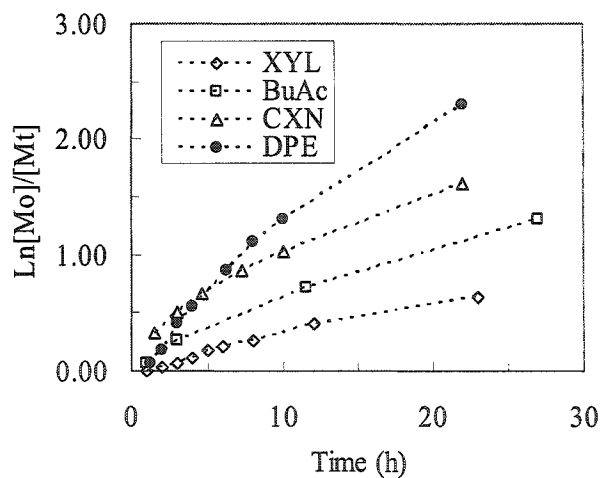


**Figure 7.** Kinetic plots for solution copolymerization of MMA with PEGMA (mol% PEGMA = 19) at 25 wt% monomer loading in the solvents shown.  $[TSC]_0$ :  $[Cu(dNBpy)_2Br]_0$ :  $[MMA] : [PEGMA] = 1:1:60:14$  at 70 °C. DPE results are reproduced from Ref. 28.

Table 2. Summary of suspension copolymerizations of MMA and PEGMA

Copolymer	Mol/Wt.% PEGMA <sup>a</sup>	Mixing speed/rpm (Time/min.)	M <sub>w</sub> /M <sub>n</sub> (1hr) <sup>b</sup>	Final M <sub>w</sub> /M <sub>n</sub>	Final conv.	Copoly. Solubility
PEGMA-10	10 / 32	500 - throughout	1.11	1.20	95	Soluble
PEGMA-19	19 / 49	500 - throughout	1.17	1.34	94	Soluble
PEGMA-30	30 / 63	500 - throughout	1.55	1.27	88	Soluble
PEGMA-10	10 / 32	1000(10); 500(TE) <sup>c</sup>	2.5 <sup>d</sup>	1.20 <sup>d</sup>	92 <sup>d</sup>	Sol-gel
PEGMA-19	19 / 49	1000(10); 500(TE) <sup>c</sup>	---	---	---	Gel
PEGMA-30	30 / 63	1000(10); 500(TE) <sup>c</sup>	---	---	---	Gel
PEGMA-10	10 / 32	1000(30); 500(TE) <sup>c</sup>	---	---	---	Gel
PEGMA-19	19 / 49	1000(30); 500(TE) <sup>c</sup>	---	---	---	Gel
PEGMA-30	30 / 63	1000(30); 500(TE) <sup>c</sup>	---	---	---	Gel
PEGMA-30 <sup>e</sup>	30 / 63	500 throughout	1.31	1.28	85	Soluble

<sup>a</sup>refers to % PEGMA in feed; <sup>b</sup>Polydispersity at 1h into suspension polymerization; <sup>c</sup>TE = till reaction end; <sup>d</sup>Data for sample drawn at 2 hr into suspension polymerization; <sup>e</sup>1% PVP added to aqueous phase as suspension stabilizer.

In the 10 and 19 mol% PEGMA copolymerizations (Entries 2 and 3, Table 2), the PDI after 1 hr of suspension polymerization was lower than that at reaction end. Also, a high MW shoulder that becomes more prominent with conversion was observed in the SEC chromatograms. This phenomenon was observed in solution copolymerizations of MMA and PEGMA<sup>28</sup> as well and we attribute it to branched polymer resulting from propagation of radicals formed by chain transfer to polymer at carbons in the pendant

PEG chains. This trend is therefore also expected in suspension copolymerizations, and suggests solution-like behavior within the oil droplets of the suspension.

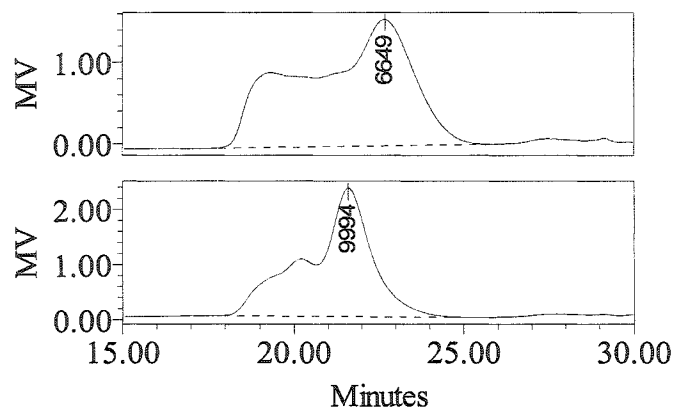


**Figure 8.** SEC chromatograms of P(MMA-co-PEGMA) prepared by suspension polymerization at 70 °C; Samples taken at 1hr into suspension polymerization (top) and at reaction end (bottom); Oil:Water = 1:2; 25 wt% monomer loading in oil phase;  $[\text{TSC}]_o$ :  $[\text{Cu}(\text{dNBpy})_2\text{Br}]_o$ :  $[\text{MMA}]$  :  $[\text{PEGMA}] = 1:1:38:16$  (30 mol% PEGMA).

At 30 mol% PEGMA (Entry 3, Table 2), the PDI of a sample taken 1hr into suspension copolymerization was high ( $M_w/M_n = 1.55$ ). Solution copolymerizations containing 30 mol% PEGMA yield low polydispersity copolymers as reported in our earlier work.<sup>28</sup> Thus, the observed high polydispersity after one hour of suspension polymerization, is indicative of loss of control in the ATRP reaction upon transfer to suspension conditions. Comparison of the SEC chromatograms of samples drawn at 1 hr in suspension and at reaction end (Figure 8) indicates that the molecular weight of the

high MW polymer that forms during the first hour of suspension polymerization does not increase with conversion. This indicates that it represents irreversibly terminated polymer chains. The PDI narrows with conversion as the low MW end of the chromatogram shifts to higher MW's. Similarly, high MW polymer formed when the 10 mol% PEGMA copolymerization was mixed at 1000 rpm for the first 10 minutes in suspension followed by 500 rpm thereafter (Entry 4, Table 2). This copolymerization yielded a sol-gel mixture as evidenced by difficulty in filtering THF solutions of the copolymer using 2 micron PTFE filters. The sol portion of a sample drawn at 2 hours into the suspension copolymerization exhibited a PDI of 2.5 that decreased to 1.2 at reaction end. These results indicate that ATRP control in suspension conditions is dependent upon the amount of PEGMA in the feed as well as the interfacial conditions in the suspension. Strong shear forces at faster mixing rates reduce the average oil droplet size. Both PEGMA macromonomer and its copolymers are amphiphilic and possibly reside at the oil-water interface in these suspensions. As well, the interfacial region is likely to have a higher water content and therefore be more polar than the interior of the oil droplets.

ATRP is known to be faster and less controlled in water-containing organic solvents.<sup>31,32</sup> Thus, with a larger interfacial area at higher mixing speeds, the locus of polymerization may well shift towards the interface leading to the observed loss of ATRP control. This would explain the observed high MW polymer and the gels formed upon transfer to suspension in the 10 mol% PEGMA copolymerization using high shear rates (1000 rpm for first 10 minutes).

Formation of gels is consistent with this hypothesis because uncontrolled conventional radical polymerization of PEGMA copolymers is known to yield gels unless chain transfer agents are used.<sup>33</sup> Furthermore, under these mixing conditions (1000 rpm for first 10 minutes), the 19 and 30 mol% PEGMA copolymerizations yielded insoluble gels (Entries 5 and 6, Table 2) that could not be analyzed by SEC. This also agrees with the above hypothesis as at high PEGMA levels, the copolymers would have a greater tendency to reside at the oil-water interface. In line with these observations, mixing the suspension at 1000 rpm for the first 30 minutes and at 500 rpm thereafter yielded gels at all three PEGMA levels (Entries 7, 8 and 9, Table 2). Furthermore, adding suspension stabilizer (1% (w/w) PVP) to the aqueous phase decreased the formation of high MW polymer in the 30 mol% PEGMA copolymerization. The PDI of the product (Entry 10, Table 2) at 1hr into suspension was significantly lower than in the absence of suspension stabilizer (1.31 versus 1.55 (Entry 9, Table 2)). Also, comparison of the SEC chromatograms (Figure 9) (obtained after careful separation of copolymer product from PVP, see experimental section for details) indicates that a much smaller proportion of high MW polymer formed upon transfer to suspension in the presence of stabilizer. This is consistent with our earlier hypothesis because PVP could displace the copolymer from the interface, thereby shifting the locus of polymerization to the less polar interior of the oil droplets where ATRP control is better. Thus, optimal conditions for suspension copolymerization are at low shear rates (500 rpm throughout) at the 10 and 19 mol% PEGMA in feed (Entries 1, 2 and 3, Table 2). At 30 mol% PEGMA in feed, addition of stabilizer improves control (Entry 10, Table 2). Figure 10 shows the MW versus

conversion plots under these conditions. The experimental MW's are in good agreement with the theoretical MW's in all cases. At 30 mol% PEGMA in the feed, the experimental MW is lower in the presence of PVP since less high MW polymer forms upon transfer to suspension in this case due to greater control of the ATRP reaction. PDI increases with conversion in the 10 and 19 mol% cases and in the 30 mol% case in the presence of PVP (Figure 11), indicating solution-like behavior within the oil droplets as explained above. Figure 11 also shows the significant narrowing of the PDI at 30 mol% PEGMA in the absence of PVP. The kinetic curves (Figure 12) are non-linear in all cases indicating diminishing radical concentrations with conversion due to irreversible termination. At 10 and 19 mol% PEGMA in feed >90% conversion to polymer was obtained, while >85% conversion was observed at 30 mol% PEGMA (Figure 13).  $^1\text{H}$  NMR showed  $8 \pm 1$ ,  $18 \pm 2$  and  $24 \pm 2$  mol% PEGMA incorporation in the copolymers at 10, 19 and 30 mol% PEGMA respectively, in the comonomer feed. That is, despite extensive partitioning into the aqueous phase (70% w/w), over 70% PEGMA is incorporated into the copolymers in all cases. Thus, using living radical polymerization amphiphilic copolymers based on oil soluble MMA and water soluble PEGMA were prepared successfully.

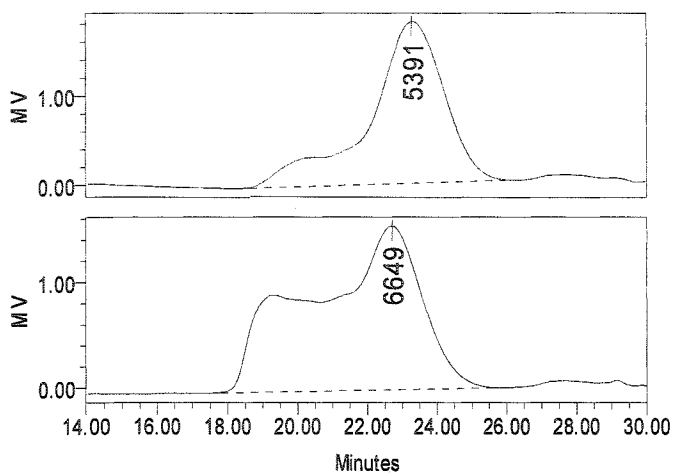


**Figure 9.** SEC chromatograms of P(MMA-co-PEGMA) prepared by suspension polymerization using 1% (w/w) PVP (top) and no suspension stabilizer (bottom); Samples taken at 1hr into suspension polymerization; Oil:Water = 1:2; 25 wt% monomer loading in oil phase;  $[TSC]_o$ :  $[Cu(dNBpy)_2Br]_o$ :  $[MMA]$  :  $[PEGMA]$  = 1:1:38:16 (30 mol% PEGMA) at 70 °C.

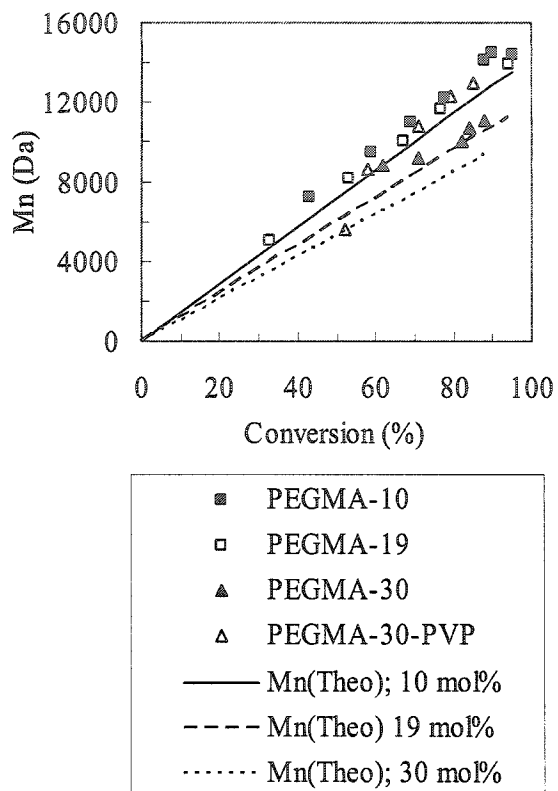


**Figure 10.** Molecular weight profiles of suspension polymerization of P(MMA-co-PEGMA) at 70 °C; Oil:Water = 1:2; 25 wt% monomer in oil phase; [TSC]<sub>o</sub>: [Cu(dNBpy)<sub>2</sub>Br]<sub>o</sub>: [MMA] : [PEGMA] = 1:1:90:10.4; 1:1:60:14; 1:1:38:16 (10, 19, and 30mol% PEGMA); PEGMA-30-PVP done with 1% (w/w) PVP in water phase of suspension.

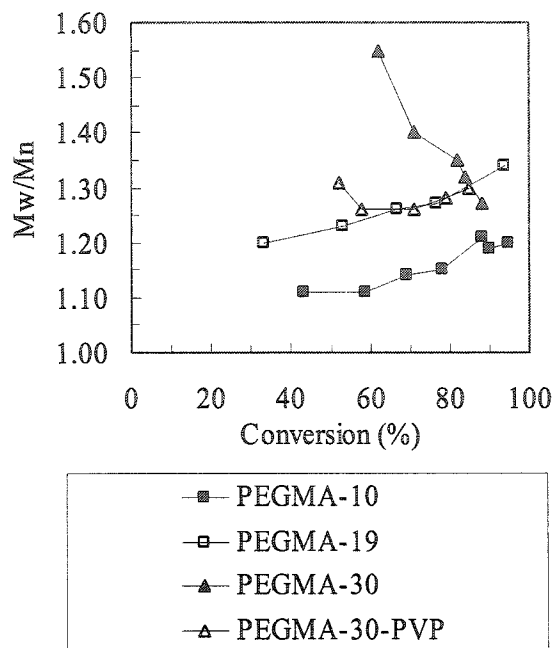


**Figure 11.** Polydispersity profiles of suspension polymerization of P(MMA-co-PEGMA); conditions as in Figure 10.

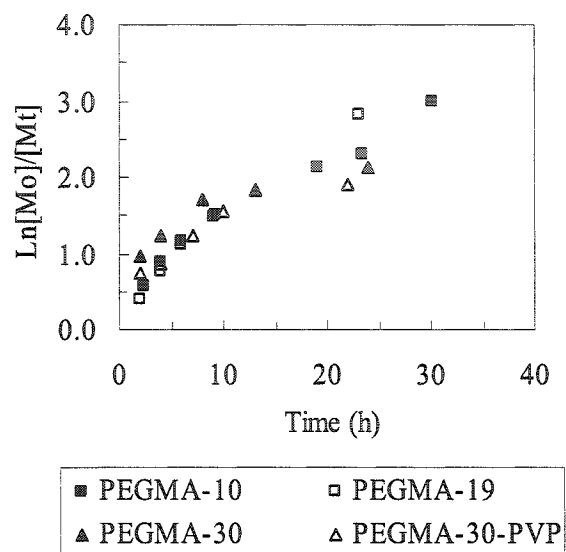


**Figure 12.** Kinetics of suspension polymerization of P(MMA-co-PEGMA); conditions as in Figure 10.

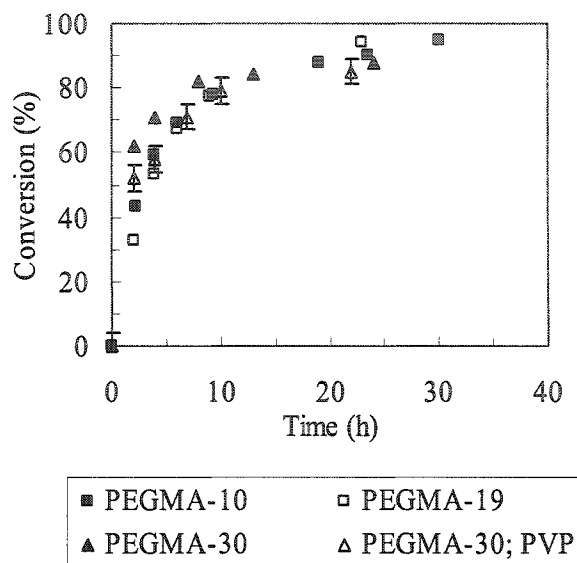


**Figure 13.** Conversion profiles of suspension polymerization of P(MMA-co-PEGMA); conditions as in Figure 10. Errors in conversion measurements in the 10, 19 and 30 mol% PEGMA copolymerization are similar to those shown for the PEGMA-30-PVP experiment but have been omitted for clarity.

#### 4.3 Polymer capsules by crosslinking suspension ATRP.

The primary objectives of this work are to synthesize amphiphilic copolymers based on oil and water soluble comonomers in suspension conditions, and to crosslink the copolymers to yield amphiphilic, surface-active gels that would migrate to the oil-water interface of the oil droplets in suspension and upon further curing yield mechanically stable polymer shells surrounding the oil droplets. Formation of such polymer capsules has two requirements. First, the copolymer must be more polar than the oil so that it is

thermodynamically favorable for the new oil-polymer and polymer-water interfaces to form at the expense of the existing oil-water interface. Second, the rate of crosslinking induced gelation (and consequent polymer precipitation) in the oil phase is slow enough to allow the initially formed microgels to migrate to the oil-water interface rather than precipitate within the oil droplet yielding polymer particles (referred to subsequently as matrix particles) rather than polymer capsules.

As demonstrated above, using ATRP polar copolymers can be prepared by incorporation of water soluble monomer in suspension conditions despite extensive partitioning of the water soluble monomer into the water phase. Also, we have earlier shown<sup>27</sup> that the slow rate of polymerization in ATRP relative to conventional radical polymerization (CFRP) allows preparation of polymer capsules under conditions where CFRP gives matrix particles. That is, when capsules are the thermodynamically favored morphology, the slow kinetics of ATRP favors the migration of polymer gels to the oil-water interface, whereas CFRP gives matrix particles due to kinetic entrapment of the gels within the oil droplets.

To evaluate the proposed advantages of using ATRP, the morphology of a series of ATRP suspension polymer particles was compared to that of analogous CFRP particles as described below. In addition, a secondary objective was to determine if the living nature of the polymer gels forming in the oil phase coupled with the presence of monomer in the water phase would yield polymer capsule walls characterized by a compositional gradient across the thickness of the capsule walls.

*Transitions in suspension particle morphology with increasing PEGMA content.*

Suspension copolymer particles were prepared by ATRP and CFRP using otherwise similar conditions (Table 3). ATR copolymerizations of MMA and PEGMA were initiated in DPE solutions at 70 °C, crosslinking monomer diethylene glycol dimethacrylate (DEGDMA) was added at 7 to 10% conversion and after mixing for 10 minutes this oligomer solution was transferred to the aqueous phase (1% in suspension stabilizer) at 70 °C. The suspensions were mixed at 1000 rpm for 30 minutes and at 500 rpm thereafter in a pressure tight baffled reactor equipped with an overhead stirrer. CFRP particles were prepared by transferring a DPE solution of MMA, PEGMA and DEGDMA to the aqueous phase at 70 °C and stirring the suspension as in the ATRP experiments described above. Final conversion to ATRP particles was lower (72 to 77%) than for CFRP particles (80 to 95%) except in the 8 mol% PEGMA experiment (Table 3). In the ATRP experiments, since crosslinker is added to a solution of prepolymers just prior to transferring the oil phase to the water phase, the formed microgels are sterically stabilized by the linear prepolymers.<sup>34</sup> This causes macrogellation at high conversions and a higher sol fraction relative to CFRP reactions. Since conversion in the encapsulation experiments was determined gravimetrically by repeated THF extractions to remove residual monomers, water and DPE (see experimental section for details), a higher sol-fraction in the ATRP particles may be responsible for the observed lower conversions. The crosslinking suspension polymerizations yielded colloidal stable polymer particles (Figure 14) of average diameter between 10 and 20 microns (Table 4).

Table 3. Morphology of suspension polymer particles<sup>a</sup>

Exp. No.	Sample code <sup>b</sup>	Polym. Method	% mon. (w/w)	Mol % / Wt. % PEGMA in feed	Final conv. (w/w)	Morphology
1	PEGMA-8L	ATRP	31	8.3 / 23	91	Matrix
2	PEGMA-13L	ATRP	31	13 / 32	72	Matrix
3	PEGMA-17L	ATRP	30	17 / 38	77	Capsule
4	PEGMA-24L	ATRP	30	24 / 49	73	Capsule (CW) <sup>c</sup>
5	PEGMA-8C	CFRP <sup>d</sup>	31	8.3 / 23	95	Matrix
6	PEGMA-13C	CFRP	31	13 / 32	85	Matrix
7	PEGMA-17C	CFRP	30	17 / 38	88	Matrix
8	PEGMA-24C	CFRP	30	24 / 49	81	Capsule

<sup>a</sup> Suspension polymerizations were conducted at 70 °C using an oil:water ratio of 1:2 with 1% (w/w) PVA in the water phase and 17 mol% cross-linker (DEGDMA); <sup>b</sup> Numbers in code refer to mol% PEGMA in the feed, “L” and “C” refer to living and conventional radical polymerization, respectively; <sup>c</sup> CW = composite wall; <sup>d</sup> Here 1% methyl cellulose was used as suspension stabilizer.

The internal morphology of the suspension polymer particles was studied by transmission electron microscopy (TEM) (Figure 15). CFRP gave matrix particles at 8, 13 and 17 mol% PEGMA (A, B and C, Figure 15), and capsules at 24 mol% PEGMA (D, Figure 15) in the feed. In contrast, ATRP gave capsules at only 17 mol% PEGMA (C, Figure 15). That is, the matrix-capsule transition occurs at lower PEGMA content when a living polymerization is used. As the ATRP gels are living, they are expected to continually

**Table 4.** Suspension polymer particle size and size distribution data<sup>a</sup>

Particle type <sup>b</sup>	L-8	L-13	L-17	L-24	C-8	C-13	C-17	C-24
Mean Dia.( $\mu\text{m}$ ) <sup>c</sup>	14	11	11	16	21	20	15	21
Std. Dev. ( $\mu\text{m}$ ) <sup>c</sup>	3	4	3	8	6	9	6	11

<sup>a</sup> Suspension polymerizations were conducted at 70 °C using an oil:water ratio of 1:2 with 1% (w/w) PVA in the water phase and 17 mol% cross-linker (DEGDMA); <sup>b</sup> Numbers in code refer to mol% PEGMA in the feed, “L” and “C” refer to living and conventional radical polymerization, respectively; <sup>c</sup> As determined by size measurements of 100 particles in one optical image for each set of particles.

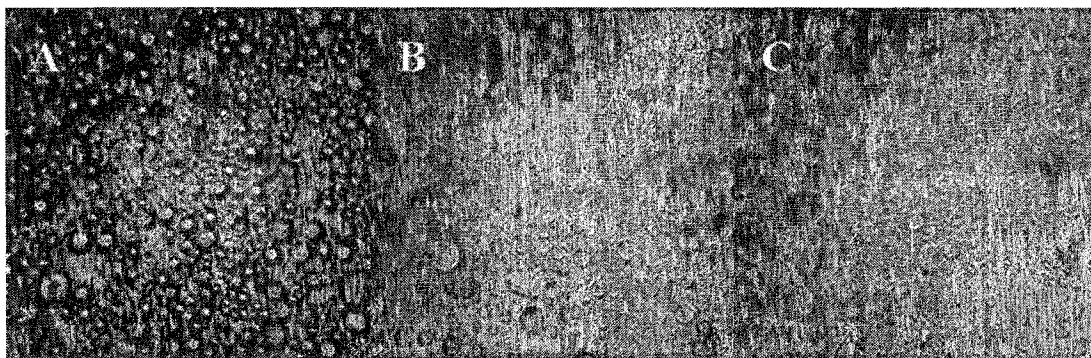
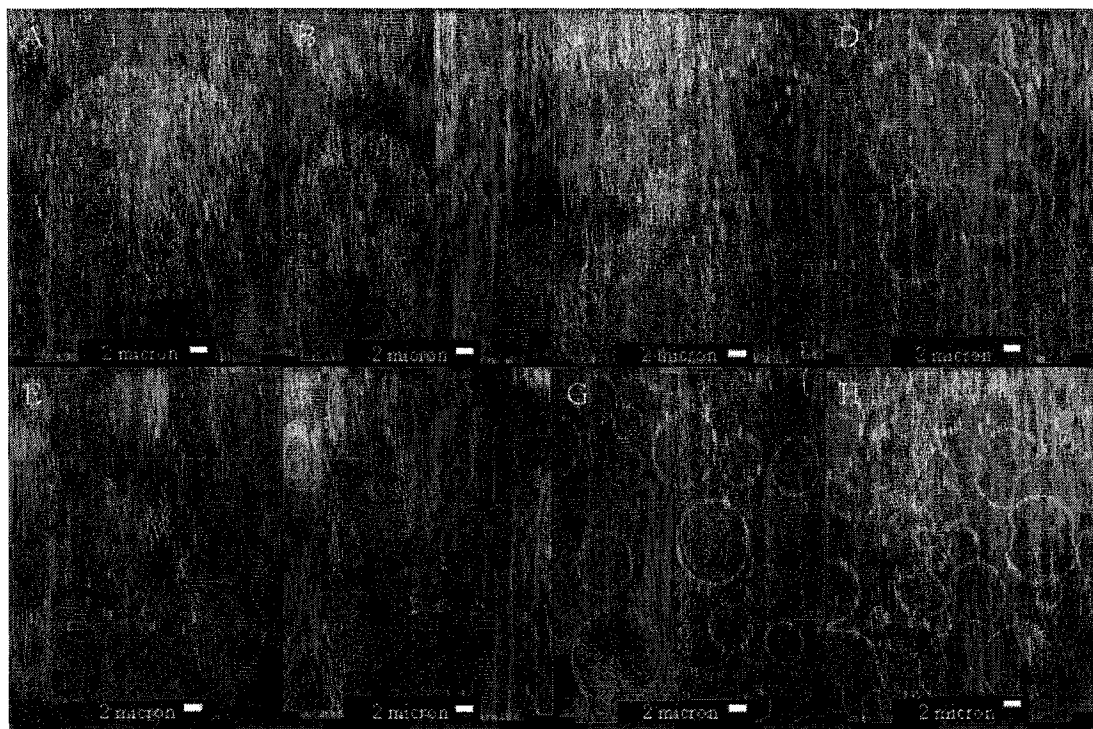
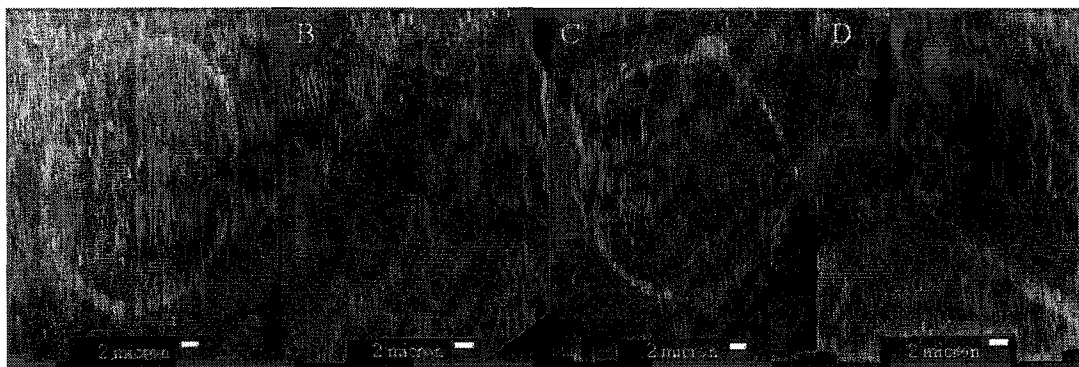


Figure 14. Optical micrographs (500  $\times$ ) of suspension polymer particles prepared by ATRP at 70 °C using an oil:water ratio of 1:2 with 1% (w/w) PVA in the water phase, 17 mol% cross-linker (DEGDMA) and A. 13 mol% PEGMA, B. 17 mol% PEGMA and C. 24 mol% PEGMA; Image A was acquired using reflected light only, while B and C were acquired using both reflected and transmitted light.



**Figure 15.** Transmission electron micrographs of suspension polymer particles prepared by convention radical polymerization (A, B, C and D) and ATRP (E, F, G and H) at 70 °C using DPE oil phase, oil:water = 1:2, and 17 mol% cross-linker (DEGDMA). In both series (A to D and E to H) the PEGMA concentration was increased incrementally (A,E = 8 mol%; B,F = 13 mol%; C,G = 17 mol%; D, H = 24 mol%).



**Figure 16.** Transmission electron micrographs of suspension polymer particles prepared by convention radical polymerization at 24 mol% PEGMA (A) and ATRP at 17 (B) and 24 mol% PEGMA (C and D) at 70 °C using DPE oil phase, oil:water = 1:2, and 17 mol% cross-linker (DEGDMA).

react with PEGMA partitioning into the oil droplets and therefore have a higher PEGMA content than the initially forming CFRP gels. The matrix-capsule transition at lower PEGMA levels in ATRP reactions is likely the combined result of the slow kinetics of the ATRP reaction as previously shown<sup>27</sup> and the higher polarity of ATRP-derived gels. Also, the CFRP particles exhibit a visibly macroporous structure (A, B and C, Figure 15) with the pore size increasing with increasing PEGMA content. The larger pores in the CFRP particles relative to the ATRP particles is likely due to the higher solubility of the ATRP gels (due to steric stabilization) and the resulting lower degree of desolvation relative to CFRP gels. It is noteworthy that while the 24 mol% CFRP capsules (CFRP-17) and the 17 mol% PEGMA ATRP (ATRP-17) capsules walls are uniformly thick, the

24 mol% PEGMA ATRP (ATRP-24) capsule walls exhibit thick and thin regions. A closer look at the three sets of capsules revealed that walls of the first two sets (A and B, Figure 16) have a single layer of polymer that exhibits no gradient in TEM contrast from the inside to the outside of the capsule wall. In contrast, the ATRP-24 capsule walls consist of two polymer layers, a uniformly thick inner layer and a bumpy second outer layer (see the circled regions in C and a close up of its boxed region, D as well as other regions of the capsule wall in Figure 16). Environmental Scanning Electron Microscopy (ESEM) of these three set of capsules showed that while the CFRP-24 capsules and the ATRP-17 capsules (A/D and B/E in Figure 17) have smooth outer surfaces, the ATRP-24 capsules (C/F in Figure 17) have a distinctly bumpy surface confirming the existence of a second layer of polymer seen in the TEM micrograms.

The TEM and ESEM sample preparation procedure (see experimental section) was designed to remove PVA prior to microscopy, thus the observed second layer is not likely to be PVA deposited on the capsule surface from the water phase. Furthermore, the absence of the second layer in similarly treated CFRP-24 and ATRP-17 particles excludes this possibility. Unlike conventional radical polymerization, in ATRP, initiator radicals form only at the start of the polymerization. In these encapsulation experiments, ATRP was initiated in DPE solution, and the prepolymer containing oil phase was transferred to suspension conditions. These prepolymers are insoluble in the water phase at the suspension polymerization temperature, and are therefore expected to remain within the oil droplets. Thus, the possibility that the second layer results from grafting of

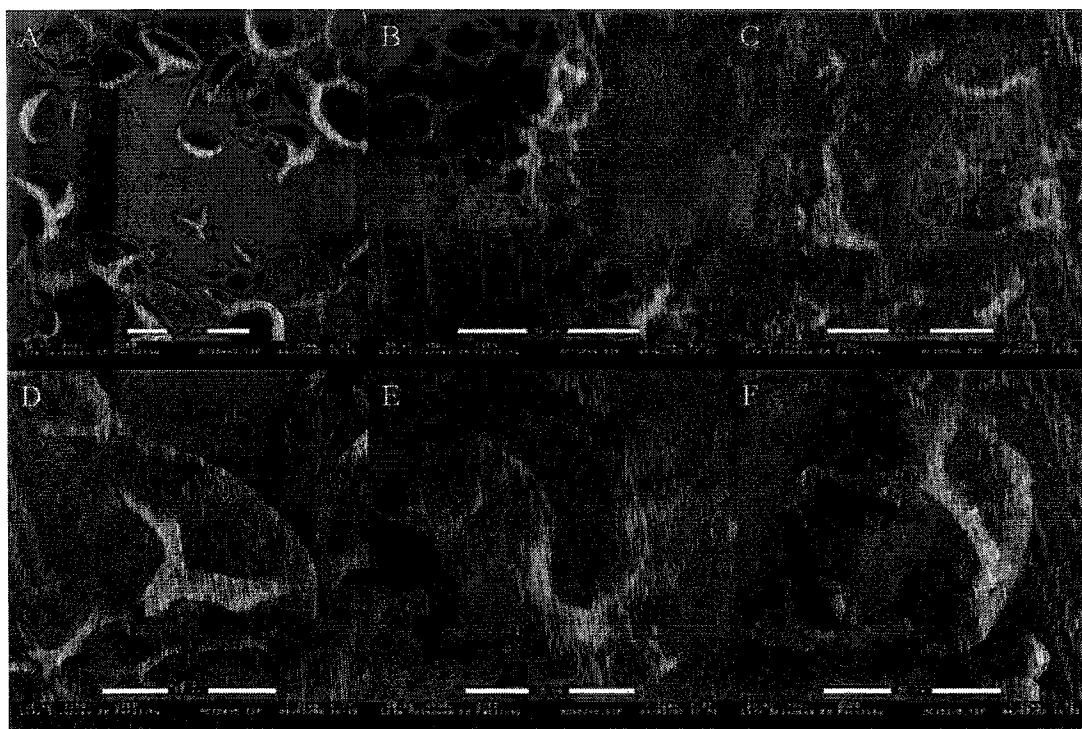


**Figure 17.** Environmental scanning electron micrographs of suspension polymer particles prepared by conventional free radical polymerization at 24 mol% PEGMA (A and D) and ATRP at 17 (B and E) and 24 mol% PEGMA (C and F) at 70 °C using DPE oil phase, oil:water = 1:2, and 17 mol% cross-linker (DEGDMA). The scale bar is 50 microns in micrographs A, B, C and F, and 35 and 15 microns in D and E, respectively.

polymer forming in the water unto the capsule surface via the residual vinyl groups of DEGDMA, is also excluded. Thus the second polymer layer must result from propagation of radicals trapped within and on the surface of the inner polymer layer. However, this requires that the dimensions these grafted-off polymer chains be of the order of several microns. Such micron sizes “giant” polymers have recently been

observed in surface-initiated ATRP.<sup>35</sup> That work supported the hypothesis that the observed micron sized polymer chains were individual macromolecules of extraordinary dimensions rather than crosslinked material resulting from inter-molecular radical transfer processes and characterized by a more moderate kinetic chain lengths. In our case, such surface initiated ATRP would be mediated by some ATRP catalyst present in the interfacial region. In addition, the second polymer layer must be rich in PEGMA as it forms on the water side of the interface were the presence of MMA and DEGDMA would be limited by their low solubility in water. We are presently evaluating the presence of a composition difference in the inner and outer polymer layers by Scanning Transmission X-ray Spectromicroscopy. The absence of a second layer in ATRP-17 particles despite the presence of a significant fraction of PEGMA in the water phase in this experiment as well, indicates that a minimum amount of PEGMA in the feed is necessary to obtain a second polymer layer. Above this critical PEGMA concentration the inner wall may be sufficiently polar to be water-swollen and the trapped radicals could become accessible to PEGMA in the water phase.

#### 4.4 Conclusions and future perspectives

Well defined soluble amphiphilic copolymers based on oil and water soluble comonomers were prepared by suspension ATRP for the first time. Copolymerizations containing up to 30 mol% (64 wt.%) water soluble PEGMA gave conversions equal to those obtained in solution conditions despite significant partitioning (70% w/w) of PEGMA into the water phase. This demonstrates that the living nature of ATRP ensures the continued incorporation of the water soluble monomer via its diffusion from the water

phase into the oil phase. Our results indicate that at high PEGMA content in the comonomer feed, the locus of polymerization may be critical for good ATRP control. In the absence of an added suspension stabilizer such as PVA or PVP, the amphiphilic copolymers occupy the oil-water interface and thus the locus of polymerization is the polar water-rich interfacial region. Consequently, the ATRP reaction is less controlled and results in the formation of high molecular weight material formed by fast uncontrolled polymerization and irreversibly terminated by coupling and disproportionation reactions that typically occur at high radical concentrations. In contrast, ATRP control is significantly enhanced by when suspension polymerization is carried out in the present of suspension stabilizer and the locus of polymerization shifts to the less polar interior of the oil droplets.

ATRP crosslinking of such amphiphilic copolymers using an oil soluble crosslinker (DEGDMA) yielded polymer capsules at 17 mol% PEGMA in the feed, while 24 mol% PEGMA was required when conventional radical polymerization was used. We conclude that this is the combined result of slower kinetics of ATRP reactions and the enhanced ability of a living polymerization to incorporate water-soluble PEGMA into the gels forming in the oil phase. Slower kinetics of polymerization gives the forming gels more time to diffuse to the oil-water interface. Thus, if the thermodynamically favored morphology is capsular under a given set of experimental conditions, then ATRP yields capsules while the analogous CFRP experiment yields matrix particles due to kinetic entrapment of the forming gels. In summary, the living nature of ATRP allowed the in

situ synthesis and crosslinking of amphiphilic polymers to yield polymer capsules via the assembly of the formed gels at the oil-water interface.

Furthermore, two-layered composite walled capsules were obtained at 24 mol% PEGMA. The difference in TEM contrast between the inner and outer layers of these capsule walls strongly suggests a compositional gradient from the inside to the outer surface. Work is in progress to spectroscopically ascertain this interesting compositional gradient.

Recent developments in room temperature ATRP of acrylic monomers using highly active aliphatic amine based catalysts<sup>36,37</sup> promises the possibility of fast (within the 1 to 2 hour time frame) room temperature encapsulations using techniques reported here. Such encapsulations could find applications in the agriculture industry where presence of residual copper species is not detrimental.

#### 4.5 Experimental Section

**Materials.** Toluene sulfonyl chloride (99+%) and 4,4'-dinonyl-2,2'-dipyridyl (97%), diphenyl ether (99%), cyclohexanol (99%), *p*-xylene (99%), poly(vinyl alcohol) (80% hydrolysed,  $M_w = 9000 - 10,000$  Da) and poly(vinyl pyrrolidone) ( $M_w = 360,000$  Da) were purchased from Aldrich and used as received. Cyclohexanone (Reagent Grade) was purchased from Anachemia Canada and distilled prior to use. Methyl cellulose (Methocell – E50) was obtained from Dow Chemical and used as received. Poly(ethylene glycol) monomethacrylate  $M_n \sim 360$  Da was purchased from Aldrich (Lot # 04023BU) and Polysciences Inc. ( $n = 200$ ; where “n” is the molecular weight of the pendant PEG chain; Lot # 519486) and purified as described earlier.<sup>28</sup> Copper (I) bromide (98%,

Aldrich) was purified according to a published procedure.<sup>38</sup> Methyl methacrylate (99%), was obtained from Aldrich and passed over a basic alumina column to remove inhibitor. n-butyl acetate (reagent grade), *iso*-propyl ether (reagent grade), neutral Alumina and basic Alumina (both Brockman Activity 1, mesh 60-325) were purchased from Fisher Scientific and used as received. Tetrahydrofuran (99%), dichloromethane (reagent grade), hexanes (reagent grade), methanol (HPLC grade), and water (HPLC grade) were purchased from Caledon Laboratories Limited and used as received.

#### **Measurement of partition coefficients of PEGMA in XYL, DPE, BuAc, CXN and CXL.**

PEGMA solutions (5% w/w) were prepared in HPLC grade water containing 100 ppm  $\text{NaN}_3$  by dissolving 400 mg PEGMA in 7600 mg of water in a 10 mL cylindrical vial (dimensions 13mm (dia.) X 70 mm (height)) equipped with a screw cap lined on the inside with a poly(propylene) organic solvent resistant seal. 3600 mg of organic solvent was then added to the vial and the suspension was shaken thrice at 10 minute intervals and then allowed to stand for an additional 10 minutes to allow the aqueous and organic layers to separate. Between shakings and until final separation of the aqueous layers, the vials were held in water baths at 25 °C or 70 °C for the respective partition coefficients. 1 mL samples of the aqueous layer were then drawn using a syringe and the residual PEGMA concentration in the aqueous layer was determined using Size Exclusion chromatography as described below.

**Quantitation of PEGMA in aqueous samples using Size Exclusion Chromatography.**

A calibration curve was developed for PEGMA using 1, 2, 3, 4, 5, 6, 8 and 10 % (w/w) solutions in 100 ppm aqueous  $\text{NaN}_3$  (the SEC mobile phase prepared by adding 400 mg of  $\text{NaN}_3$  to 4 L of HPLC grade water). To build the calibration curve, the total area under the peaks eluting between 34.6 and 71.6 minutes (Figure 1) was used as a measure of PEGMA concentration. This calibration curve was then employed to determine residual PEGMA concentrations in the aqueous layers after extraction with organic solvents, enabling the calculation of the partition coefficients.

**ATRP solution copolymerizations in XYL, DPE, BuAc, CXN and CXL.**

The following is a description of the ATRP synthesis of poly(MMA-co-PEGMA) containing 19 mol% PEGMA and is typical of all other solution copolymerizations. CuBr (72.8 mg, 0.5 mmol), dNBpy (408.8 mg, 1.0 mmol), MMA (2.00 g, 20 mmol), PEGMA (2.85 g, 7 mmol), and solvent (17.53 g) were placed in a round bottomed flask in a nitrogen filled glove bag and closed with a septum. TSC (95.3 mg, 0.5 mmol) was dissolved in MMA (1.00 g, 10 mmol) in a vial equipped with a septum inside a nitrogen filled glove bag. The monomer(s) and catalyst solution was degassed in a stream of argon for 30 minutes and then transferred to an oil bath at 70 °C. The initiator solution was introduced in one aliquot via a syringe that had been previously degassed with a stream of argon for 3 minutes. Samples (1 mL) were drawn periodically via a previously degassed syringe for Size Exclusion Chromatography (SEC) and conversion measurements. SEC samples (0.2 mL) were prepared by diluting with THF (1 mL) and passing over a neutral alumina column to remove catalyst followed by filtration using 2

micron PTFE filters. Conversion was determined gravimetrically. This involved dilution of 0.8 mL samples to 2 mL with THF, followed by precipitation in 18-19 mL iso-propyl ether in 20 mL vials; the vials were then centrifuged at 3500 rpm, the supernatant decanted and the precipitate vacuum dried (at 40 °C) in the dark to constant weight. The copolymerizations typically proceeded to 80 – 95% conversion.

**ATRP suspension copolymerization of MMA and PEGMA using DPE as oil phase.**

The following is a description of the suspension ATRP synthesis of poly(MMA-*co*-PEGMA) containing 19 mol% PEGMA and is typical of all other suspension copolymerizations. A solution polymerization was initiated in solution conditions (as described above). At 1 hour reaction time (7 to 15 % conversion), the oligomer solution was transferred into twice its weight of previously degassed (by bubbling a stream of Argon for 1 hour) HPLC grade water at 70 °C in a pressure tight baffled reactor equipped with a propeller type overhead stirrer. The suspension was mixed at a controlled speed (500 rpm throughout, or 1000 rpm for 10 or 30 minutes followed by 500 rpm until reaction end). Suspension samples (typically 3 to 4 g) were drawn via syringe, placed in pre-weighed 20 mL vials and used for GPC and conversion measurements as follows. The suspensions samples were freeze dried to remove water and the residue was dissolved in 2 to 3 mL THF. This copolymer solution was precipitated in 17 to 18 mL of di-*iso*-propyl ether, and the procedure repeated to ensure complete removal of unreacted monomers and solvent prior to vacuum drying at room temperature in the dark to constant weight, for conversion measurements. When PVP was used as suspension stabilizer, its presence in the final dried samples is accounted for in the conversion

calculations. SEC samples were prepared as described above except when PVP was used as suspension stabilizer. To remove PVP selectively, 20 – 30 mg samples were dissolved in a 2 mL THF : MeOH (19:1) mixture in 20 mL vials, and passed over an alumina column to remove catalyst. The resulting catalyst free solutions of copolymer and PVP were added to 17 to 18 mL THF to precipitate the PVP selectively. The precipitate was separated by centrifugation of the vials at 3500 rpm and subsequent decantation of supernatant. The supernatant, now containing only copolymer was evaporated under a stream of nitrogen at room temperature and used for SEC analysis after filtration using 2 micron PTFE filters.

#### **ATRP and CFRP encapsulations using DPE oil phase.**

ATRP encapsulation experiments were done in the same manner as the suspension copolymerizations described above except that prior to transferring the oligomer solution to the water phase, a calculated amount of crosslinker (for instance, 1696 mg DEGDMA with amounts of MMA and PEGMA in the suspension copolymerizations described above gives a feed composition of MMA : PEGMA : DEGDMA = 64:17:17 mol%) was added to the solution polymerization mixture and stirred for 10 minutes to ensure homogenous mixing before transfer. In these experiments the aqueous phase contained 1% (w/w) suspension stabilizer (PVA or methyl cellulose). The suspension was mixed at 1000 rpm for 30 minutes followed by 500 rpm until reaction end. Suspension samples were drawn periodically and treated as follows for gravimetric conversion determination. Suspension samples (3 to 4 g) were drawn with syringe, placed in a pre-weighed 20 mL vial, and diluted with 16 to 17 mL water. The

diluted suspension was shaken to disperse the polymer particles homogeneously prior to sedimenting the polymer particles by centrifugation at 3500 rpm for 10 minutes. This process was repeated three times to remove unreacted PEGMA and suspension stabilizer (PVA or methyl cellulose) in the water phase. Effective removal of the stabilizer was checked qualitatively by precipitation of the washings into a 20 fold excess of ethanol. These washed samples were then swollen in 16 to 17 mL THF (by rolling the vials gently in a hot dog roller over night at room temperature) and the polymer particles were sedimented with the aid of centrifugation as above. This process was repeated three times (swelling the particles with THF for only 20 to 30 minutes in the second and third extraction) to ensure removal of solvent and unreacted monomers. The THF swollen polymer particles were then precipitated by adding 10 to 15 mL *iso*-propyl ether. The precipitated particles were settled by centrifugation as above and the supernatant was decanted before drying the samples to constant weight in a vacuum oven (at 60 °C) for gravimetric conversion determination. In CFRP encapsulations (at a feed composition of MMA : PEGMA : DEGDMA = 64:17:17 mol%), MMA (3.00 g, 30 mmol), PEGMA (2.85 g, 7 mmol), DEGDMA (1.69 g, 7 mmol), benzoyl peroxide (226 mg, 3 wt.% with respect to monomers) and solvent (17.53 g) were placed in a round bottomed flask in a nitrogen filled glove bag and closed with a septum. The solution was degassed in a stream of argon for 30 minutes and then transferred to twice its weight of previously degassed (by bubbling a stream of Argon for 1 hour) HPLC grade water (1% in PVA or methyl cellulose) at 70 °C in a pressure tight baffled reactor equipped with a propeller type overhead mixer. The suspension was mixed at 1000 rpm for 30 minutes followed by

500 rpm until reaction end. Suspension samples for conversion measurements were drawn periodically and worked up as described above for ATRP particles.

#### **Sample preparation for Electron Microscopy.**

The surface and internal morphologies were determined using a Phillips-2020 Environmental Scanning Electron Microscope (ESEM) and a JEOL 1200EX Transmission Electron Microscope (TEM), respectively. For TEM analysis, suspension samples were worked-up as described above and the resulting polymer particles were embedded in Spurr epoxy resin and microtomed to ~ 100 nm thickness. ESEM samples were prepared by depositing dilute aqueous dispersions of polymer particles (after washing three times with water as described above to remove suspension stabilizer) on cover glass slips fixed to aluminum stubs using double sided adhesive carbon tape, drying at room temperature for 24 hours and sputter coating with a 4 nm layer of gold.

#### **Size Exclusion Chromatography (SEC) instruments and conditions.**

Polymer molecular weight was determined by SEC using a Waters 515 HPLC Pump connected to three Waters 5  $\mu\text{m}$  (7.8 X 300 mm) Styragel (HR2, HR3 and HR4) linear columns (exclusion limits 500-20,000 Da, 500-30,000 Da, and 5000-600,000 Da) and a Waters 2414 Refractive Index Detector. The HPLC pump was equipped with a Water 717 plus Autosampler and computer controlled using the Millennium 32 Chromatography Manager. The column and detector temperature were set at 40.0 °C and 35.0 °C, respectively. Tetrahydrofuran was used as elution solvent (flow rate = 1 mL/min), and narrow disperse linear polystyrene standards were used for calibration. Aqueous SEC was used for quantitation of PEGMA in aqueous samples. A Waters 515

HPLC Pump connected to three Waters 6  $\mu\text{m}$  ( $7.8 \times 300$  mm) Ultrahydrogel (120, 250 and 500) linear columns (exclusion limits 0-3000 Da, 0-50,000 Da, and 2000-300,000 Da) and a Waters 2414 Refractive Index Detector. The HPLC pump was equipped with a Water 717 plus Autosampler and computer controlled using the Millennium 32 Chromatography Manager. HPLC grade Water containing 100 ppm  $\text{NaN}_3$  was used as elution solvent at a flow rate = 0.8 mL/minute; Injection volume = 30  $\mu\text{L}$ ; Column temperature ( $^{\circ}\text{C}$ )/RI detector temperature ( $^{\circ}\text{C}$ )/run time (minutes) = 35/30/140.

#### **Acknowledgements**

We acknowledge NSERC and 3M Canada for funding this research and Dr. Nicholas Burke and Wen Hui Li for valuable suggestions.

## References:

- (1) Discher, E. D.; Eisenberg, A. *Science* **2002**, *297*, 967-973.
- (2) Arshady, R. *Microspheres, Microcapsules Liposomes* **1999**, *1*, 11-45.
- (3) Thurmond, II, K. B.; Kowalewski, T.; Wooley, K.L. *J. Am. Chem. Soc.* **1996**, *118*, 7239-7240.
- (4) Bütün, V.; Wang, X. -S.; de Paz Báñez, M. V.; Robinson, K. L.; Billingham, N. C.; Armes, S. P. *Macromolecules* **2000**, *33*, 1-3.
- (5) Stewart, S.; Liu, G. *Chem. Mater.* **1999**, *11*, 1048-1054.
- (6) Discher, B. M.; Bermudez, H.; Hammer, D. A.; Discher, D. E.; Won, Y. -Y.; Bates, Frank. S. *J. Phys. Chem. B* **2002**, *106*, 2848-2854.
- (7) Discher, B. M.; Won, Y., -Y.; Ege, D. S.; Lee, J. C. -M., Bates, F. S.; Discher, D. E.; Hammer, D. A. *Science* **1999** *284*, 1143-1146.
- (8) Discher, B. M.; Hammer, D. A.; Bates, F. S.; Discher, D. E. *Curr. Opin. Colloid Interface Sci.* **2000**, *5*, 125-131.
- (9) Chen, L. X.; Jenekhe, S. A. *Macromolecules* **2000**, *33*, 4610-4612.
- (10) Breitenkamp, K.; Emrick, T. *J. Am. Chem. Soc.* **2003**, *125*, 12070-12071.
- (11) Heming, A., M.; Mulqueen, P. J.; Scher, H. B.; Shirley, I. M. WO Patent 02/100525 A3, 2002.

- (12) Arshady, R. *Polym. Eng. Sci.* **1990**, *30*, 905-914.
- (13) Arshady, R. *Polym. Eng. Sci.* **1989**, *29*, 1746-1758.
- (14) Arshady, R. *Polym. Eng. Sci.* **1990**, *30*, 915-924.
- (15) Beestman, G. B.; Deming, J. M. U.S. Patent 4, 417, 916, 1983.
- (16) Arshady, R. *J. Microencapsulation* **1989**, *6*, 13-28.
- (17) Berg, J.; Sundberg, D.; Kronberg, B. *J. Microencapsulation* **1989**, *6*, 327-337.
- (18) Tiarks, F.; Landfester, K.; Antonietti, M. *Langmuir* **2001**, *17*, 908-918.
- (19) Van Zyl, A. J. P.; Sanderson, R. D.; Wet-Roos, D. D.; Klumperman, B. *Macromolecules* **2003**, *36*, 8621-8629.
- (20) McDonald, C; Chonde, Y.; Cohrs, W. E.; MacWilliams, D. C. U.S. Patent 4, 973, 670, 1990.
- (21) Kasai, K.; Hattori, M.; Takeuchi, H.; Sakurai, N. US Patent 4,798,691, 1989.
- (22) Kasai, K.; Hattori, M.; Takeuchi, H.; Sakurai, N. U.S. Patent 4, 908, 271, 1990.
- (23) Torza, S.; Mason, S., G. *J. Colloid Interface Sci.* **1970**, *33*, 67-83.
- (24) Sundberg, D. C.; Casassa, A. P.; Pantazopoulos, J.; Muscato, M.R. *J. Appl. Polym. Sci.* **1990**, *41*, 1425-1442.

- (25) McDonald, C. J.; Bouck, K. J.; Chaput, A. B.; Stevens, C. J.; *Macromolecules* **2000**, *33*, 1593-1605.
- (26) Kasai, K.; Hattori, M.; Takeuchi, H.; Sakurai, N. U.S. Patent 4, 908, 271, 1990.
- (27) Ali, M. M.; Stöver, H. D. H. *Macromolecules* **2003**, *36*, 1793-1801.
- (28) Ali, M. M.; Stöver, H. D. H. Accepted for publication in *Macromolecules* pending minor modifications (Dec. 2003).
- (29) Li, M.; Matyjaszewski, K. *J. Polym. Sci., Part A: Polym. Chem.* **2003**, *41*, 3606-3614.
- (30) Matyjaszewski, K.; Qiu, J.; Shipp, D. A.; Gaynor, S. G. *Macromol. Symp.* **2000**, *155*, 15-29.
- (31) Wang, X. -S.; Jackson, R. A.; Armes, S. P. *Macromolecules* **2000**, *33*, 255-257. (32) Natzmer, P. V.; Bontempo, D.; Tirelli, N. *Chem. Comm.* **2003**, 1600-1601.
- (32) Nanda, A. K.; Matyjaszewski, K. *Macromolecules* **2003**, *36*, 599-604.
- (33) Bo, G.; Wesslén, B.; Wesslén, K. B. *J. Polym. Sci. : Part A: Polym. Chem.* **1992**, *30*, 1799-1808.
- (34) Ali, M. M.; Stöver, H. D. H. in "Advances in Controlled/ Living Radical Polymerization"; Editor: Matyjaszewski, K.; *ACS Symposium Series* **854**, **2003**, *36*, 299-315.

- (35) Natzmer, P. V.; Bontempo, D.; Tirelli, N. *Chem. Comm.* **2003**, 1600-1601.
- (36) Queffelec, J.; Gaynor, S. G.; Matyjaszewski, K. *Macromolecules* **2000**, *33*, 8629-8639.
- (37) Matyjaszewski, K.; Göbelt, B.; Paik, H. -J.; Horwitz, C. P. *Macromolecules* **2001**, *34*, 430-440.
- (38) Keller, R. N.; Wycoff, H. D. *Inorg. Synth.* **1946**, *2*, 1-4.

## Conclusions

### 5.1 Summary

In this work, two types of amphiphilic methacrylate based copolymers were prepared using Atom Transfer Radical Polymerization (ATRP) in solution and suspension polymerization conditions. The ability of these amphiphilic polymers to assemble at the oil water interface (of oil droplets) in suspension polymerization was controlled by the ratio of non-polar to polar comonomer. Cross-linking the copolymers yielded stable suspension polymer particles whose morphology was tuned from solid to core-shell capsular particles by increasing the polar comonomer content in the feed. The morphology of these ATRP particles was compared to suspension polymer particles prepared using Conventional Free Radical Polymerization (CFRP) at analogous comonomer ratios. This illustrated that the ATRP particles exhibited the capsular morphology at lower concentrations of polar comonomer in the feed relative to CFRP particles. A summary of specific observations and conclusions reached as well as suggestions on possible future research directions are presented in the following sections.

### 5.2 The Poly(MMA-*co*-MPEGMA) system

Copolymers of methyl methacrylate (MMA) and 9.5, 18 and 39 mol% poly(ethylene glycol) monomethyl ether methacrylate (MPEGMA) were prepared in diphenyl ether (DPE) solution at 70 °C using tosyl chloride (TSC) initiator and the copper (I) bromide/dinonyl bipyridyl (Cu(I)Br/2dNBpy) catalyst. The copolymerizations yielded narrow disperse polymers ( $M_w/M_n < 1.2$ ) in over 90 % wt. % yields with good agreement

between experimental ( $M_n(\text{SEC})$ ) and theoretical ( $M_n(\text{Theo})$ ) molecular weights indicating well controlled ATR copolymerizations. In suspension conditions, polydispersity increased ( $M_w/M_n < 1.3$ ) and conversion decreased (>80 %) slightly, but  $M_n(\text{SEC})$  matched  $M_n(\text{Theo})$  indicating that the catalyst is confined to the oil droplets and effectively mediates the ATRP reaction.

Crosslinking suspension polymerizations using diethylene glycol dimethacrylate (DEGDMA) yielded colloiddally stable polymer particles. Increasing the polarity of the copolymer by increasing its MPEGMA content from 0 to 31 mol% led to a transition in suspension particle morphology from matrix to multi-hollow and capsular particles. In contrast, comparable suspension particles prepared by conventional free radical polymerization (CFRP) only showed matrix structure. Thus, we demonstrated for the first time that the use of a living/controlled polymerization characterized by slow rate of polymerization allows the thermodynamically favored morphology to be achieved. This finding is particularly important for encapsulation of polar core oils where the driving force for polymer migration to oil water interface is correspondingly weaker.

### 5.3 The Poly(MMA-co-PEGMA) solution polymerization system

Novel well defined amphiphilic copolymers ( $M_w/M_n < 1.2$ ) based on hydrophobic MMA and water soluble poly(ethylene glycol) methacrylate (PEGMA) (10, 18, 24, 30, 40 and 100 mol% PEGMA) were prepared in several organic solvents using TSC - Cu(I)Br/2dNBpy as initiator - catalyst system at 70 °C. The PEGMA homopolymer and copolymers containing more than 24 mol% (57 wt.%) PEGMA were water-soluble and

exhibited sharp lower critical solution temperatures (LCST) that increased with increasing PEGMA content as expected (mol% PEGMA = 24, 30, 40; LCST = 42.7, 49.8, 55.8 °C, respectively). <sup>1</sup>H NMR showed that the composition of the copolymers matched the comonomer feed composition throughout the polymerization. This indicates that random rather than gradient copolymers formed. These thermosensitive copolymers bearing a pendant poly(ethylene glycol) chain are potentially useful in diverse areas such as controlled drug delivery, reversible surfactants and chromatography.

#### **5.4 The Poly(MMA-*co*-PEGMA) suspension polymerization system**

Suspension copolymerizations using DPE oil phase proceeded to high conversions similar to those observed in solution conditions (> 80% w/w) despite significant partitioning of PEGMA (70 wt. %) into the water phase. This work indicates for the first time that the living nature of ATRP allows the synthesis of highly amphiphilic copolymers based on oil and water soluble comonomers in suspension polymerization conditions. Copolymers with high PEGMA content contained a significant proportion of high molecular weight material formed *via* uncontrolled polymerization unless PVA was added to stabilize the oil droplets. This suggests that the locus of polymerization is critical for ATRP control in suspension conditions.

Crosslinking suspension polymerization using DEGDMA gave capsules at as low as 17 mol% PEGMA using ATRP, while CFRP only led to capsules at 24 mol% PEGMA in the feed. ATRP causes particle-capsule transition at lower PEGMA levels, reflecting the slower ATRP kinetics and possibly higher polarity of ATRP-derived gels due to more

uniform incorporation of PEGMA into the gels. Suspension ATRP using 24 mol% PEGMA in the feed gave two-layered capsule walls bearing a uniformly thick TEM-visible inner layer and TEM/ESEM-visible irregular outer layer suggesting a compositional gradient across the capsule wall. Capsules bearing a PEGMA rich outer surface are potentially useful for medical applications owing to the biocompatibility and non-immunogenic nature of poly(ethylene glycol) based hydrogel materials.

### 5.5 Future work

In our present work, polymer capsules based on oil and water soluble, methacrylate based comonomers were prepared by *in situ* suspension ATRP. The locus of polymerization was the oil droplets and thus confinement of the ATRP catalyst to the oil droplets was critical for well controlled ATRP. While this system successfully demonstrated the advantage of slow ATRP kinetics towards obtaining the thermodynamic morphology, it suffers from two significant drawbacks which stem from the oil phase being the locus of polymerization. First, ATRP of methacrylates in organic solvents is slow, typically requiring over 12 hours and high temperature (>60 °C) for quantitative conversion. Second, the copper based ATRP catalyst remains trapped within the polymer capsules imparting color and toxicity thereby limiting the possible applications of such capsules. These limitations can be overcome if the wall forming copolymer forms in the water phase and subsequently precipitates onto the surface of dispersed oil droplets. Water soluble acrylates and acrylamides undergo fast ATRP in water and water/alcohol mixtures using highly reactive ATRP catalysts based on aliphatic amine ligand. Such

polymerizations are fast, typically requiring less than 5 hours at room temperature for quantitative conversion. Furthermore, catalyst free capsules are potentially accessible by separation of the capsules from the aqueous continuous phase by simple filtration or decantation. Deposition of wall forming polymer from the continuous aqueous phase of course presents new challenges with regards to colloidal stability, unless the forming polymer forms liquids coacervates.

The present work suggests that composite-walled capsules characterized by an inner polymer layer rich in the hydrophobic monomer and an outer hydrophilic monomer rich layer form at high concentrations of water soluble monomer in the aqueous phase. We have hypothesized the presence of a compositional gradient based on TEM observations. While TEM contrast is generally caused by differences in chemical composition, it may result from differences in the density of material as well. As such, the presence of a compositional gradient in these systems needs to be confirmed by spectroscopy. Scanning Transmission X-ray Spectromicroscopy (STXM) may be used as this technique is potentially capable of mapping compositional differences on the 50 – 100 nm length scale. Alternatively, tagging the PEGMA comonomer with a chromophore could permit comparison of its concentration in the inner and outer layers of the composite capsule wall. If a gradient in chemical composition is ascertained, then the ability of ATRP to yield such materials in one step may be further harnessed in the development of composite capsules based on polymers that differ in their diffusional, mechanical, or chemical properties.

In this work, we developed the synthesis of potentially biocompatible thermosensitive copolymers whose lower critical solution temperature could be controlled through the comonomer ratio. Surface grafting of these thermosensitive copolymers can potentially be used for the development of materials whose surface polarity can be reversibly switched between hydrophilic and hydrophobic states triggered by changes in temperature.

## APPENDIX I:

Summary of the experimental used approaches to favor the hollow or capsular particle morphology in the preparation of capsules using the *in situ* polymerization technique

Approaches to tailor thermodynamics	Approaches to tailor kinetics	Research groups*
Use of polar comonomers e.g., AA, AN, AAM or HEMA, to impart high polarity	Use of chain transfer agents e.g., R-SH, to lower polymer molecular weight and hence viscosity	Kasai et al. McDonald et al.
Use of hydrophobic seed particles e.g., PS latex, to drive forming polymer to the oil water interface	Use of high swelling ratio (monomer/diluents to seed) to impart low viscosity	Kasai et al., Okubo et al. El Aasser et al. McDonald et al.
Use of surfactants/stabilizers e.g., SDS, CTAB, PVA or PVP, to modify the oil-water and polymer-water interfacial tensions.	Use of continuous monomer addition to lower monomer concentration	Sundberg et al. Others
Use of water miscible alcohols e.g., MeOH, EtOH, to modify interfacial tensions, partitioning of monomers between oil and water, and lower polymer molecular weight.	Use of a temperature ramp to lower polymerization rate i.e., polymer concentration and hence viscosity	McDonald et al.

\*See references in Chapter 1 for specific journal articles authored by these researchers and their coworkers.

## APPENDIX II:

Summary of preliminary experiments aimed at developing the ATR polymerization of MMA in some organic solvents\*

Mon.	Mon. Conc. (w/w)	Sol.	Rxn. Temp. (°C)	Ini.	Catalyst	M <sub>n</sub> (Theo); M <sub>n</sub> (exp); PDI
MA	20	OC	50	EBiB	CuBr/BPMOA	17,000; 15,000; 1.6
MA	40	MIBK	60	EBiB	CuBr/BPMOA	17,000; 3000; 1.1
MA	40	MIBK	70	EBiB	CuBr/BPMOA	68,000; 10,000; 1.2
MMA	40	MIBK	50	EBiB	CuBr/BPMOA	20,000; 24,000; 1.2
MMA	5	MIBK	50	EBiB	CuBr/BPMOA	20,000; 16,000; 1.4
MMA	5	BuBz	60	EBiB	CuBr/BPMOA	20,000; 16,000; 1.2
MMA	5	BuBz	70	EBiB	CuBr/BPMOA	20,000; 17,000; 1.4
MMA	50	NMP	60	EBiB	CuBr/HMTETA	10,000; 12,000; 1.3

\*Abbreviations: Mon. = Monomer; Sol. = Solvent; Ini. = Initiator; MA = Methyl acrylate; MMA = Methyl Methacrylate; OC = *iso*-octane; MIBK = Methyl *iso*-butyl ketone; BuBz = Butyl benzoate; NMP = 1-methyl-2-pyrrolidinone; EBiB = Ethyl bromo *iso*-butyrate; BPMOA; *Bis*-pyridyl methyl octylamine; HMTETA = Hexamethyl triethylene tetraamine; M<sub>n</sub>(Theo) = Number Average molecular weight based on the initial monomer to initiator used; M<sub>n</sub>(exp) = Experimentally observed Number Average molecular weight determined by Size Exclusion Chromatography; PDI = Polydispersity Index.